



UNIVERSIDADE FEDERAL DE SÃO CARLOS  
CENTRO DE CIÊNCIAS EXATAS E DE TECNOLOGIA  
PROGRAMA DE PÓS-GRADUAÇÃO EM ENGENHARIA QUÍMICA

ELISÂNGELA KRAUSS

DESENVOLVIMENTO DE METODOLOGIA PARA MONITORAMENTO CONTÍNUO  
DE CONCENTRAÇÃO DE EMISSÃO DE  $PM_{10}$  EM FONTES ESTACIONÁRIAS  
INDUSTRIAIS

METHODOLOGY DEVELOPMENT FOR CONTINUOUS MONITORING OF THE  
EMISSION CONCENTRATION OF  $PM_{10}$  IN INDUSTRIAL STATIONARY SOURCES

SÃO CARLOS – SP

2020

ELISANGELA KRAUSS

DESENVOLVIMENTO DE METODOLOGIA PARA MONITORAMENTO CONTÍNUO  
DA CONCENTRAÇÃO DE EMISSÃO DE PM<sub>1</sub> EM FONTES ESTACIONÁRIAS  
INDUSTRIAIS

METHODOLOGY DEVELOPMENT FOR CONTINUOUS MONITORING OF THE  
EMISSION CONCENTRATION OF PM<sub>1</sub> IN INDUSTRIAL STATIONARY SOURCES

Tese apresentada ao Programa de Pós-Graduação  
em Engenharia Química da Universidade Federal  
de São Carlos, para obtenção do título de doutora  
em Engenharia Química.

Orientadora: Prof.<sup>a</sup> Dr.<sup>a</sup> Mônica Lopes Aguiar

SÃO CARLOS – SP

2020



**UNIVERSIDADE FEDERAL DE SÃO CARLOS**

Centro de Ciências Exatas e de Tecnologia  
Programa de Pós-Graduação em Engenharia Química

---

**Folha de Aprovação**

---

Defesa de Tese de Doutorado da candidata Elisângela Krauss, realizada em 31/08/2020.

**Comissão Julgadora:**

Profa. Dra. Mônica Lopes Aguiar (UFSCar)

Prof. Dr. Rafael Sartim (UFES)

Profa. Dra. Vádila Giovana Guerra Béttega (UFSCar)

Profa. Dra. Simone Andréa Pozza (UNICAMP)

Prof. Dr. Marcos Vinicius Rodrigues (UNIFAL)

Prof. Dr. Bruno de Araújo Lima (UFSCar)

O presente trabalho foi realizado com apoio da Coordenação de Aperfeiçoamento de Pessoal de Nível Superior - Brasil (CAPES) - Código de Financiamento 001.

O Relatório de Defesa assinado pelos membros da Comissão Julgadora encontra-se arquivado junto ao Programa de Pós-Graduação em Engenharia Química.

## ACKNOWLEDGEMENTS

Ao sistema público de ensino, com seus professores e servidores guerreiros sobrevivendo à tantas investidas para retroceder o desenvolvimento do Brasil. Esse sistema que me propiciou 22 anos de educação gratuita e de altíssima qualidade, desde a primeira série em escola rural multiseriada até o doutorado.

A Mônica por ter saído de sua zona de conforto para seguir comigo nesse projeto e ter sempre uma palavra de apoio quando precisei, um exemplo de educadora em tempos de escuridão.

Til Ole Bjørn Jensen, Vibeke Rasmussen og Sigbjørn Vestmoen som har støttet denne prosjekt og meg selv med tid og tålmodighet.

Ao Claiton pela parceria de cuidar da Clara e da Anna enquanto eu estudava termodinâmica aos sábados e ficava depois do horário no trabalho. Pela imensa compreensão nas minhas ausências.

Às irmãs Eli e Regina por ouvir minhas reclamações sem julgar.

Agradeço a jornalista Regina Krauss e ao engenheiro Jakub Bujalski pela revisão e comentários.

À teimosia vinda do Ovídio e a coragem da Maria Nilce.

*“Menina, o mundo, a vida, tudo está aí. Nossa gente não tem conseguido quase nada. Todos aqueles que morreram sem se realizar, todos os negros escravizados de ontem, os supostamente livres de hoje, se libertam na vida de cada um de nós, que consegue viver, que consegue se realizar. A sua vida, menina, não pode ser só sua. Muitos vão se libertar, vão se realizar por meio de você. Os gemidos estão sempre presentes. É preciso ter os ouvidos, os olhos e o coração abertos”.*

Becos da memória – Conceição Evaristo

## TABLE OF FIGURES

Figure 1 Map of potential aspects to be explored in the research .....	16
Figure 2 Process flow diagram of NPK prilling process.....	18
Figure 3 Optical Scatter Principle and application example. Source: Adapted from PCME (2019) .....	24
Figure 4 Example of electrodynamic diffusion charger. Source: adapted from (PCME, 2019) .....	29
Figure 5 Cascade impactor operation principle. Source: adapted from Dekati (2011).....	30
Figure 6 ELPI instrument schematic. Source: adapted from Dekati (2011). .....	31
Figure 7 Schematic of airflow in the PT .....	37
Figure 8 Test rig where (a) shows the stack with 3 sensors installed and (b) the detail of the probe for GS .....	38
Figure 9 Layout of analyzers and GS probe in the stack under study.....	40
Figure 10 Fiberglass pad filter employed in the research project. ....	40
Figure 11 OSA probe which one goes inside the stack.....	42
Figure 12 External part of EDA and probe rod.....	42
Figure 13 Industrial Prilling Tower set-up.....	49
Figure 14 Layout of analyzers in the stack under study.....	49
Figure 15 Effect of human factor evaluated based on the result of the test for equal variances, from the GS performed by 2 operators considering normal distribution. ....	52
Figure 16 PM concentration as a function of product type over different seasons.....	53
Figure 17 Standard deviation of calibration factors for sensors OSA/ EDA over different seasons.....	54
Figure 18 Standard deviations for calibration factors from OSA/ EDA under different product grades .....	54
Figure 19 PM concentration read from OSA over 600h .....	55
Figure 20 Results from the span check performed by the OSA every 15min where 80% is the reference to inspect the instrument.....	56
Figure 21 PM concentration read from EDA over 600h in fall .....	56
Figure 22 (a) Laser sensor from OSA day 1 (span 80%). (b) Laser sensor from OSA day 15 (span 71%).....	57
Figure 23 (a) Sampling probe from EDA day 1 (self-check 100%). (b) Sampling probe from EDA day 15 (self-check 100%). ....	57
Figure 24 Online analyzers output during start-up of the plant. ....	58
Figure 25 EDA outputs for reducing the steam injection frequency.....	59
Figure 26 EDA (red squares) and OSA (blue circles) results under sudden high changes on PM concentration. ....	60
Figure 27 Web search on keywords in Science Direct from 2010 – 2020.....	65
Figure 28 Industrial Prilling Tower (PT) set-up with 6 stacks.....	66
Figure 29 Cumulative particle size distribution of mineral fertilizer aerosol in each impactor stage (95% confidence interval for the mean).....	69
Figure 30 (a) Stage 1.24 $\mu$ m aerodynamic diameter support, aluminum foil, substrate and UFPs. (b) Magnification of 180 times of one of the UFP agglomerates.....	70
Figure 31 Magnification of 1500 times of UFP agglomerate with particles named as A, B and C. ....	70
Figure 32 Standardized effect for EDA PM concentration for significance level of 5%.....	72
Figure 33 Residuals for EDA UFP concentration model over time.....	73
Figure 34 Probability plot of OSA model versus data set.....	75

Figure 35 Residuals between OSA model and data sets .....	76
Figure 36 Standardized effects of parameters. Level of significance 5% .....	77
Figure 37 Process flow diagram of NPK prilling process.....	81
Figure 38 Proposed Methodology to Continuous Measure UFP in PT.....	82
Figure 39 Standardized off-spec flowrate per run (9 runs each campaign) for the two campaigns performed .....	86
Figure 40 Standardized NP-liquor temperature per run (9 runs each campaign) for the two campaigns performed .....	86
Figure 41 Probability plot for the flowrate ratios of raw materials to the final product .....	87
Figure 42 Test for equal variances on air temperature considering normal distribution with confidence level of 97.5%.....	88
Figure 43 Test for equal variances on relative humidity with confidence level of 98.3% considering normal distribution .....	89
Figure 44 ELPI linear regression model .....	91
Figure 45 Residuals over time for ELPI regression model (18 experiments data set).....	92
Figure 46 OSA linear regression model residuals.....	94
Figure 47 EDA model residuals over the experiments .....	95
Figure 48 ELPI measurement vs off-spec flowrate and NP-liquor temperature.....	97
Figure 49 ELPI PM concentration vs K-salts temperature and bucket speed.....	98

## LIST OF TABLES

Table 1 Guide to application parameters for technologies.....	23
Table 2 Manual equipment employed.....	39
Table 3 Range of parameters during gravimetric sampling.....	41
Table 4 ELPI specifications .....	44
Table 5 Mapping of potential parameters to be included in the analysis.....	45
Table 6 Range of parameters during gravimetric sampling.....	50
Table 7 Data set employed to build the model.....	64
Table 8 Chemical composition of particles from stage 1.24 $\mu$ m .....	71
Table 9 Terms included in the EDA PM concentration model with significance level.....	72
Table 10 Model coefficients for OSA PM concentration .....	75
Table 11 Parameters mapped from the volume of control.....	83
Table 12 Design of Experiment from Minitab19® .....	85
Table 13 Summary of quality parameters generated by the regression models from ELPI/ OSA/ EDA.....	90
Table 14 ELPI regression model coefficients and significance .....	91
Table 15 OSA/EDA PM concentration model coefficients .....	94

## ACRONIMS

AN	Ammonium nitrate – $\text{NH}_4\text{NO}_3$
ANN	Artificial Neural Networks
ANOVA	Analysis of Variance
BAT	Best Available Technique
CAN	Ammonium Calcium Nitrate
CFD	Computational Fluid Dynamics
CN	Calcium Nitrate
CPC	Condensation Particle Counter
DC	Diffusion Charger
DCS	Distributed Control System
DoE	Design of Experiments
EDA	Electrodynamic Diffusion Charger
ELPI	Electrical Low-Pressure Cascade Impactor
$\text{FNO}_3$	Ammonium Fluoride
GS	Gravimetric Sampling
$\text{K}_2\text{SO}_4$	Potassium sulphate
KCl	Potassium Chloride
LRM	Linear Regression Model
$\text{NH}_3$	Ammonia
NPK	Nitrogen- Phosphorus- Potassium Mineral Fertilizer
OPC	Optical Particle Counter
OSA	Optical Scattering
PM	Particulate Matter
PM1	Particulate matter with diameter less than $1\mu\text{m}$
PM10	Particulate matter with diameter less than $10\mu\text{m}$
PM2.5	Particulate matter with diameter less than $2.5\mu\text{m}$
PSD	Particle Size Distribution
PT	Prilling Tower
RM	Raw Material
RSM	Response Surface Model
SEM/EDS	Scanning Electron Microscopy / Energy Dispersive X-ray Spectroscopy
$\text{SiF}_4$	Silicon Tetrafluoride
UFP	Ultrafine Particles – Particles with Diameter from $100\text{nm}$ to $2.5\mu\text{m}$
X1, X2	Variables in a Model
Y	Response from a Model



## RESUMO

As partículas ultrafinas (UFP) emitidas por torres de prilling apresentam potencial de causar doenças degenerativas no cérebro quando inaladas. Estas são voláteis e instáveis (como o caso de sulfatos e nitratos), o que torna a determinação da sua concentração em massa imprecisa, especialmente se o monitoramento contínuo dessa concentração através de sensores é exigido pelas agências ambientais, uma vez que o procedimento padrão de calibração dos sensores é baseada em amostragens gravimétricas, que, por sua vez, atingiram seu limite de detecção nessa faixa granulométrica. Nesse contexto, este trabalho avaliou o desempenho de dois sensores de monitoramento contínuo para medição de UFP em uma torre de prilling industrial. Os princípios testados foram difusão de carga eletrodinâmico (EDA) e dispersão ótica (OSA), instalados na fonte estacionária na qual amostragens gravimétricas foram realizadas. Os dados destes sensores foram coletados por quatro estações no norte da Europa, simultaneamente com os parâmetros meteorológicos e de processo. Uma metodologia baseada em um experimento controlado foi testada na qual as vazões de matérias-primas foram mantidas estáveis enquanto a concentração em massa de UFP foi medida também com o impactador de cascata (ELPI) com todos os experimentos sendo realizados em uma mesma estação do ano. Os resultados mostraram que o OSA segue as variações do processo e os fatores de calibração obtidos com as amostragens gravimétricas variaram 0,5 desvios padrão entre as estações e mudanças de produto. O EDA identificou mudanças pontuais de concentração no seu limite de detecção, mas os fatores de calibração medidos foram de três desvios-padrão independentemente da estação do ano ou produtos. EDA também indicou erroneamente concentrações elevadas de UFP devido a injeção de vapor no processo. A contaminação dos sensores por poeira afeta a leitura de ambos os sensores, mas somente o OSA indica a necessidade de manutenção. Na modelagem dos dados coletados de todo o período foi observado que o EDA não apresenta correlação com o processo nem tampouco com os parâmetros meteorológicos ( $r$ -quadrado menor que 10%) o que pode ser causado por partículas não serem eletricamente carregadas uniformemente e o fato de o equipamento apresentar resolução comprovada para partículas maiores que  $10\mu\text{m}$ . O modelo obtido pra OSA apresentou  $r$ -quadrado de 45% e correlação com os dois grupos de parâmetros monitorados, com erro padrão de  $0,21\text{ mg/m}^3$ , indicando uma potencial aplicação no monitoramento de UFP, se os parâmetros meteorológicos forem incluídos no modelo, prática já em uso na modelagem de UFP em ar ambiente. Finalmente, os modelos de regressão linear criados empregando a metodologia aqui proposta mostraram que os sensores comerciais não possuem resolução suficiente em condições controladas para UFP enquanto o modelo gerado pelo ELPI apresentou  $r$ -quadrado de 94,13% e um erro padrão de  $0,02\text{ mg/m}^3$  não sendo influenciado pelas condições da chaminé e sendo capaz de detectar variações no processo. Desta forma o ELPI apresenta potencial para uso na calibração de sensores comerciais em substituição à amostragem gravimétrica, a qual apresenta limitações nessa faixa de diâmetros de partículas. O emprego dessa metodologia, portanto, apresenta potencial para assegurar que as torres de prilling possam instalar monitoramento contínuo, calibrar os sensores e otimizar o processo empregando o ELPI, contribuindo, portanto, para a redução da emissão de material particulado fino para o ambiente e reduzindo seu dano potencial.

**Palavras chave:** Torre de prilling industrial. Partículas ultrafinas. Scanner por laser ótico. Efeito eletrodinâmico. ELPI.

## ABSTRACT

Among the processes that generate emissions of ultrafine particles (UFP), which are known by their high potential to cause brain diseases when inhaled, the prilling towers have a significant contribution, as those processes use flow rates up to 10 times higher than other dryers. From the monitoring perspective, UFP are generally unstable and volatile (as the case of sulfates and nitrates) making its mass concentration determination inaccurate, especially if continuous mass monitoring is intended to be installed. Also, the environmental agencies have demanded that particulate matter from the stacks must be continuously monitored, with the standard procedure for calibration being the gravimetric sampling. In this context, this research has evaluated the performance of two continuous sensors on measuring UFP mass concentration in an industrial fertilizer prilling tower. The sensors tested were electrodynamic diffusion charger (EDA) and optical scattering (OSA). The analyzers were installed at same stack where gravimetric sampling (GS) was performed to find calibration factors. Data was collected over four seasons in Northern Europe, including the particulate matter from the analyzers, meteorological and process parameters. A controlled experiment where flows and meteorological parameters were kept stable was run to test electrical low-pressure cascade impactor (ELPI) performance compared to the other sensors. The results show that OSA follows the process changes and the calibration factors obtained from GS varied on 0.5 standard deviations over products and seasons. EDA represents better sudden variations up to its operating range, but the calibration factors measured were over three standard deviation, independent of seasons and products. EDA also presented an artificially high emission due to intermittent steam injection in the stream. Dust deposition on the sensors affects the reading on both analyzers but only OSA indicates it. While modelling the data collected over the period, it was found that EDA was neither correlated with process nor meteorological parameters (r-squared less than 10%) what can be caused by particles not being charged evenly or droplets read as particles. The OSA concentration model showed r-squared of 45% and strong correlation with meteorological parameters and raw material flow rates. The model presented a standard error of 0.21 mg/Nm<sup>3</sup>. OSA has potential to be employed for ultrafine particles monitoring if the influence of particle characteristics under industrial operation is considered and meteorological parameters are included, as already in practice for ultrafine particles monitoring outdoors. Finally the linear regression models built based on the methodology here proposed, showed that the commercial sensors did not have enough precision while ELPI analyzer output presented a model with adjusted r-squared of 94.13% and a standard error of 0.02 mg/m<sup>3</sup> not including any air stream parameter and detecting changes in the process that allow optimization of those to reduce the UF emission. The ELPI shows potential to be used as calibration device to other in-situ continuous dust monitoring when dealing with UFP, once gravimetric sampling has reached its detection limit for UFP. By applying the methodology here proposed there is potential to install and calibrate continuous sensors at stationary sources emitting UFP with ELPI as well as optimizing the process to reduce the concentration of UFP and by doing so, decreasing the potential impact of those in the environment and on the human health.

**Keywords:** Industrial prilling tower; Ultrafine particles; Optical laser scanner; Electrodynamic diffusion charger; ELPI;

## TABLE OF CONTENTS

<b>ACKNOWLEDGEMENTS</b> .....	<b>4</b>
<b>TABLE OF FIGURES</b> .....	<b>5</b>
<b>LIST OF TABLES</b> .....	<b>7</b>
<b>ACRONIMS</b>	<b>8</b>
<b>RESUMO</b>	<b>9</b>
<b>ABSTRACT</b>	<b>10</b>
<b>TABLE OF CONTENTS</b> .....	<b>11</b>
<b>1. INTRODUCTION</b> .....	<b>13</b>
<b>2. OBJECTIVES</b> .....	<b>14</b>
2.1. General Objective .....	14
2.2. Specific Objectives.....	14
<b>3. BIBLIOGRAPHIC REVIEW</b> .....	<b>15</b>
3.1. The Process Under Analysis.....	15
3.2. Techniques for Continuous PM Concentration Monitoring.....	20
3.2.1. Optical detection methods .....	22
3.2.2. Probe electrification .....	27
3.2.3. Electrical low-pressure cascade impactor.....	29
3.3. Statistical Modeling Applied to Experimental Investigations .....	33
<b>4. GENERAL MATERIALS AND METHODS</b> .....	<b>37</b>
4.1. Gravimetric Sampling.....	38
4.2. Manual Data Collection.....	41
4.3. Continuous Monitoring Equipment.....	41
4.3.1. Optical dust analyzer .....	41
4.3.2. Electrodynamic dust analyzer .....	42
4.3.3. Calibration of online analyzers/ self-quality checks.....	43
4.3.4. Electrical low-pressure impactor .....	43
4.4. Data Extraction and Handling .....	45
<b>5. PERFORMANCE AND CHALLENGES OF ONLINE FINE PARTICULATE MATTER MONITORING IN A MINERAL FERTILIZER INDUSTRIAL PLANT</b> .....	<b>47</b>
5.1. INTRODUCTION .....	47
5.2. MATERIAL AND METHODS.....	48
5.2.1. Manual Gravimetric Sampling.....	49
5.2.2. Online PM Analyzers .....	50
5.2.3. Electrodynamic PM analyzer .....	50
5.2.4. Optical PM analyzer.....	51
5.2.5. Calibration of Online Analyzers/ Self-Quality Checks .....	51
5.3. RESULTS AND DISCUSSIONS .....	52
5.3.1. Calibration Campaigns Results.....	52
5.3.2. Performance of Instruments Over Time.....	55
5.3.3. Saturated Steam Effect on EDA Outputs.....	57
5.3.4. Analyzers Responses to Sudden Changes on PM Concentration.....	59
5.4. CONCLUSIONS.....	60
<b>6. DEVELOPMENT OF A REGRESSION MODEL TO PREDICT ULTRAFINE PARTICLES EMISSION IN AN INDUSTRIAL PLANT COMBINING METEOROLOGICAL AND PROCESS VARIABLES</b> .....	<b>62</b>
6.1. INTRODUCTION .....	62
6.1.1. Mapping of Potential Parameters in Prilling Fertilizers with AN/CAN.....	63
6.1.2. Ultrafine Particle Concentration Methods .....	64
6.1.3. Modelling Techniques for Experimental Data .....	65
6.2. MATERIAL AND METHODS.....	66
6.2.1. Industrial Process Set-up.....	66
6.2.2. Equipment Employed to Characterize and Measure Concentration of UFP .....	67

6.2.3.	Dataset Preparation and Regression Techniques .....	67
6.3.	RESULTS AND DISCUSSIONS .....	68
6.3.1.	Characterization of PM Under Study.....	68
6.3.2.	EDA UFP Concentration as a Function of Process and Meteorological Parameters	71
6.3.3.	OSA UFP Concentration as a Function of Meteorological and Process Parameters	74
6.4.	CONCLUSIONS.....	77
<b>7.</b>	<b>NEW METHODOLOGY TO MEASURE AND CALIBRATE ULTRAFINE PARTICLES EMISSION IN INDUSTRIAL PRILLING TOWERS.....</b>	<b>79</b>
7.1.	INTRODUCTION .....	80
7.2.	MATERIALS AND METHODS .....	81
7.3.	Process Description .....	81
7.4.	Proposed Methodology .....	82
7.5.	RESULTS AND DISCUSSION.....	85
7.5.1.	Data Quality Control.....	85
7.5.2.	Linear Regression Models Generated .....	89
7.5.3.	Application of the model to recommend actions to reduce dust emission .....	96
7.6.	CONCLUSION .....	98
<b>8.</b>	<b>GENERAL CONCLUSIONS AND RECOMMENDATION FOR FUTURE WORKS</b>	<b>100</b>
<b>9.</b>	<b>BIBLIOGRAPHIC REFERENCES.....</b>	<b>102</b>
<b>10.</b>	<b>APPENDIX.....</b>	<b>110</b>
10.1.	Unique ELPI Data Sheet for Impactor 10270.....	110
10.2.	Operating Procedures for ELPI.....	111
10.3.	Perform Leakage Test on ELPI.....	112
10.4.	Perform Zeroing Test on ELPI .....	113

## 1. INTRODUCTION

A clean outdoor and indoor air is considered a basic right by WHO (World Health Organization) once air pollution is ranked among the top risks for mortality and lost years of healthy life, which affects everyone in urban and rural areas and in both developing and developed countries (WHO, 2017).

The human exposure to respirable particulate matter (PM) is correlated with an increase in cardiac and respiratory morbidity and mortality (Dhananjayan, et al., 2019). Studies of the size and composition of atmospheric PM have demonstrated the usefulness of separating them into its fine PM<sub>2.5</sub> (PM with diameter less than 2.5 $\mu$ m) and coarse components (PM with diameter between 10 $\mu$ m and 2.5 $\mu$ m), especially when evaluating the health impact of PM, as worldwide epidemiological studies have shown (Wilson, et al., 2002).

While airborne PM<sub>2.5</sub> is a pollutant that is found in all urban environments and it is predominantly generated by traffic and domestic fuel combustion (Martins & Carrilho da Graca, 2018), an even smaller fraction of PM has raised attention, the ultrafine particles (UFPs).

The UFPs have particle sizes in the range of 0.1 – 2.5 $\mu$ m and can also be agglomerates of UFPs, nanoparticles or nanoclusters (Fahlman, 2007) which are mainly generated in industrial plants (Liou, 2007) and can travel hundreds of kilometers before settling on the ground. They not only get to the lungs while breathing, but also to the blood system, what can cause degenerative brain diseases, as such Alzheimer, Parkinson and Huntington (Maher, et al., 2016) (Win-Shwe & Fujimaki, 2011) to such an extent of concern that WHO works on a new guideline for concentration of particulate matter with a diameter smaller than 1 $\mu$ m (PM<sub>1.0</sub>).

The mineral fertilizer industry, for instance, produced in 2018 around 62 million tons of ammonium nitrate/ calcium ammonium nitrate (AN/CAN) over the world (IFA, 2019). When producing those fertilizers there is emission of ultrafine particles, (UFP) mainly formed in gas phase, no matter which production process is employed. This issue becomes critical when using prilling towers (PT) due to the high flow of air employed (order of thousands of m<sup>3</sup> per hour). Prilling towers are not only used in this segment, but also in food, hygiene, pharmaceutical and other chemical industries (Couper, et al., 2012) what means UFP emission an issue in many areas around industries.

The industries face a challenge to comply with the regulations from the environmental agencies that demand online monitoring of PM although the commercial available online sensors are designed to handle with accuracy up to PM<sub>2.5</sub>, not smaller than this (as the UFPs

are), as extensively discussed by Wilson et al. (2002). Since then, no relevant sensor development was achieved for this size range. On the other hand, the agencies have established standards to calibrate the online sensors with results from gravimetric sampling (GS) (EPA, 2018), which ones can have, for instance for nitrates sampling, up to 50% losses according to Wilson et al. (2002).

There is clearly a technology and methodology gap between the current standards for industrial stationary sources measurement of PM, the continuous monitoring sensors available in the market and the certified methodology in use to calculate the emission of PM containing mainly UFPs as Hoeflinger & Laminger have pointed out when proposing a PM<sub>2.5-0</sub> alternative methodology for evaluating efficiency of equipment for emission control (Hoeflinger & Laminger, 2017).

## **2. OBJECTIVES**

### **2.1. General Objective**

The aim of this work is to investigate which parameters are critical to both provide reliable results from continuous monitoring and reduce emission of UFP, by optimizing the process, and to propose a methodology to calibrate the sensors using an electrical low-pressure cascade impactor.

### **2.2. Specific Objectives**

- Selecting and testing the performance and challenges faced by two distinct commercial continuous PM analyzers, based on the main commercially available techniques, in a mineral fertilizer industrial PT over one year, in Northern Europe.
- Calibrating the sensors installed with several GS measured under different product composition and seasons in Northern Europe.
- Developing a regression model that could correlate both process and meteorological parameters to predict the UFP concentration over the four seasons in the Northern Europe at an industrial stationary source.
- Performing a controlled experiment in the industrial plant to find the most important controllable parameters impacting on dust emission expressing it in the form of a regression model, studying the operating windows to reduce the UFPs concentration at the stack

and finding the best measurement technique of dust emission among online analyzers and electrical low pressure cascade impactor.

- Proposing a new methodology to measure and calibrate the online sensors for the stationary sources containing mainly UFPs and contribute to the knowledge of UFPs continuous monitoring and statistical methods under industrial environment.

### **3. BIBLIOGRAPHIC REVIEW**

Here is presented a general bibliographic review related to the study performed. In order to help understanding the intersectional areas involved on this matter Figure 1 was prepared to show the potential aspects to explore in this research. The approach employed was to consider the prilling tower as volume of control and all the potential parameters impacting on UFPs generation and emission were mapped as highlighted in light gray. On the other hand, the potential options to quantify the UFPs concentration in the stack were analyzed both continuous and batch sampling. Each of the aspects is discussed on the next sections.

#### **3.1. The Process Under Analysis**

The Nitrophosphate process starts with phosphate rock being dissolved in nitric acid (called digestion process). Calcium Nitrate (CN) is produced as a byproduct in the process and sent to a plant where it is used to produce calcium ammonium nitrate fertilizer (CAN) (Hussain, 2012).

After separation of calcium nitrate, the so-called mother liquid is neutralized by addition of ammonia. The N/P ratio is corrected by using nitric acid or ammonium nitrate. The resulting neutralized liquid is called NP-liquor. The water content in the NP-liquor is thereafter decreased by using a shell and tube heat exchanger in combination with cyclone separators working under a decreased pressure. Before the NP-liquor is added to the mixer, small adjustments are made to the NP-ratio by addition of ammonia (NH<sub>3</sub>) gas. The next steps of the process are showed in Figure 2 where the main equipment are the evaporators, mixer, prilling bucket, prilling tower and sieves together with the potential measured parameters (circled in red). Note that liquid, solid and gas streams are illustrated using blue, brown and green arrows, respectively.

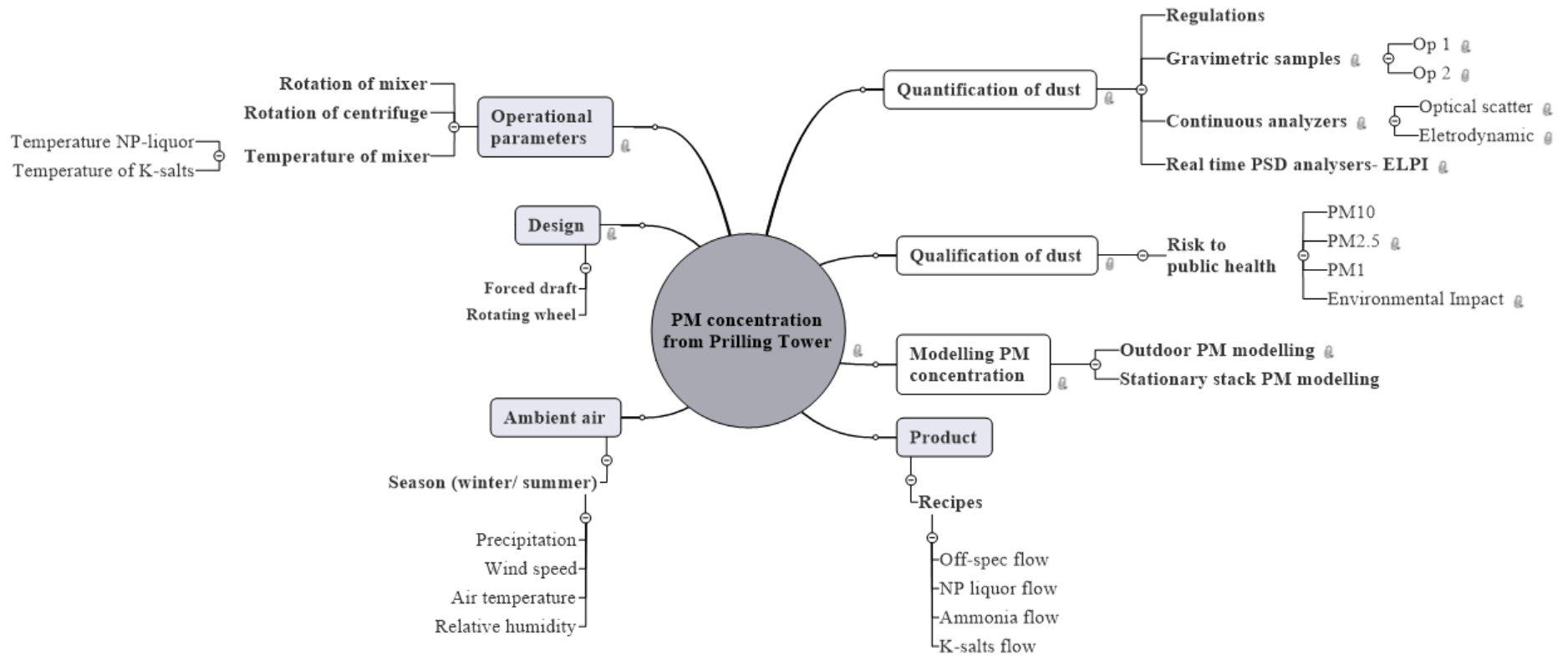


Figure 1 Map of potential aspects to be explored in the research



The pre-processed raw materials (NP-liquor, ammonia, K-salts/minerals) enter the mixer as a three phase (gas, liquid and solid) mixture that needs to be heated and intensively agitated to create a homogeneously mixed melt and to prevent solidification. This melt is thereafter sent to a rotating prilling bucket that sprays the liquid melt into the prilling tower.

The rotational speed (rpm) of both mixer and prilling bucket as well as the temperature of the mixer are measured.

The melt is sprayed from the bucket into a prilling tower, to let the melt solidify and create uniform spherical particles with a diameter of 2-4 mm. The falling liquid is cooled by using ambient air in counter-current flow that is dragged into the PT by using six fans located at the outlet stacks at the top of the tower. The primary emission is the dust or fume of ammonium nitrate from the PT. The material is of submicron size and, therefore, highly visible (Vallero, 2014). The temperature, relative humidity and pressure is measured at the air inlet at the bottom of the tower while the temperature, relative humidity and velocity is measured in the stack.

After solidification, the prills must be classified by particle size on the sieves as can be seen in Figure 2. This process uses several sieves in series that classify the particles in oversized, undersized and the final product. The oversized particles are sent to a crusher and then back to the screening while the undersize particles (called off-spec in Figure 2) are sent back to the mixer together with dust collected from bag filters of other process equipment.

The NPK (Nitrogen – Phosphorus and Potassium) fertilizer product is stored or transported after being cooled and treated. The flowrate of the product and off-spec are measured.

The dust emitted from the stack is composed mainly by small particles that are dragged up by the upward velocity inside the stack and can be the NPK fertilizer itself or can be in the form of ammonium nitrate ( $\text{NH}_4\text{NO}_3$ ) that is produced from a side reaction of the acidic media with ammonia, added in the mixer for keeping the pH stable, as can be seen from the chemical reaction as Equation 1 shows.



Most of the bibliography material related to PT is quite often general, once the specific applications are protected from patents. This is the case, for instance, of NPK prilling towers so few processes related material is available, and this review tries to cover the subject in the best possible way.

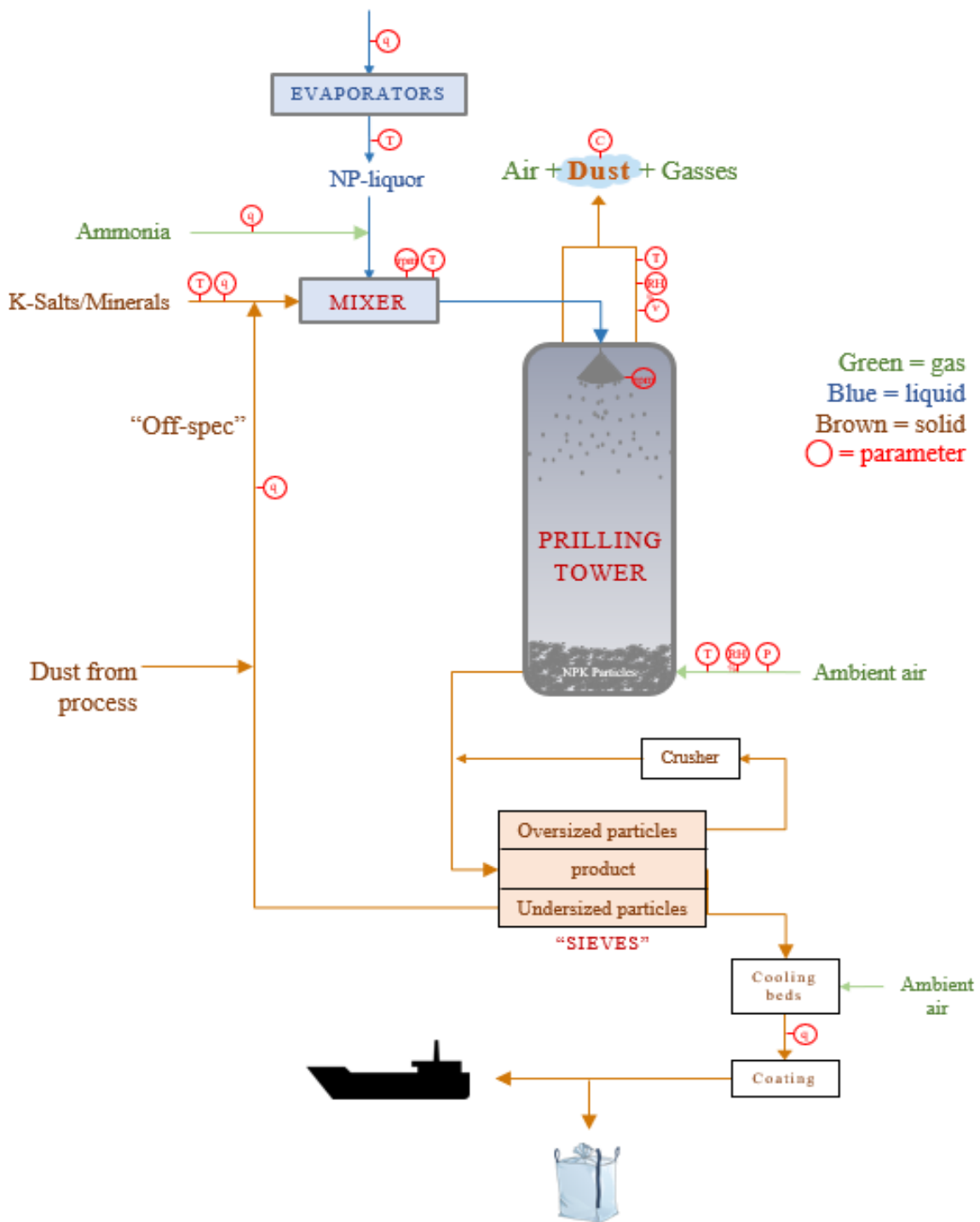


Figure 2 Process flow diagram of NPK prilling process.

PT are also called spray dryers and they are employed mainly to feeds like solutions, pumpable pastes and slurries. Such a material is atomized in a nozzle spray wheel and when in contacted with air solidifies and is removed from the bottom of the tower (Couper, et al., 2012). The authors point at the two main characteristics of spray drying are the short drying time, the

porosity and small, rounded particles of product. Short drying time is an advantage with heat sensitive materials. Porosity and small size are desirable when the material subsequently is to be dissolved (as foods or detergents) or dispersed (as pigments, inks, etc.).

The mean residence time of the gas in a spray dryer is the ratio of vessel volume to the volumetric flow rate, what leads to huge towers to ensure proper cooling of the droplets sprayed. An attempt was made by Yuan et al. (2007) to reduce the height of the PT, where is proposed a combined tower with a fluidized bed so that the height of equipment was greatly decreased, and it exhibited satisfactory performance in industrial application. Besides being promising, to the authors knowledge no further industrial installation was built.

Atomization is key in spray drying and there are three devices of commercial value that can be used which are pressure nozzles, pneumatic nozzles and rotating wheels of various designs. To achieve a suitable range of prill sizes for determined feed, parameters as pressure, nozzle diameter, flow rate and motive pressure for nozzles can be adjusted. While from the design point of view, the geometry and rotation speed of wheels (Couper, et al., 2012).

Spray dryers are capable of large evaporation rates (5 to 7 t/h) and the spherical sprayed particles often are preferable to drum dryer flakes. The completely enclosed operation of spray dryers also is an advantage when strong chemicals are handled, as in the NPK fertilizer application.

The patent from Shirley et al. (1996) describes an improvement in prilling whereby water is atomized into a PT to promote faster solidification of the prills, resulting in a major reduction in air pollution potential in the form of both fume and particulate. Specifically, the invention was related to quick-freezing the outside surface of the prills by flash evaporation of finely atomized water particles on the surface of the prills or in extremely close proximity to the prills to greatly lower the vapor pressure at the prills surface. The potential application could be of value for water sensitive materials, in particular ammonium nitrate, urea, potassium nitrate and other water-soluble melts, which normally absorb water or go into solution readily at ambient conditions in their solid state. This work has emphasized the importance of promoting the quick surface cooling on the droplets to reduce emission of UFPs.

As highlighted in the patent mentioned earlier, the effect of cooling on the generation of UFPs is significant, what turns the attention to the media used to promote this effect which is ambient air without conditioning. Chen et al. (2019), for example, when studying PM<sub>2.5</sub> compositions in coastal areas, originated from ships (up to 35% contribution at port areas) concluded that ships emissions contribution to PM<sub>2.5</sub> exhibited an obviously seasonal variation

with the highest contribution in fall (6.2%), followed by summer (5.4%), spring (3.6%) and winter (1.2%) for the land areas. In general, models for ambient air pollution consider the meteorological parameters. Being the UFPs instable with potential change in both size, mass and composition in different air conditions, it becomes clear the need to include the seasonal factors in the evaluation of UFPs concentration from PT.

In addition to the ambient air seasonal characteristics, the authors Saleh and Barghi (2016) have found that the geometry and design of the air exit configuration had a significant impact on the airflow behavior inside the PT. Besides that, the formation of a quiescent zone near the showerhead was essential in minimizing droplet breakup due to secondary disintegration and fine particle formation. While CFD (Computational Fluid Dynamics) modelling the system, the authors were able to obtain the optimum location for the installation of showerhead. While these authors have used a pilot PT, the presented project here deals with an industrial tower. Anyhow, the explanation of the droplet breakup mechanism can help on identifying the source of the PM emitted at stack and provide recommendation on how to improve the current design.

Besides not employing PT, the authors Ji et al. (2017) when studying the influence of raw materials (RM) on the characteristics of PM<sub>2.5</sub> and measuring it to reduce emissions used four different sources of RM on steelworks in their investigation. The results showed that a well positive correlation existed between the emission concentration of K (potassium) and Cl (Chloride), and their contents in raw materials, what can be also explored in prilling towers once under production of different NPK, there are different amounts of K (potassium) source needed.

### **3.2. Techniques for Continuous PM Concentration Monitoring**

There is very broad and consolidated research regarding PM measurement techniques (Sullivan, et al., 2018) (Giechaskiel, et al., 2014) (Liou, 2007) so here the main focus will be given to commercial available sensors, especially the ones able to provide continuous or semi continuous results due to the objectives stated before, mainly related to potential industrial application.

Instruments that for decades were standard equipment in focus areas as vehicles emission for engine test cells, such as smoke meters and opacity meters, have become obsolete over a rather short time span, unable to provide the sensitivity required by the new standards (Giechaskiel, et al., 2014). In addition, in the fertilizer's industry, where the best available

technique (BAT) mentions emission levels of  $5\text{mg}/\text{Nm}^3$  for NPK production (COM, 2007) with almost 90% of the PM below  $1\mu\text{m}$ , well established principles do not meet the standards required. Furthermore, high time resolution measurement (seconds or less) has become a necessity to understand particles formation and to develop control and aftertreatment strategies (Giechaskiel, et al., 2014).

The physical and chemical properties of exhaust aerosol continuously change after their formation, both along the exhaust system and after emission into the atmosphere. A rather rapid change occurs as exhaust exits the tailpipe and abruptly dilutes and cools in the ambient air. These changes have created a demand for new instruments that are capable of real time measurement and enhanced sensitivity (Giechaskiel, et al., 2014), (Liou, 2007).

The current research focus is on newly evolving instrumentation, including scattering, absorption and instruments based on the electrical detection of exhaust aerosols. Meanwhile GS is still the general standard to calibrate those instruments.

GS is performed by collecting particles onto a filter. The emission rate is then calculated by weighing the filter before and after the test. The filter collects all particle size fractions (nucleation, accumulation and coarse modes). The collection method also provides an operational definition of PM, as the material mass collected on a filter. Conventional filters are made of glass fibers and an inter-coating (e.g. Polytetrafluoroethylene PTFE) protects the surface from chemical reactions. Filter measurements are affected by vapor adsorption on substrates, by evaporative losses during or after sampling and by reactions between collected particles as nitrates and sulphates. Filter handling and loss of material from the filter surface can also play an important role, particularly for quartz fiber filters. The conditioning of the filter in the weighing room can also affect the final result by a few  $\mu\text{g}$ . For this reason, filters are typically conditioned under controlled relative humidity and temperature conditions. The effect of the ambient air pressure is considered with a buoyancy correction. For process with modern aftertreatment technologies or emission close to BAT levels, the gravimetric method is reaching its detection limits. At the lowest emissions levels, the artifacts and measurement uncertainties discussed above can contribute more than 90% of the recorded mass increase (Giechaskiel, et al., 2014). The lack of sensitivity of the gravimetric method has been one prime reason for looking into alternative detection techniques.

Table 1 shows one example of a guide where the continuous measurement technology available is related to parameters to help the user on selecting the most adequate principle for a defined application. The supplier here mentioned PCME (2018) offers three different

principles: probe electrification, transmissometry and scattered light. Those principles are offered by different suppliers as Sick (2020) and Palas (2020), for example. A set of parameters is presented, based on regulations applicable, process and PM characteristics to help end users on the selection.

Even though it looks straight forward, the list presented on Table 1 is not complete as (Giechaskiel, et al., 2014) discuss. The authors summarized the main criteria to select the equipment to measure PM concentration. These include representativeness (emissions as they would be in real world dilution and aging conditions), accuracy (uncertainties include random error and systematic error), detection limit, traceability (international standards or basic physical constants or properties), robustness (a method continues to function despite the existence of faults in its subsystems or component parts), user friendliness and cost (capital and maintenance).

The main principles on which the commercially available instruments are based are discussed in the following next.

### **3.2.1. Optical detection methods**

The study and applications of optical methods have been enormously simplified and extended with the availability of reliable laser sources over a wide range of wavelengths (Glatter, 2018) (Giechaskiel, et al., 2014) (Liou, 2007). (Wu & Chu, 2000).

In optical detection methods, the interaction of aerosol particles with incident light serves as basis for real time measurement of particle concentration. Aerosol particles illuminated by a beam of light reradiate it in all directions (scattering) and simultaneously transform part of it into other forms of energy called absorption and extinction (Babick, 2020) (Sullivan, et al., 2018) (Giechaskiel, et al., 2014) (Wu & Chu, 2000). Some of this modified light is collected at a receiver, usually placed very close to the transmitter, and often using the same optical device as illustrated on Figure 3. The return signal light is then analyzed to derive information about the target. Some of the applications areas of light sensing are meteorology, atmospheric measurement, chemical species and pollutants, gas detection and space-borne measurements as clouds and global wind field (Vaughan, 2002). Optical detection can be used to measure PM concentration although the main application is still particle size distribution determination (PSD).

Table 1 Guide to application parameters for technologies

Measurement Technology	Technology	Stack Diameter (m)	Concentration (mg/m <sup>3</sup> )		Filter Type	Certification		Dry	Humid	Wet	ATEX IECEx Hazardous Zone		Type of Dust		Velocity Dependant	
			Min	Max		EU	USA				Gas	Dust	Same	Changing		
Probe Electrification	Charge Induction (AC)	PCME ElectroDynamic™	0.2 - 4	0.05	1000	Bag, Cyclone, Drier, Scrubber <sup>(5)</sup> None <sup>(8)</sup>	QAL1 TUV MCERTS <sup>(7)</sup>	MACT, PM detector	✓	✓	x	✓ <sup>(7)</sup>	✓	✓	x	No <sup>(8)</sup>
	Contact Charge Transfer (DC)	DC Triboelectric	0.2 - 2	1	1000	Bag, Cyclone	x	MACT	✓	x	x	?	✓	✓	x	Yes
	Combination AC & DC	Combination AC & DC/Tribo	0.2 - 2	1	1000	Bag, Cyclone	TUV	MACT	✓	x	x	✓	✓	✓	x	Yes
Transmissometry	Radiometric Opacity	PCME DynamicOpacity™	1 - 8 (PCME VESTA 500 HRC) 1 - 15 (PCME STACK 602)	10 <sup>(3)</sup>	1000	Bag <sup>(1)</sup> , Cyclone, EP, None	TUV	PM detector	✓	x	x	x	x	✓	x	No
		Dynamic Detection Principle	0.5 - 12	20	1000	Bag <sup>(1)</sup> , Cyclone, EP, None	x	x	✓	x	x	x	x	✓	x	No
	Opacity	PCME Opacity	2 - 10 <sup>(1)</sup>	30 <sup>(4)</sup>	1000	EP, None	TUV	PS-1	✓	x	x	✓	✓	✓	x	No
		Other Transmittance	0.5 - 12	30	10000	EP, None	TUV	PS-1	✓	x	x	✓	✓	✓	x	No
Scattered Light	Scattered Light (Forward)	PCME ProScatter™	1 - 4 <sup>(2)</sup>	0.02	300 <sup>(10)</sup>	Bag, Cyclone, EP, none	QAL1 TUV MCERTS	PS-11, PM detector	✓	x	✓ <sup>(9)</sup>	POA <sup>(7)</sup>	POA <sup>(7)</sup>	✓	x	No
		Other Forward Scatter	1 - 3 <sup>(2)</sup>	0.1	200 <sup>(10)</sup>	Bag, Cyclone, EP, none	QAL1 TUV MCERTS	PM detector	✓	x	✓ <sup>(9)</sup>	✓	✓	✓	x	No
	Scattered Light (Back/Side)	Back/Side Scatter	1 - 4 <sup>(1)(2)</sup>	25	500 <sup>(10)</sup>	Bag <sup>(1)</sup> , Cyclone, EP, none	TUV	PM detector	✓	x	x	?	?	✓	x	No
		PCME ProScatter™ /Backscatter	2 - 10	10	500	Bag <sup>(1)</sup> , Cyclone, EP, none	x	PM detector	✓	x	x	x	x	✓	x	No

- Notes:**
- (1) Concentration dependant
  - (2) Repeatable Flow dependant
  - (3) Application specific
  - (4) Stack diameter dependant
  - (5) No water droplets
  - (6) No filter - not advised
  - (7) Model specific
  - (8) Velocity range 8-20m/sec
  - (9) Using Wet Stack monitor
  - (10) Must have constant clean air purge supply 24/7

The above statements are for guidance only and fulfill the majority of application parameters, however, the actual stack conditions will dictate suitability, therefore, a Site Survey Form should always be undertaken to confirm suitability. If in doubt ask PCME Ltd for advice.

Source: adapted from (PCME, 2018)

Light absorption is mainly used in atmospheric studies related to climate change, due to fact of greenhouse pollutants strongly absorbs light. The most common techniques for measuring aerosol absorption are the difference method, where absorption is derived from the difference between extinction and scattering, the filter based methods that measure the light attenuation by PM collected on a filter, and photoacoustic spectroscopy and Laser Induced Incandescence, which measure PM concentration via the heat particles gain as they absorb light. (Glatter, 2018) (Giechaskiel, et al., 2014).

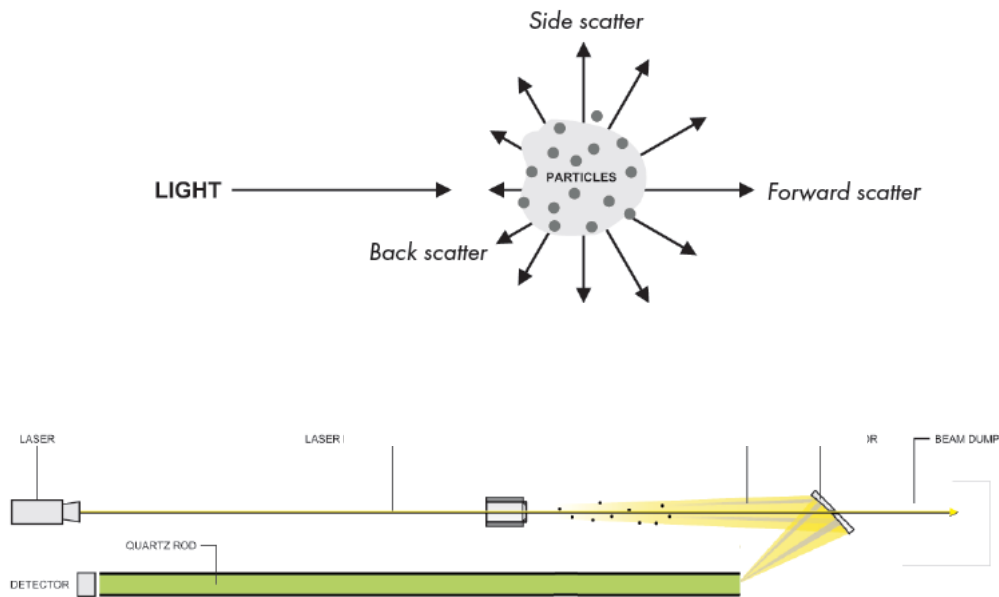


Figure 3 Optical Scatter Principle and application example.

Source: Adapted from PCME (2019)

The Opacity meter measures the fraction of light transmitted through a given exhaust volume (path). Light extinction (also referred to as opacity or smoke opacity) by absorption and scattering is the difference between incident and transmitted light. Extinction based measurements quantify particle concentrations via the Beer–Lambert–Bouguer law, where the ratio of transmitted to incident light intensity is an exponential function of the path length and the extinction coefficient. Opacity depends on particle size and light wavelength, as well as particle shape and composition. This is difficult to estimate theoretically for most particles in the real world (Giechaskiel, et al., 2014).

Two types of opacity meters are common: sampling opacity meters, which sample a fraction of the exhaust flow through a measuring chamber and inline opacity meters, which do not have a separate measuring chamber, but send a light beam to a microphone detector. In the last one, some new features as sampling pumps to have constant flow and heated windows to protect the optical components have improved the accuracy of the opacimeters (Glatter, 2018).



Light scattering (Figure 3), has seen considerable application in particle size and concentration measurement, e.g. for soot in flames, incinerators and cement plants. The light scattering pattern and intensity are strongly dependent on the ratio of the particle size to the wavelength of incident light. For very small particles compared to the wavelength, particles act as dipoles, therefore scattering is symmetrical in the forward and backward directions, and the scattering intensity is independent of particle shape. This defines the Rayleigh scattering regime. In the case of non-spherical particles, the radius must be replaced by a “characteristic length” of the particle. As particle size approaches the wavelength of light the Mie scattering regime is entered. The formulas in this regime are rather complex and cannot be calculated in closed form. The scattering intensity of particles much larger than the wavelength is proportional to the square of the particle size (Wu & Chu, 2000).

For particles in the size range of some hundred nanometers up to several micrometers perfectly fit into the accessible range of a light scattering; this makes a detailed structural analysis possible. However, one is confronted with two main difficulties: one must use Lorenz–Mie theory, and the situation is often complicated by multiple scattering. In these cases, a low-resolution shape analysis is possible for monodisperse systems. Polydisperse systems can be analyzed in terms of size distributions of spheres by using Lorenz–Mie theory. High-quality experimental data allow the determination of this value from the measured data during size analysis. Multiple scattering contributions can be reduced by contrast matching, or by special experimental set-ups like thin, flat cells. May lead to sharp resonant scattering (Glatter, 2018). Due to the high scattering power of these large particles one runs into the problem of multiple scattering with increasing concentration much earlier, before one can see the influence of excluded volume effects. If the particles are larger than several micrometers, then the regime is Fraunhofer diffraction, which probes only the silhouette of the particles. The original work of Lorenz and Mie related to spherical particles only, but these names are now often used for arbitrarily shaped scattered light in this size. This theory describes the propagation of electromagnetic radiation in an inhomogeneous dielectric medium and considers that the interaction of the electric field with the inhomogeneities becomes more complicated. We can no longer assume that the electric field strength is the same everywhere in the probe volume. Currently there are at least modern numerical algorithms that allow computation of the scattering problem for simple regular particles like spheres and prolate and oblate ellipsoids, and cylinders (Glatter, 2018).

As discussed, the particle shape is a drawback of light scattering and many approaches have been developed for the calculation of light scattering by non-spherical particles and broad range of PSD because of the need for precise scattering information in optics, geophysics, remote sensing, astrophysics, engineering, medicine, and biology (Glatter, 2018), (Liou, 2007).

Light scattering can be classified in either static or dynamic. Static light scattering occurs in which the angular dependence of the time-averaged scattering intensity is measured while in a dynamic light scattering experiment the time-dependence of the scattered light at a fixed scattering angle is measured. These time dependent fluctuations correlate with the displacement of the scattering centers due to diffusion processes (Brownian motion), or due to intra-molecular mobilities.

In static scattering experiments that are primarily diluted systems, where the scattering centers are fixed in a single particle, so the relative distances of the scattering centers are fixed in time. Many systems in the size range between 100 nm and several micrometers, like emulsions, show a distinct polydispersity in size, and one can hardly find strictly monodisperse particles in practical applications. When assuming a certain shape, like spheres for emulsions — one is interested in a determination of the size distribution. However, there is a difficulty: of combining the Lorenz-Mie theory with multiple scattering (Glatter, 2018).

The situation is quite different for dynamic light scattering what is a method of studying dynamics in a system, in most cases translational diffusion dynamics. The technique is primarily used for particle sizing and can be applied in a wide size range, from nanometer up to micrometers, but it is a low-resolution technique (Bras & Hammel, 2019). Moreover, Babick (2020) points out at when dynamic light scattering is used to quantify the properties of individual particles, the sample should be properly diluted to exclude any impact of particle concentration. There are several sources of such impacts, which depend on the particulate phase (size, shape, and optical and interfacial properties) and instrumentation (wavelength and scattering angle). For practical reasons, it is not possible to completely avoid the occurrence of these effects (Babick, 2020).

For practical industrial applications two kinds of instruments exist: light scattering by an ensemble of particles as scattering photometers, which measure the scattered light intensity at one or more angles and light scattering by single particles represented commonly by the Optical Particle Counter (OPC). A special category of the last one is the Condensation Particle Counter (CPC), where the particles are grown by condensation to optically detectable sizes.

### **3.2.1.1 Scattering photometer**

Light scattering photometers measure the combined light scattered from all particles present in the optical sensing volume typically at angles centered at 90°, 45°, or less than 30°. Most commercial light scattering instruments use visible light, e.g., 600 nm. Light scattering instruments have sufficient sensitivity to detect particle emissions from for example, relatively low emitting vehicles. However, their responses are dominated by large particles and therefore, are strongly dependent on particle size distribution. One can calibrate the instrument response to particle mass, but this is sensitive to deviations in particle size and composition from that of the calibration aerosol. (Bras & Hammel, 2019).

### **3.2.1.2 Optical particle counter (OPC)**

OPCs are similar to photometers. The major difference is that the OPC optical sensing volume, formed by the intersection of a focused light beam with a narrow particle beam, is much smaller so that only one particle is illuminated at a time. The scattered light is detected by a photo detector as an electrical pulse. The pulse height depends on particle properties (size, refractive index and morphology). A disadvantage of OPCs is that uncertainty in refractive index often leads to significant variability in derived size distributions, even for the ideal case of homogeneous spherical aerosol particles (Liou, 2007) (Galvão, et al., 2018).

### **3.2.1.3 Condensation Particle Counters (CPCs)**

CPCs use light scattering to count particles after they are grown to micron size. The three types of CPCs, depending on the method that is used to achieve supersaturation and particle growth, utilize either adiabatic expansion of the aerosol–vapor mixture, or conductive cooling, or mixing of cool and warm saturated air, but only limited use of this type of CPCs has been reported (Giechaskiel, et al., 2014).

### **3.2.2. Probe electrification**

The ability of particles to acquire electrical charge provides the opportunity to design simple, low cost, sensitive PM sensors. A number of processes can contribute to the charging of aerosol particles: static electrification, thermionic emission, photoemission, and charging by small ions. The electrical charge acquired by a particle from static electrification is difficult to predict thus no instruments are based on this technique. Likewise, there are no thermionic based instruments used for exhaust PM emissions (Giechaskiel, et al., 2014).

Charging by small ions is a technique that has been used to characterize ambient aerosols and vehicle exhaust aerosols. On a Diffusion Charger (DC) the ions, usually from a corona discharge, attach to particles and an electrometer registers a current proportional to the number of particles times the average charge per particle. Theoretically, the measured current is proportional to particle diameter squared in the free molecular regime and proportional to particle diameter in the continuum regime. Experimentally, for the size range of interest, which lies in the transition regime, an exponent of 1–1.4 to particle mobility diameter is found. (Giechaskiel, et al., 2014) This varies with the charging area design and with particle losses at and downstream of the charging area. If entering particles are already charged with the same polarity as the corona, they can exhibit higher apparent charging efficiency than expected, by up to 30%. Aerosol detection based on diffusion charging offers fast response (1 s), very good sensitivity, simplicity, repeatability, and a wide dynamic range (Sullivan, et al., 2018). Diffusion chargers (DC) have a strong potential to be used alone to measure relative changes in particle emissions or in combination with other instruments to provide additional information on particle properties, such as the mean diameter when combined with a CPC. This instrument combination was designed for ambient ultrafine particle measurement and an applicability to other systems like diluted engine exhaust needs further investigation (Giechaskiel, et al., 2014).

An example of application of electrodynamic diffusion charger (EDA) is showed on Figure 4. EDA stably traps charged aerosol particles by balancing the aerosol particle in an electric field. This stable trap requires a feedback loop between the potential applied to the electrodes and the position of the particle, which is sensitive to changes in mass. The electric field strength required to stably trap the particle thus provides an accurate real-time measurement of the mass of the particle if the charge state is known.

The particles studied in the EDA range are typically greater than 10  $\mu\text{m}$  in diameter, and the trap can be easily loaded using an ink-jet nozzle to dispense droplets. As the trapping capabilities of the EDA do not depend on particle shape, and thus the EDA is not restricted to spherical particles as is the traditional optical detection methods. This makes the EDA ideal for phase transition experiments, such as salt efflorescence and the freezing of water, because crystalline particles are readily trapped (Sullivan, et al., 2018).

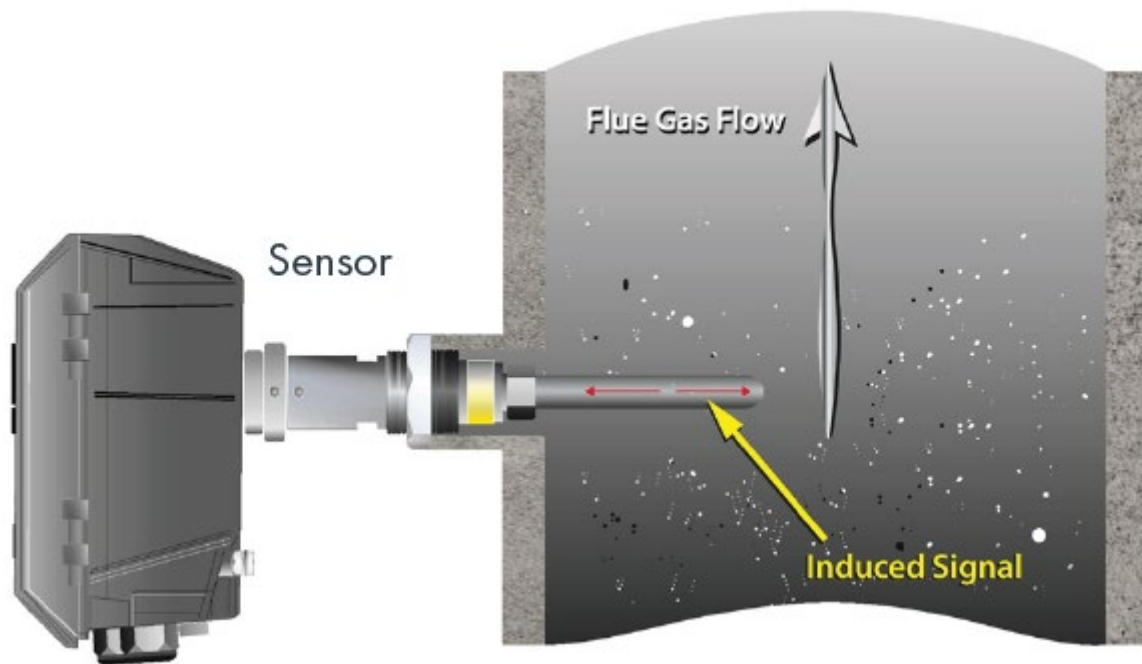


Figure 4 Example of electrodynamic diffusion charger. Source:  
adapted from (PCME, 2019)

A case study performed by PCME (2018) provides a comparison of results for monitoring the same stack with an EDA instrument and an optical forward scatter installed at outlet of a bag filter from an incinerator. The author concluded that both instruments track short-term variations in dust levels associated with bag cleaning in a similar fashion. Besides that, instruments have dissimilar results during plant stop and start up when there are water condensation issues. This issue appears to be related to the different effects of water vapor on both instruments.

### 3.2.3. Electrical low-pressure cascade impactor

As presented above, all techniques presented to measure PM concentration at the stack have their results affected by the particles properties, as the shape for optical measurements and the charging properties to electrodynamic DC. Because of this, it was raised the need for instruments to be able to provide more information regarding the particle as PSD over time and its chemical properties.

From the commercial available continuous monitoring instruments, it can be seen they are based on two principles, OPC already discussed in item 3.2.1 and electrical low-pressure impactor (ELPI).

Low-pressure impactors (LPI) have been introduced to measure nanosized particles (Brachert, et al., 2014). In cascade low-pressure impactors, the pressure is reduced either by having a separate pressure-reducing stage or by gradually reducing the pressures by using high jet velocities as shown in Figure 5.

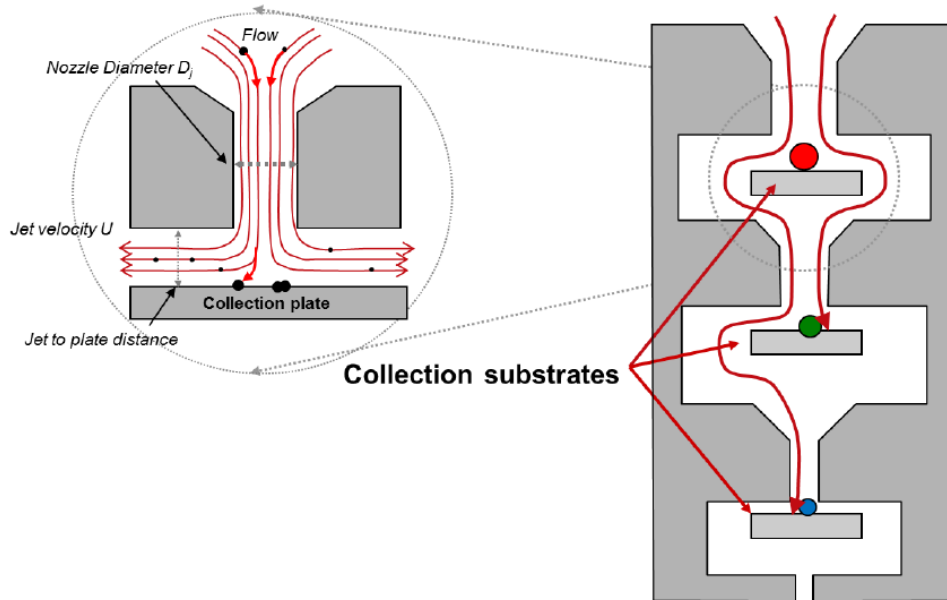


Figure 5 Cascade impactor operation principle. Source: adapted from Dekati (2011)

To make LPI measurements in real-time and to improve the sensitivity, Keskinen et al. (1992) developed the electrical low-pressure impactor (ELPI) to achieve real-time operation of a low-pressure cascade impactor. According to the authors, a multichannel electrometer is constructed using low cost monolithic electrometer amplifiers. The zero-check technique is applied to achieve a lowest detectable current of  $10 \times 10^{-15} \text{A}$ .

In the ELPI, the aerosol is sampled through a unipolar corona charger as presented on Figure 6. The charged particles then pass into a low-pressure cascade impactor consisting of electrically isolated collection stages (13 impactor stages and one filter stage). As particles impact on a specific stage, they produce an electrical current that is recorded in real-time by an electrometer. Particles below the lowest cut diameter are collected by a filter stage enclosed in an isolated Faraday cage. The ELPI impactor classifies particles according to their aerodynamic diameter, from  $10 \mu\text{m}$  to  $6 \text{nm}$ . The concentration measurement is based on calibration of the corona discharge for charging efficiency, impactor collection efficiency, and current measurement. The charging probability is calibrated against mobility equivalent diameter. (Dekati, 2020).

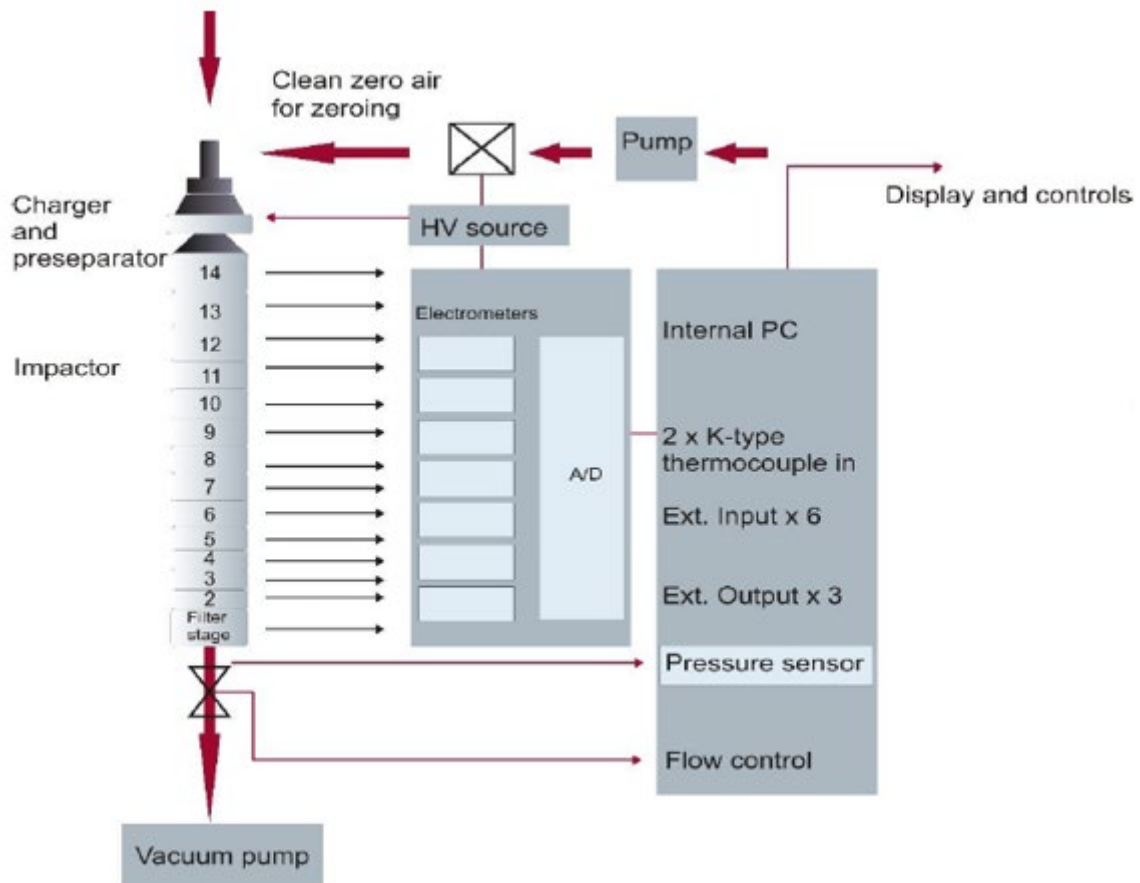


Figure 6 ELPI instrument schematic. Source: adapted from Dekati (2011).

To reconcile the mobility-based charging efficiency with the aerodynamic size measurement, as well as to determine PM mass, the effective density of the particles needs to be known or estimated. ELPI is used quite often for research in engine tests beds and generally, the agreement with the PM mass is within 10% for non-diesel fueled vehicles. At low emission levels the agreement is not so good due to the filter artifact. With other instruments the agreement at low levels (e.g. 0.3 mg/m<sup>3</sup>) is better than 10–20%. The combination of aerodynamic and mobility size data is used to estimate particle effective density and, thereby, enable conversion of the impactor data into a real time mass concentration. The agreement with gravimetric PM mass can be quite good (within 20%) if the instrument is kept clean and not overloaded with high PM concentrations. (Giechaskiel, et al., 2014)

The calibration of the ELPI is based on the realistic shape of particle collection efficiency curves. To ensure that a used impactor is performing in the same aerodynamic range allowed for new impactors, one must also satisfy the other, secondary factors of cascade impaction aerodynamics, most notably the distance to the collection surface relative to the nozzle diameter. Muller et al. (2012) states that the performance of a cascade impactor is

difficult to define because it includes the number of the measurement channels per order of magnitude in the size axis, the time response, the shape of the kernel functions, and the sensitivity of the instrument.

Arffman et al. (2014) investigated the performance mainly from the perspective of distinguishing both modes of bimodal size distributions and determining the lower limit at which the relevant information from a size distribution can still be resolved. Results of the instruments were consistent by taking into account that soot particles have fractal structure. It is important to highlight that the performance of the ELPI has been evaluated using monodisperse aerosols. The good agreement between the two measured size distributions shows the capability of the ELPI for near real-time particle size measurements.

Dong et al. (2004) studied the inversion processing of cascade impactor data to construe continuous size distributions within fine particulate matter (PM<sub>2.5</sub>) is examined for residential oil furnace and fireplace appliance emissions. The oil furnace aerosol offers an opportunity to apply data inversion to study a bimodal lognormal distribution in which much of the aerosol mass is impactor-penetrating nanoparticles (< 30 nm). The fireplace emissions on the other hand cover the issue of a chemical size distribution, which is subject to particle loss and characterized by a single lognormal, accumulation mode peak. Raw cascade impactor data was inverted with the knowledge of individual stage collection efficiencies to create a continuous and complete particle size distribution.

The ELPI present losses of fine particles. Those were calculated by Virtanen et al. (2001) considering three different loss mechanisms: diffusion, space charge, and image charge deposition. Diffusion losses were determined experimentally in particle size range of 10 μm to 400 nm. The measured values varied from 0.1 to 6% depending on particle size and impactor stage. In the measurement range of the instrument, i.e. above 30 nm, the losses were below 2%. Image charge losses exceeded the diffusion losses when particle size was larger than 200 nm, but the combined loss in this size range was below 0.5%. Space charge losses were determined both experimentally and through calculations. The space-charge effect was found to be a dominant loss mechanism in ELPI when measured concentrations were high.

ELPI has being used in the field of droplets formation in wet flue gas cleaning process, sometimes coupled with a FTIR as mentioned by Mertens et al. (2014) when studying sulfuric acid droplets formation in an amine absorption column or either coupled with the condensation particle counter from Palas (2020) in the investigation of sulfuric acid aerosol on a wet flue gas scrubber as discussed by Brachert et al. (2014). These authors concluded that the condensation



particle counter provides information about the number concentration while with the ELPI also the size evaluation is possible. Both measurement methods revealed number concentrations above  $10^8 \text{ cm}^{-3}$  under well-controlled conditions in a pilot plant and the good conformance of the both methods are shown. In case of the ELPI, the overestimation of number concentration has been observed as well when measuring very small sizes with the ELPI. Consequently, for smaller sulfuric acid concentrations the number concentration can only be measured with the CPC as the ELPI have overestimated it by a factor of 2–5 times.

### **3.3. Statistical Modeling Applied to Experimental Investigations**

Statistical modeling helps in understanding the variables responses in experimental investigations among many engineering related areas. Govaerts et al. (2020) explains that an established scientific approach consists of first defining a statistical model. This model aims to describe the system of interest using a simple mathematical equation containing one or more random terms, which account for experimental and measurement errors or natural variation between subjects. Once the model is defined, it is then fitted to a set of process data collected according to a given experimental design. Finally, the fitted model is used to answer the questions of interest.

The family of linear models includes simple linear model (LRM), used for example in calibration models, single variable polynomial model, multiple regression model, response surface model (RSM), analyses of variance (ANOVA) and its related approaches furthermore analysis of covariance model. These models share three common characteristics, the response  $Y$  explained by the model is always assumed to be observed on a quantitative continuous scale, the expression of the model equation is a sum of parameters multiplied by the values of some predictors of interest in the study and the last term added to the model is an error term  $e$ , which accounts for some or all of the random components of the process of interest. The word linear does not mean that the systematic part of the model has a linear shape. For example, the response surface model has a nonlinear shape but is a linear statistical model because it is expressed as a linear function: a sum parameter multiplied by transformations of the factors of interest ( $X_2$  and  $X_1X_2$  as an example).

Linear models are mostly used in experimental studies, i.e. studies where data are intentionally generated from a given process (analytical, experimental or industrial) in order to answer a specific scientific question. Ideally, these data are generated based on an experimental design to guarantee that they will contain the information targeted by the study and have a

balanced structure. Data used to develop linear models can also come from an observational study, where data are not produced for a given purpose, but are rather collected from a process or in a certain context. Such data often present a high degree of collinearity between predictors; contain very influential observations and outliers that are badly spread in the domain of the factors of interest.

In this context, the linear model family is certainly the most used model because of its ease of implementation and versatility. Understanding how to express the random part of the process is also of the utmost importance in contexts where one is involved or must be able to accurately quantify the uncertainty of measurement systems, as the inclusion of the constant term in the LRM to ensure the random effects are taken into account.

The main statistical indicators used to evaluate the model result are coefficient S (standard error in the regression) measured in absolute numbers and complementary to that r-squared which is the percentage of response variation explained by a linear model.

The significance of parameters which is given by p-value, based on the hypothesis of at least 95%, e.g., of the data set can be explained by the model proposed ( $p\text{-value} \leq 0.05$  in this example), residual (or lack-of-fit) equivalent to the vertical distance between a data point and the regression line being employed to evaluate how close is the fit of the linear model to the dataset and if their distribution is random (residuals are distributed evenly along positive and negative values) what means there is only error left in the model (Sarabia, et al., 2020) (Benyounis, 2019).

The decision to move from a simple linear model to RSM according to Sarabia et al. (2020) is due to the fact that the model relating some controllable variables with a response either is not available or is very complex, so a collection of mathematical and statistical techniques can help analyzing, by an empirical model.

Usually, the full model consists of insignificant model terms that need to be eliminated, such as terms that have p-value greater than the level of significance specified. This elimination can be done manually or automatically. The three automatic procedures of evaluating all possible selection of variables are forward selection procedure where the procedure begins with only the constant term, and the first variable added is the one with the highest simple correlation with response Y. If the regression coefficient of this variable is significant it will remain in the equation and a new search for the second variable with highest correlation with the response is begin, after Y has been adjusted for the effect of the first variable and the significance of the regression coefficient of the second variable is then tested. The second method is by backward

elimination procedure: in this procedure, full equation is fitted and sequentially eliminates one variable each time. The variable with the smallest contribution to the reduction of error is eliminated first, and so on. The last procedure is stepwise regression where the possibility of eliminating a variable that might be added in earlier stage, as in backward procedure, is considered. This procedure has the advantage of assuming different or similar levels of significance for inclusion or deletion of variables from the regression equation (Benyounis, 2019).

Allegrini and Olivieri (2020) explain that some alternative methodologies have been developed to handle nonlinearities, such as polynomial functions and kernel-partial least squares. The most powerful and flexible in this regard is the use of artificial neural networks (ANN), which have also been applied in multivariate calibration.

Artificial neural networks are mathematical models inspired in the way the human brain is supposed to work. Indeed, the ANN nomenclature reminds biological units such as neurons, and biological processes such as neuron activation, interneuron connections, etc. However, in the analytical multivariate calibration context, ANNs are useful tools employed to model nonlinear relationships between multivariate signals (e.g., spectra) and one or more analyte concentrations or sample properties as targets. In this context, they can be viewed as nothing else than calibration models with several adjustable parameters, which are able to universally fit nonlinear relations between targets and instrumental responses.

For solid or semisolid materials where the component concentrations may be far from the linear range when using NIR (near infrared spectra), or when calibrating for a global sample property, such as organoleptic aspects, octane number in gasoline, consumer acceptance of industrial or food products, etc., deviations from the linearity in the signal-target relationship may be found and ANN are often chosen to address this challenge. Model interpretability remains an active research area for the neural network community, once the key operating unit of an ANN is the neuron. Independently of its biological meaning, in multivariate calibration problems a neuron is a function receiving an input and generating an output through a suitable mathematical expression. A typical ANN setup or “architecture” contains three layers of neurons: input, hidden and output. The input layer serves to accommodate the variables, either real or latent; the variables from the input layer are first linearly combined, and then become the input for the hidden layer. The coefficients of the linear combination are adjustable parameters called “weights,” one for each input variable. The weighted average value activates the nonlinear function of each of the hidden neurons, yielding an output that is transmitted to

the output layer. From the modeling standpoint, optimizing a neural network means to find the value of the weights resulting in the best input–output modeling from the experimental data.

Setting the weights based on training data and the desired output is the central problem in neural networks implementation. The back-propagation algorithm is the most often used method for training, due to its relative simplicity and wide applicability. The goal of back-propagation is to iteratively change the weights in a manner that minimizes the error, defined as the squared difference between nominal and network output values for all training objects. Given a set of training samples with known nominal concentration values, back-propagation may continue until the error approaches zero. This carries the risk of overfitting the data that is, modeling the noise as well as the signal-target relationship. In this sense, the application of ANN for calibration against well-defined standards is suitable while when modelling process parameters, a good model fit not necessarily will help to understand the relation between parameters and the response.

The result of a web search in science direct (Elsevier, 2020) from 2019 shows that methodologies here presented are widely applied, but mainly in experiments in both laboratory and pilot scale while few of them deal with industrial final use application, only Saleem et al. (2019) when studying levels of disinfection by products in aquatic centers published a work on this field. The authors have employed LRM (linear regression model) which was also the choice for Mohtashami & Shang (2019) in wastewater painting treatment and Gonzalez-Soto et al. (2019) while studying exposure to different sized polystyrene in mussels.

Response surface methodology (RSM) has been applied by Tonday & Tigga (2019) in electrical discharge machinery, Boulila et al. (2019) on manufacturing of gas turbines, Kahraman et al. (2019) for grinding wheel, Changra & Bhattacharya (2019) when studying pyrolysis of biochar, Heydari et al. (2019) evaluating electrodes nanostructure, Lee et al. (2019) and Su et al. (2019) for clean technologies in biodiesel production, Balamurugan et al. (2019) for waterjet cutting of abrasives, Parida & Maity (2019) machining parameter for flank wear, Ozturk et al. (2019) when grinding flat glass and Singh et al. (2019) for rotary soil tillage operation.

Analyses of variance (ANOVA) was employed by Fernandez-Lopez et al. (2019) for heavy metal bio removal while Kavimani et al. (2019) for graphene process production, Ramesh et al. (2019) when improving stability of impact dampers and Muaz & Choudhury (2019) for milling process and Sivaiah & Chakradhar (2019) for manufacturing process in machining of 17-4 PH stainless steel.

The artificial neural network method was employed by Ghimire et al. (2019) when modelling meteorological parameters and Alizadeh & Omrani (2019) for CO<sub>2</sub> cutting.

In research related to PM emission Padoan et al. (2017) employed LRM for road dust emissions while Moser et al. (2017) for aerosol emission on post combustion pilot plant have applied ANOVA.

#### 4. GENERAL MATERIALS AND METHODS

The experimental tests in this project research were performed in a fertilizer unit, which produces mainly AN based fertilizers employing a prilling tower. The air is dragged in the PT by six fans, each one located at a single stack as schematic showed in Figure 7.

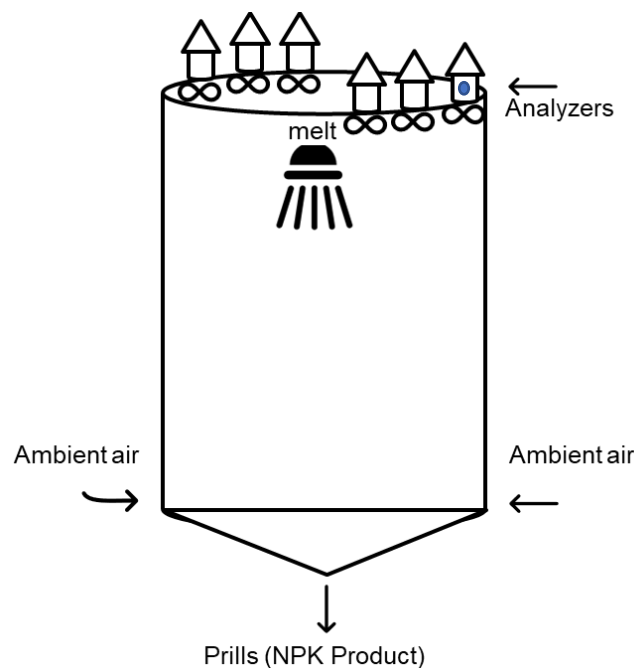


Figure 7 Schematic of airflow in the PT

The six exhaust fans had the same capacity and there was no frequency inverter installed, so for the entire period they were running at same rotational speed. All the tests were performed in the stack number 3. The stacks had the same diameter of 1700mm.

The test rig was assembled as shown in Figure 8 where (a) shows the continuous PM concentration monitoring employing optical scattering (here called OSA) and a second one employing electrodynamic DC (called here EDA) mounted at the same height of the stack but with angle 0° and 180°, respectively and (b) shows the probe for GS and ELPI. The sampling point employed was located on a level 600mm higher than the continuous instruments (OSA and EDA) as showed. In this specific situation, the sampling point was connected to the probe when performing GS.



(a) (b)  
 Figure 8 Test rig where (a) shows the stack with 3 sensors installed and (b) the detail of the probe for GS

#### 4.1. Gravimetric Sampling

Gravimetric sampling was performed according to Environmental Protection Agency standard for stationary stacks (EPA, 2018) with some adaptations described below on the stack number 3 at PT. The stack had a total height of 25,000mm and diameter of 1,700mm with the sampling point located 20,000mm above the top of the PT. The sampling point was located 12 diameters over the PT top and 3 diameters below the gas stream exits to the atmosphere.

For the determination of isokinetic stack gas velocity and volumetric flow rate (type S pitot tube) the method 2 was employed (EPA, 2016) while for determination of PM emissions from stationary sources the method 5 was utilized (EPA, 2019). According to method 5 the samples should be dried from 2-3h at 105°C, but to avoid decomposition of ammonium nitrate, after the sampling period, the samples were left to cool down at silica gel desiccator for 30 min and then taken to the oven at 110 °C for 1 h.

Table 2 shows the equipment used to perform GS. The scale employed for PM mass determination was Mettler Toledo AE100 which range is in conformity with Method 5 from EPA (2019). All instruments had valid calibration certificate over the duration of the experiments.

Figure 9 shows a cross section view of the probe position related to the other installed instruments. The stack was sampled in 8 points to get isokinetic velocity and temperature profiles as the standard reference requires (EPA, 2016), while PM concentration was measured

at the center point for the whole study due to the fact the PM here presents a PSD of minimum 90% below 1 $\mu$ m leading to main mechanism of motion being Brownian motion and therefore not dependent of flow in the stack (Mertens, et al., 2014). EDA has a probe length of 900mm while OSA 710mm.

Table 2 Manual equipment employed

<b>Equipment</b>	<b>Model</b>	<b>Parameter obtained</b>
<b>Digital pressure indicator</b>	Druck DPI 705	Pressure stack 70 or 200 mbar, accuracy of $\pm 0.1\%$ Vacuum in the pump suction -200mbar, accuracy of 0.1%
<b>Pitot</b>	Kimo MP210	Temperature profile at stack From -100 to +750°C, accuracy of $\pm 0.4^\circ\text{C}$ Velocity profile at stack range from 2 to 100m/s, accuracy of $\pm 0.2$ m/s
<b>Gas meter</b>	Ritter Bellows BG4	Temperature of gas sampled 5 to 40°C Volume sampled 40l/h to 6000l/h, accuracy of 2%
<b>Compressed air</b>	6 bar	Supplied from the plant
<b>Digital Scale</b>	Mettler AE100	readability range between 0.01 mg and 0.1 mg, and capacities up to 320 g
<b>Nozzle</b>	Teflon®	Adjust for isokinetic velocity with gas meter Diameter of 3.5, 4 and 4.5mm used
<b>Sampling filter</b>	Tube with fiber glass	Desiccated for 24h minimum 24 to 27g of fiber glass

Figure 9 shows a cross section view of the probe position related to the other installed instruments. The stack was sampled in 8 points to get isokinetic velocity and temperature profiles as the standard reference requires (EPA, 2016), while PM concentration was measured at the center point for the whole study due to the fact the PM here presents a PSD of minimum 90% below 1 $\mu$ m leading to main mechanism of motion being Brownian motion and therefore not dependent of flow in the stack (Mertens, et al., 2014). EDA has a probe length of 900mm while OSA 710mm.

Filters were made of fiberglass pads (Figure 10) previously desiccated according to Method 5 (EPA, 2019). The probe nozzle employed to get isokinetic sampling had a range between 3.5mm to 4.5mm. No sample recovery was needed once the filter was located at the inlet of the probe, inside the stack as Figure 9 shows.

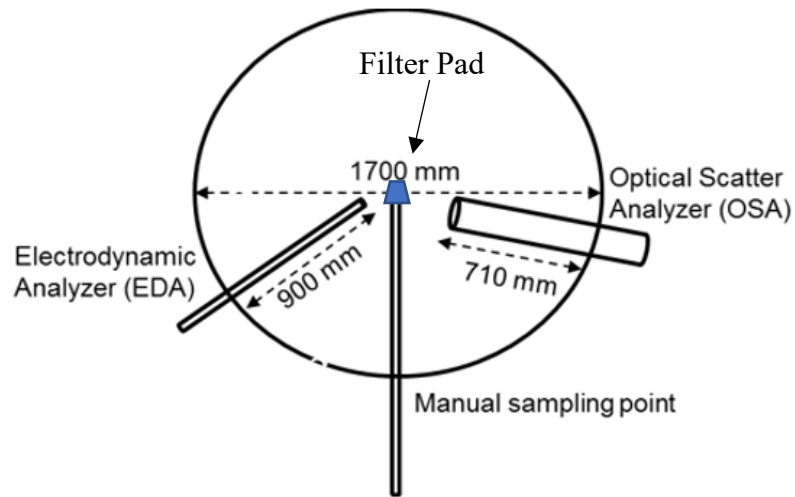


Figure 9 Layout of analyzers and GS probe in the stack under study



Figure 10 Fiberglass pad filter employed in the research project.

The range of main parameters is showed on Table 3 where can be seeing large variations due to meteorological conditions in the region where the study was conducted. The ambient air employed receives no preconditioning before its use in the process as showed in Figure 7.

GS was performed minimum 3 times for each production batch to evaluate potential variations over time but also twice in the same day to evaluate repeatability and reproducibility of the method, under same product batch.



Table 3 Range of parameters during gravimetric sampling

Parameter	Unit	Minimum	Maximum	Weighted Average
Temperature	°C	2	40	22
Velocity	m/s	16	27	20
Air mass flow	Kg/h	162,000	273,000	206,000

## 4.2. Manual Data Collection

For the third part of the research the Testo 440, Druck 705 and Kimo MP 210 were used to perform manual measurements. The details about range and accuracy were listed previously according to Table 2. The average velocity over the whole diameter of the stack (1700mm) was measured at 8 points. These manual measurements were done always at the beginning of the each designed experimental run.

## 4.3. Continuous Monitoring Equipment

The continuous PM monitoring was performed by two different instruments, OSA and EDA. The choice was made to evaluate distinct principles in this application.

### 4.3.1. Optical dust analyzer

The OSA was selected from PCME Ltd manufacturer (now called ENVEA UK), model QAL 181, which utilizes forward-scattering, called ProScatter® featuring patented options for enhanced reliability. The optical scatter analyzer from PCME Ltd, model QAL 181. The forward-scattered light collected by the concave mirror is then focused onto a quartz rod where the light is transmitted towards the light detector positioned within the electronic enclosure located outside the stack. The amount of light detected is proportional to the particulate concentration and calibration is based on manual isokinetic sampling. Figure 11 shows the external part of OSA which one is inserted on the stack. The space between the two cylinders is the area where the particles flow and are reached by the laser (PCME, 2019) as showed by the red arrow.

OSA model PCME QAL 181 had a certification range of 0-15mg/Nm<sup>3</sup> and measurement capability of 0-300mg/Nm<sup>3</sup>.



Figure 11 OSA probe which one goes inside the stack.

#### 4.3.2. Electrodynamic dust analyzer

To test the electrification technique the chosen PM analyzer was EDA from PCME Ltd. (now called ENVEA UK) prospect, model STACK 980 (Figure 12).



Figure 12 External part of EDA and probe rod

The instrument measures the current signal created by particles interacting with the sensing rod in the stack. The sensor extracts a specific frequency band of this signal and electronically filters out the direct current caused by particle collisions. The signal may be

correlated to dust concentration by comparison to the results of one manual isokinetic sample for those types of industrial applications for which the instrument is designed.

PCME (2018) states the core features of the Electrodynamic® Probe Electrification are that the signal generated is unaffected by contamination on the sensor rod, operates on velocity range of between 8 m/s and 20 m/s and air temperature range from -20 °C to 50 °C.

EDA model PCME STACK 980 had a certification range of 0-15mg/Nm<sup>3</sup> and measurement capability of 0-500mg/Nm<sup>3</sup>.

#### **4.3.3. Calibration of online analyzers/ self-quality checks**

The calibration of both PM concentration analyzers is done with a single point calibration applying a factor as given by Equation 2 (PCME, 2018).

$$\text{Emission} \left( \frac{\text{mg}}{\text{Nm}^3} \right) = \text{Raw instrument reading} \times \text{Calibration factor} \quad \text{Eq.2}$$

To get the calibration factor, the same formula is applied considering the average of the instrument reading in the same period of when GS was performed.

Both analyzers perform self-quality checks to ensure reliability of the outputs. The PCME STACK 980 sensor includes automatic functionality checks to provide high quality assurance as a probe rod short-circuit check enable the operator to know when the sensing rod may be electrically shorted to the stack.

The PCME QAL 181 performs a span check every 15 min. During this test, it closes the reading from the process and reads only the channel. The result, expressed in percentage is equivalent to the material accumulated in the channel, not actually PM from the process.

Cleaning on both sensors were performed once every month or when the span test from OSA reached results below 75 %.

#### **4.3.4. Electrical low-pressure impactor**

The Electrical low-pressure impactor (ELPI) from Dekati was chosen for the work performed on Chapter 7, due to the fact it offers a different measuring principle from the two online analyzers employed for the continuous monitoring at the stack under study, it is extractive and provides a real-time particle spectrometer for measuring airborne PSD and mass concentrations.

In the ELPI, after dehydrating the stream, the particles are charged to a known charge level and size classified in 14 size fractions ranging from 6nm to 10µm. All the impactor stages are electrically insulated which means that the produced electrical current at each stage is

measured and discharged. This current is proportional to the number concentration, and consequently proportional to the mass concentration of particles on each stage when using the calculated density of the stream (Dekati, 2011).

The main specifications of the equipment are described in the Table 4. The flow to the equipment is fixed at 10 l/min so in order to reach the closest isokinetic setup the nozzle employed was 3.5mm. As already discussed by Mertens et al. (2014) the isokinetic sampling was not critical under the PSD range studied, but still an attempt was made to fit the closest nozzle to get isokinetic sampling with the fixed flow.

Table 4 ELPI specifications

Nominal air flow	10 l/min	Particle size range	0.006 – 10 $\mu\text{m}$
Ambient humidity	0–90 % RH, non-condensing	Ambient temperature	10–35 $^{\circ}\text{C}$
Sample gas temperature	< 60 $^{\circ}\text{C}$	Sampling rate	10 Hz
Number of channels electrically detected + pre-separator stage	14	Pump requirements	25 m <sup>3</sup> /h at 40 mbar
Electric power	100–250 V	50–60 Hz,	200 W
Charger current	1 $\mu\text{A}$	Charger voltage	3.5 kV +/- 0.5 kV

Each impactor has a unique data sheet with the calibration specifications. For the equipment used in this research, the information is detailed in Appendix 10.1.

The stages were cleaned daily after sampling. The operation procedure is available in the Appendix 10.2. It was taken about one hour to clean and reassemble the equipment after a day of sampling.

Leakage test were performed every time the impactor was disassembled for cleaning, e.g. daily. The procedure is available in Appendix 10.3.

Zeroing test was performed before each experimental run. The procedure is available in Appendix 10.4.

The interpolated minute average data from ELPI was recorded and each experiment had a duration of 13min (the period where was expected the plant to run stable after each change without compromising the productivity levels).

#### 4.4. Data Extraction and Handling

The data needed to be extracted and organized at the same temporal interval from the different sources. For instance, the raw data from OSA/EDA/ ELPI and the plant distributed control system (DCS) were logged as interpolated minute average, while manual measurements were taken at beginning of the running and meteorological parameters from nearest meteorological station located at 1.2km far from the PT, in straight line. The last data set was only available on hourly average data (see Table 5). It was chosen to organize all the data in a minute-average way to improve the accuracy of the measurements and it was chosen to only take specific experimental periods where the process was assumed to be in stable operation (standardized production rates from 37 to 57t/h).

Table 5 Mapping of potential parameters to be included in the analysis

Type of parameter	Parameter description	Unit
	Fertiliser grade	text
	Date	text
	Time	text
Process parameters	Off-spec flowrate	t/h
	NP-liquor temperature	°C
	Flowrate of salts	t/h
	Flowrate of NP-liquor	m <sup>3</sup> /h
	Flowrate of NH <sub>3</sub>	kg/h
	Flowrate of product	t/h
	Temperature of salts	°C
	Temperature of mixer	°C
	Mixer rotation	rpm
	Bucket rotation	rpm
	Inlet temperature	°C
Manually sampled parameters	Inlet relative humidity	%
	Inlet temperature	°C
	Stack relative humidity	%
	Stack temperature	°C
	Stack velocity	m/s
Meteorological parameters	Air pressure	hPa
	Air temperature	°C
	Relative humidity	%
	Precipitation	mm
	Wind speed	m/s
Output of dust analysers	ELPI	mg/m <sup>3</sup>
	OSA	u/m <sup>3</sup>
	EDA	u/m <sup>3</sup>

For the statistical analysis of data set it was used Minitab® 19 software and LRM, which models the relationship between categorical or continuous predictors and one response, to include interaction and polynomial terms, or transform the response if needed.

The industrial application investigated was a constraint in terms of which statistical approach could be employed due to sudden changes in process parameters to build potential experiments, what led to the choice of regression model.

The results will be presented as chapters, which are manuscripts, submitted for publication. Chapter 5 deals with the performance and challenges of continuous monitoring of UFPs under industrial application, considering two distinct sensors; while in the Chapter 6 (manuscript accepted for publishing) models the correlation between the relevant parameters impacting the concentration of UFP and the output of the sensors. Finally, in Chapter 7 a methodology is proposed and tested, based on a controlled experiment to improve the model found in Chapter 6 and test the potential of using a cascade impactor (ELPI) to calibrate the commercial online PM sensors.

## 5. PERFORMANCE AND CHALLENGES OF ONLINE FINE PARTICULATE MATTER MONITORING IN A MINERAL FERTILIZER INDUSTRIAL PLANT

Elisangela Krauss<sup>1\*</sup>, Jo-Ela Johansen<sup>2</sup>, Monica Lopes Aguiar<sup>1</sup>

<sup>1</sup>PPGEQ – Chemical Engineering Post Graduation Program, Federal University of Sao Carlos

<sup>2</sup> Energy and Environmental Technology, University of South Eastern Norway

\*Corresponding author: krausselisangela@gmail.com

### Abstract

The increased need to accurately measure continuous fine particulate matter (PM) concentration at stacks is addressed in this work by evaluating performance of analyzers, electrodynamic (EDA) and optical scatter (OSA) in an industrial mineral fertilizer plant. The analyzers were installed at same stack where gravimetric sampling (GS) was performed to find calibration factors. The results show that OSA follows the process changes to a good extent and the calibration factors obtained varied on 0.5 standard deviations over products and seasons. EDA represents better sudden variations up to its operating range, but the calibration factors measured were over three standard deviation for the same product over different meteorological conditions but also under same meteorological and product conditions. EDA also presented an artificially high emission every 15 min due to intermittent steam injection in the stream. PM deposition on the sensors affects the reading on both analyzers but only OSA indicates it (span test result less than 75%). From the parameters here evaluated, OSA is recommended for industrial continuous monitoring of fine PM once provides feedback on the sensor condition and smaller effect of seasonal conditions and product grades.

**Keywords:** prilling tower, optical laser scanner, electrodynamic induced signal, continuous monitoring, ammonium nitrate

### 5.1. INTRODUCTION

Mineral fertilizer plants usually employ Prilling Towers to get nutrients as Nitrogen, Phosphorous and Potassium bound together in the same granule with uniform particle size distribution (Yuan, et al., 2007). By 2018 there was a yearly production of ammonium nitrate/ calcium ammonium nitrate (AN/CAN) over the world of 62 million tons (IFA, 2019).

As mentioned by Brechet & Tulkens (2009), the best available techniques should be the best from the Society's point of view, not only in terms of private interests. In this sense, the recognized gravimetric sampling (GS) method provides an instant picture for the particulate

matter (PM) concentration but it is not able to follow the process behavior or instabilities that can affect the air quality in the surrounding of the industrial plants.

The total PM concentration at industrial stacks can be generally measured by several different methods as GS (Kalaiarasan, et al., 2018), conventional or diluted GS (England, et al., 2000), cascade impactor technique (Ehrlich, et al., 2007) (Muller, et al., 2012), optical scattering and electrification diffusion charger (Koval, et al., 2018) (Wozniak, et al., 2018) (Sullivan, et al., 2018). For each specific application, parameters as stack diameter, estimated concentration and particle size distribution, type of gas cleaning equipment, flow conditions as temperature, relative humidity and velocity must be analyzed to get the best possible result from the analyzer. Even with many commercial analyzers available, no literature was found to the author's knowledge that tackle reliability and operability of such equipment in industrial environments. For instance, Ehrlich et al. (2007) sampled many industrial stacks using a manual cascade impactor technique, but no correlation was possible to be performed between the results with process or environment changes.

Lingling et al. (2017) studied a gas-liquid crossflow array system to remove fine particles measured concentration with a Welas® digital 2000 (Palas GmbH) device with a series of probes sampling isokinetically. The relative errors between the calculated values and the actual values were below 5%. Besides applying online measurement, the authors kept PM concentration fixed, due to the purpose of their work.

Sullivan et al (2018) points out limitation of available technologies as the typical assumption of particles are spherical, so the transmission bias of all such inlets against non spherical particles, which diverge more from the inlet's centerline than spherical particles do. This particle detection event can also trigger the firing of the laser beam.

With the purpose of reducing the knowledge gap on online industrial monitoring of fine PM, this project aims to evaluate the performance and challenges faced by two distinct online PM analyzers in a mineral fertilizer industrial Prilling Tower over time, calibrating it with several GS measured under different product composition and season in Northern Europe.

## **5.2. MATERIAL AND METHODS**

This work was performed at an industrial fertilizer plant, where over 40 different recipes of AN/CAN (Nitrogen, P<sub>2</sub>O<sub>5</sub> and K<sub>2</sub>O) are currently produced, during summer/ fall season. The process is based on reaction from phosphate rock and nitric acid and after some separation steps the called mother liquor is mixed with potassium chloride and ammonia (also some formulas



take small amounts of other nutrients source), generating a melt in high temperature which is pumped to a centrifugal bucket with small holes inside the Prilling Tower (Hussain, 2012). As showed on Figure 13, the AN/CAN melt falls in the tower and is cooled down by ambient air in counter-current flow. The prills go to the bottom of the Prilling Tower and then to the size classification process, while the PM is carried over to the top of the Prilling Tower and flow through six fans installed each one in a stack.

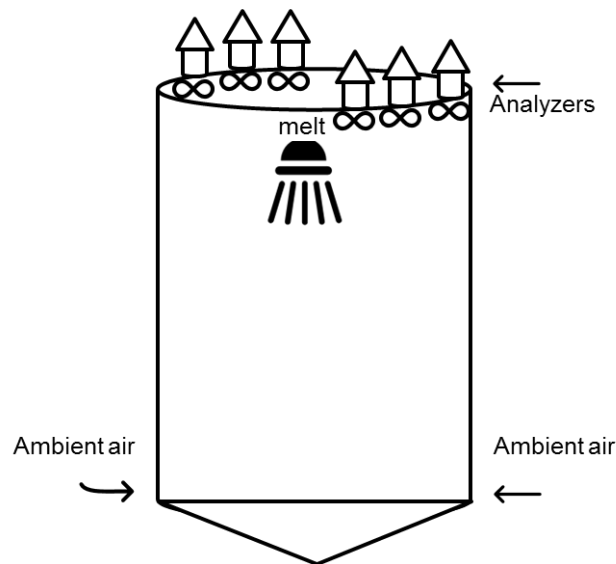


Figure 13 Industrial Prilling Tower set-up

### 5.2.1. Manual Gravimetric Sampling

The GS was performed at one among 6 stacks at AN/CAN Prilling Tower at the same level where the two online PM analyzers were installed as per Figure 14.

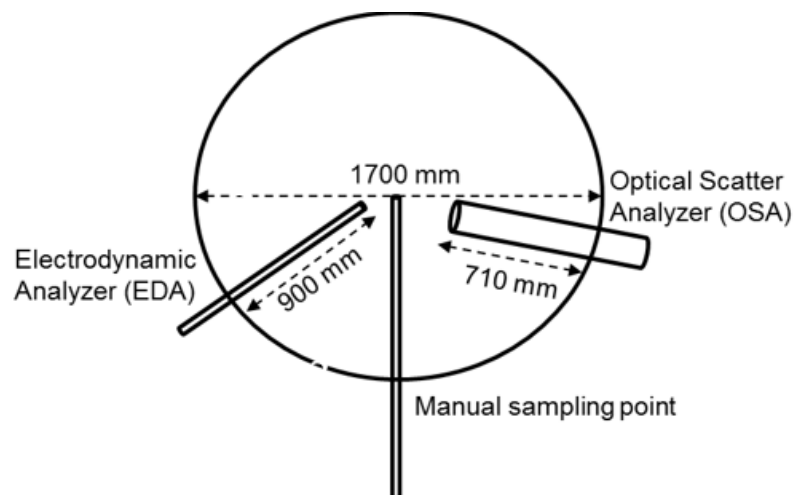


Figure 14 Layout of analyzers in the stack under study

The procedure was done according to EPA standards of performance for new stationary sources (EPA, 2018). To avoid decomposition of ammonium nitrate, after the sampling period,

the samples were left to cool down at silica gel desiccator for 30 min and then taken to the oven at 110 °C for 1 h.

The stack had a total height of 25,000mm and diameter of 1,700mm with the sampling point located 20,000mm above the top of the PT. The sampling point was located 12 diameters over the PT top and 3 diameters below the gas stream exits to the atmosphere.

The stack under analysis was sampled in 8 points to get isokinetic velocity, temperature profiles and PM concentration (EPA, 2018). The range of main parameters is showed in Table 6, where can be seeing large variations due to meteorological conditions in the region where the study was conducted once the ambient air employed receives no pre conditioning before its use in the process as showed in Figure 29.

Table 6 Range of parameters during gravimetric sampling

Parameter	Unit	Min	Max	Average
Temperature	°C	2	40	22
Velocity	m/s	16	27	20
Air mass flow	Kg/h	162,000	273,000	206,000

GS was performed minimum 3 times for each production batch to evaluate potential variations over time but also twice in the same day to evaluate repeatability and reproducibility of the method.

### 5.2.2. Online PM Analyzers

This section shows the details about the two instruments employed and how they are calibrated.

### 5.2.3. Electrodynamic PM analyzer

One of the chosen PM analyzers was electrodynamic PM analyzer (EDA) from PCME Ltd. (now called ENVEA UK) prospect, model STACK 980.

The operating manual from the supplier PCME (PCME, 2018) states the sensor uses unique and patented Electrodynamic® Probe with electrification technology. The instrument measures the current signature created by particles interacting with the sensing rod in the stack. The sensor extracts a specific frequency band of this signal and electronically filters out the DC current caused by particle collisions.

PCME (2018) states the core features of the electrodynamic® probe are that the signal generated is unaffected by contamination on the sensor rod (which may cause signal drift issues

for other systems), not affected by velocity variations within typical bag filter velocity ranges (of between 8 m/s and 20 m/s) and the air temperature range could be from -20 °C to 50 °C.

#### 5.2.4. Optical PM analyzer

The second analyzer selected from PCME Ltd manufacturer (now called ENVEA UK) prospect was the optical scatter PM analyzer (OSA), model QAL 181.

According to PCME (2018), the QAL 181 utilizes an improved forward-scatter technique *ProScatter*® featuring patented options for enhanced reliability.

As particles travel through a beam of light, each particle scatters light in all directions with the strongest intensity of light being scattered in a forward direction. The beam of laser light then continues through a concave mirror to the beam dump.

The forward-scattered light collected by the concave mirror is then focused onto a quartz rod where the light is transmitted towards the light detector positioned within the electronic enclosure located outside the stack. The amount of light detected is proportional to the particulate concentration and calibration is also based on one manual isokinetic sampling.

#### 5.2.5. Calibration of Online Analyzers/ Self-Quality Checks

The calibration of both PM concentration analyzers is done with a single point calibration applying a factor as Equation 3 (PCME, 2018).

$$\text{Emission} \left( \frac{\text{mg}}{\text{Nm}^3} \right) = \text{Raw instrument reading} \times \text{Calibration factor} \quad \text{Eq.3}$$

To get the calibration factor, the same formula is applied considering the average of the instrument reading in the same period of GS.

Both analyzers perform self-quality checks to ensure reliability of the outputs.

The PCME STACK 980 sensor includes automatic functionality checks to provide high quality assurance as a probe rod short-circuit check enables the operator to know when the sensing rod may be electrically shorted to the stack.

The PCME QAL 181 performs a span check every 15 min. During this test it closes the reading from the process and reads only the channel. The result, expressed in percentage is equivalent to the material accumulated in the channel, not actually PM from the process. According to the PCME (2018) when span test reaches results below 75 % it is needed to perform inspection/ cleaning.

### 5.3. RESULTS AND DISCUSSIONS

#### 5.3.1. Calibration Campaigns Results

It was performed 34 GS campaigns during one year, from August 2018 to July 2019 by 2 operators and under 11 different product grades. A complete design of experiments was not possible to be performed due to the challenges of industrial sampling under unstable conditions as well as the seasonal product grades, which are defined by demand from the market, according to the region and type of nutrients required by the different crops.

Wilson et al. (2002) highlighted that the measurement of volumetric flow in the stack can itself be a source of error up to 30%, due to the human factor. So, to evaluate the human factor as a potential source for errors in the gravimetric sampling, it was employed the test for equal variances, once the data was normally distributed.

Figure 15 shows that both operators have performed sampling according to an adequate standard once the corresponding standard deviations are mostly in the same range as the blue lines are overlapping each other. Besides that, the p-value obtained from the database was 0.988 what means that the the standard deviation from Operator 1 was 98.8% similar to the one obtained from Operator 2.

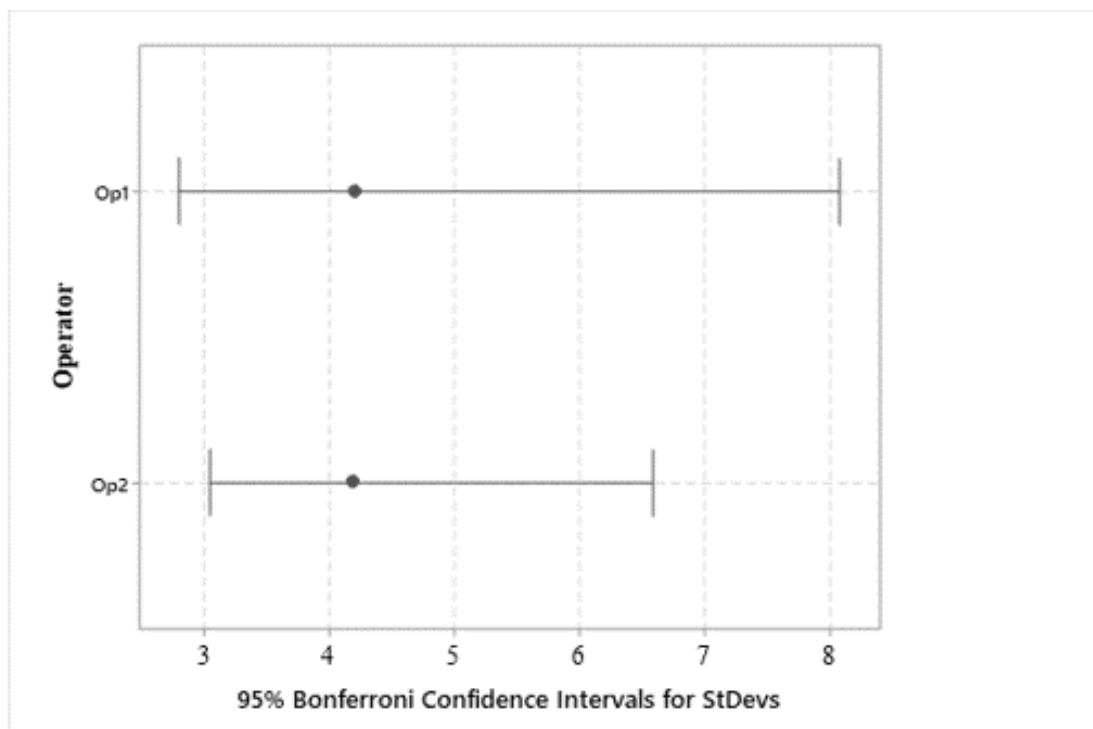


Figure 15 Effect of human factor evaluated based on the result of the test for equal variances, from the GS performed by 2 operators considering normal distribution.

It is observed although, that the range obtained from Operator 1 is wider than the one from Operator 2, indicating that the last one is performing a more systematic work. For this analysis, it was excluded four data sets where the plant was operating with an extra source of fine dry product dust to the stack during fall. The extra emission was not coming from the prilling tower itself but from the dedusting system from the plant.

In Figure 16 it can be seen that PM concentrations are higher during summer for all products studied and lower in wintertime, what is due to the use of ambient air without pretreatment to the prilling tower. In winter time the cold air makes the droplets to solidify faster into prills reducing the PM concentration, as Shirley et al. (1996) observed. Ideally, the PM monitoring instruments should be able to follow this trend in an extent that calibration factors would be the same over seasons what is not observed as per Figure 16. Here the effect of seasons in each instrument reading is presented in terms of standard deviation. EDA shows up to over 4 standard deviations than OSA among seasons and a consistent trend about 67% overestimated emissions from one season to the next (winter to fall) in Northern Europe. OSA wider variation identified was about 40%, from fall to winter/summer.

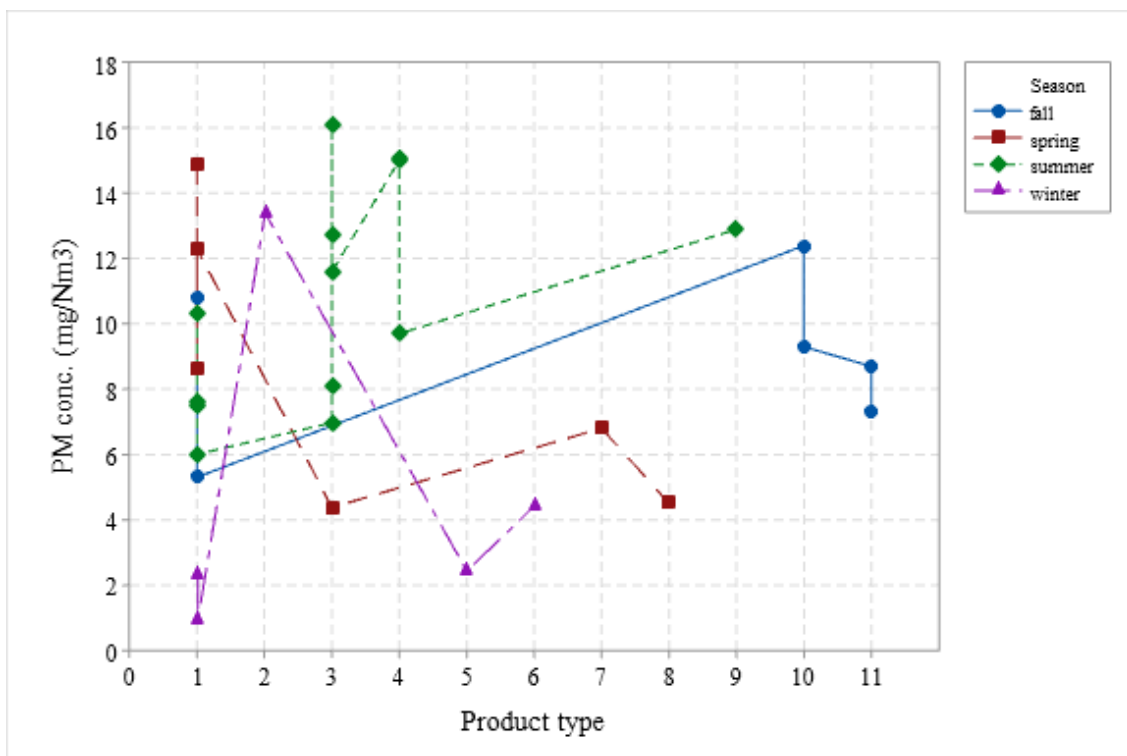


Figure 16 PM concentration as a function of product type over different seasons.

When sampling different product types it can be expected to have variation between calibration factors as presented on Figure 18. For instance, OSA reading is influenced by the optical and reflective properties of PM under study (Koval, et al., 2018) (Sullivan, et al., 2018).

This study proved to consistent with the known phenomena once the standard deviation found among products was 0.5 from product 1 to product 10. EDA presented standard variation of 3 from product 3 to product 11 what could be due to the particles being charged electrically and interacted with the probe in distinct intensities.

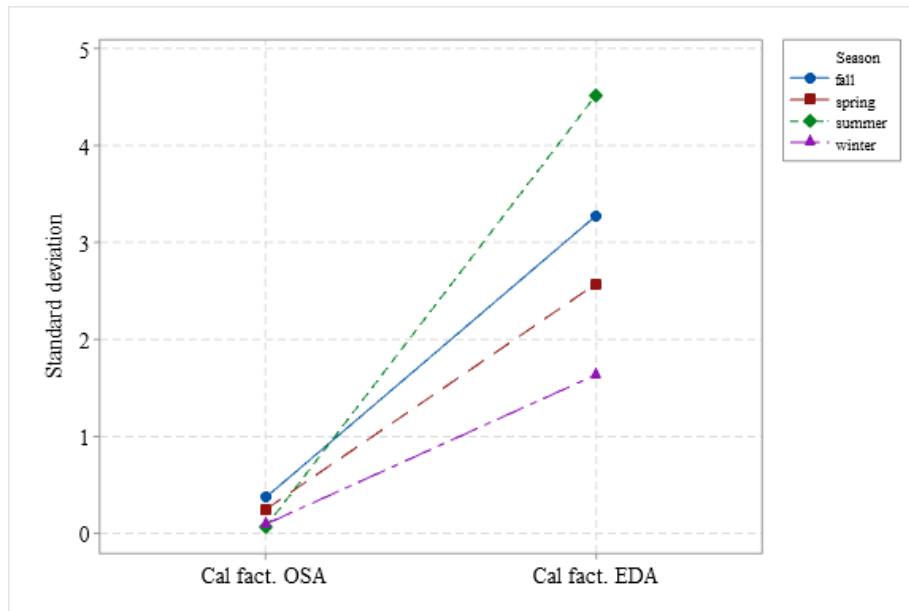


Figure 17 Standard deviation of calibration factors for sensors OSA/ EDA over different seasons.

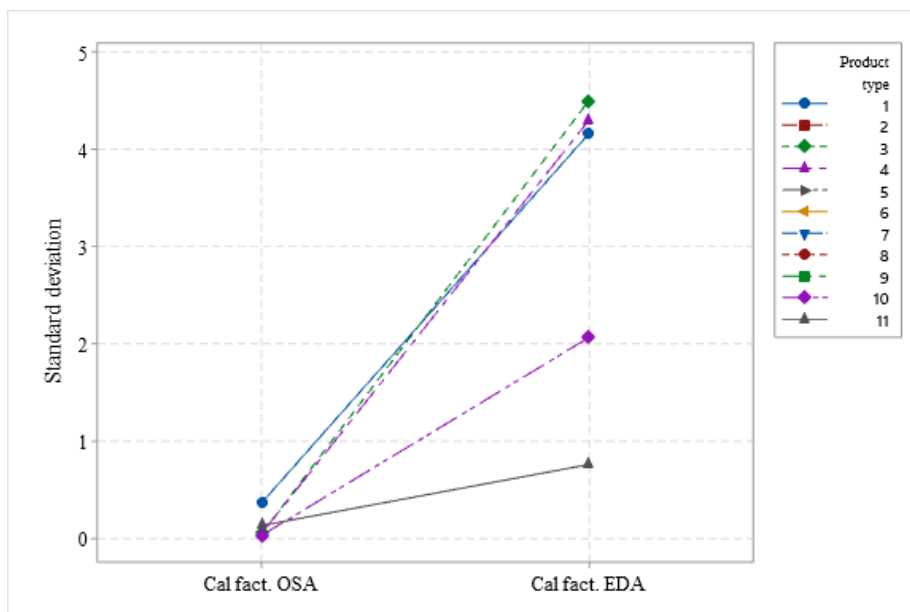


Figure 18 Standard deviations for calibration factors from OSA/ EDA under different product grades

### 5.3.2. Performance of Instruments Over Time

After having performed the GS campaigns, the calibration factors from each period were applied to the database collected from the online PM analyzers. It can be seen from Figure 19 that results from the OSA vary from no emission up to over  $70 \text{ mg/Nm}^3$ , giving realistic results, during a tested period of over 30 days. The peaks occurring approximately every 8h correspond to the start-up of the plant after a cleaning stop performed every working shift. Also, a higher emission level was measured in one of the start-ups (hour 504).

The span test results for the period under study are showed in Figure 20, when between cleaning intervals, the test got values lower than 80, so the data collected during this period was discarded from the database.

Unlike the OSA, EDA showed results as per Figure 21 from no emission until above  $5,000 \text{ mg/Nm}^3$ . These results are not realistic, once no change was identified on process/environment parameters during that time that could lead to higher emission levels. Besides that, plumes with such low particle size (90% particles with less than  $1 \mu\text{m}$  measured by electrical low-pressure impactor from Dekati) are highly visible during sun light as other authors have demonstrated (England, et al., 2013) (Abreu, et al., 2007) (Presotto, et al., 2005).

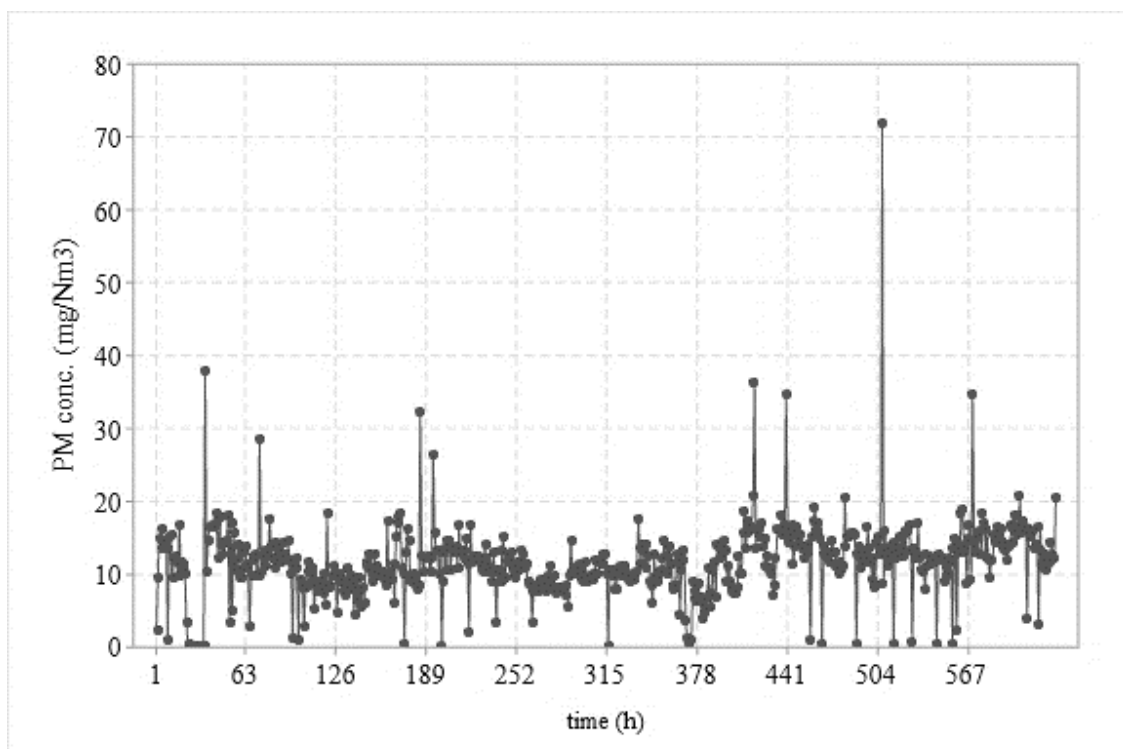


Figure 19 PM concentration read from OSA over 600h

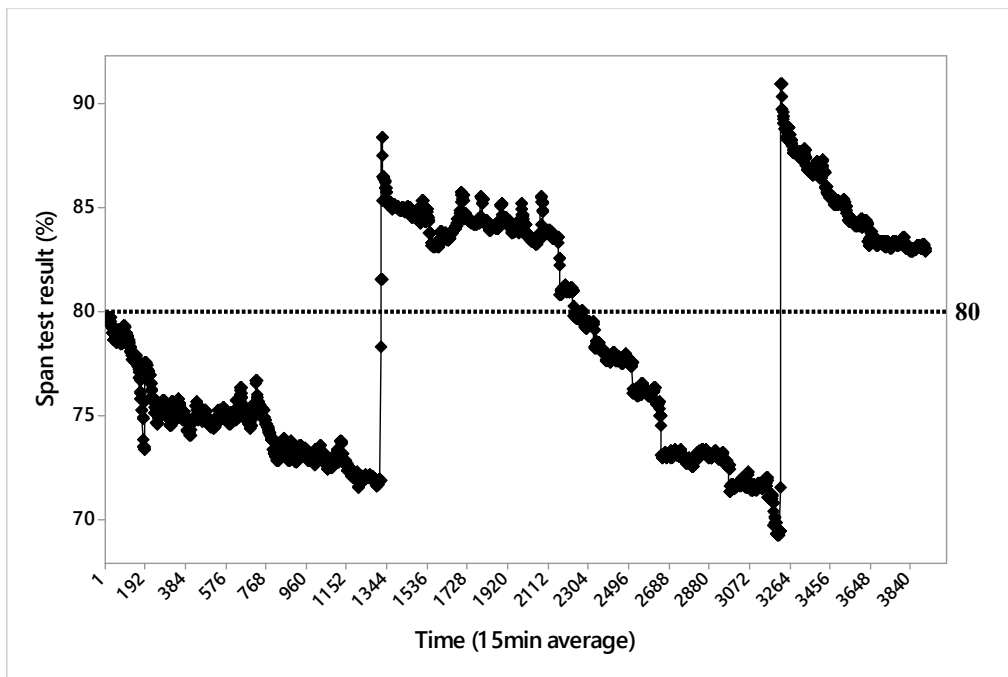


Figure 20 Results from the span check performed by the OSA every 15min where 80% is the reference to inspect the instrument.

The span test for the EDA was also performed automatically and always returned value of 100%, with no indication of disturbances or problems in the sensor, but when inspected on hour 315, the sensor rod had significant layer of material build-up. Once the rod was cleaned, the output results returned to current range of reading (from hour 315 on Figure 21).

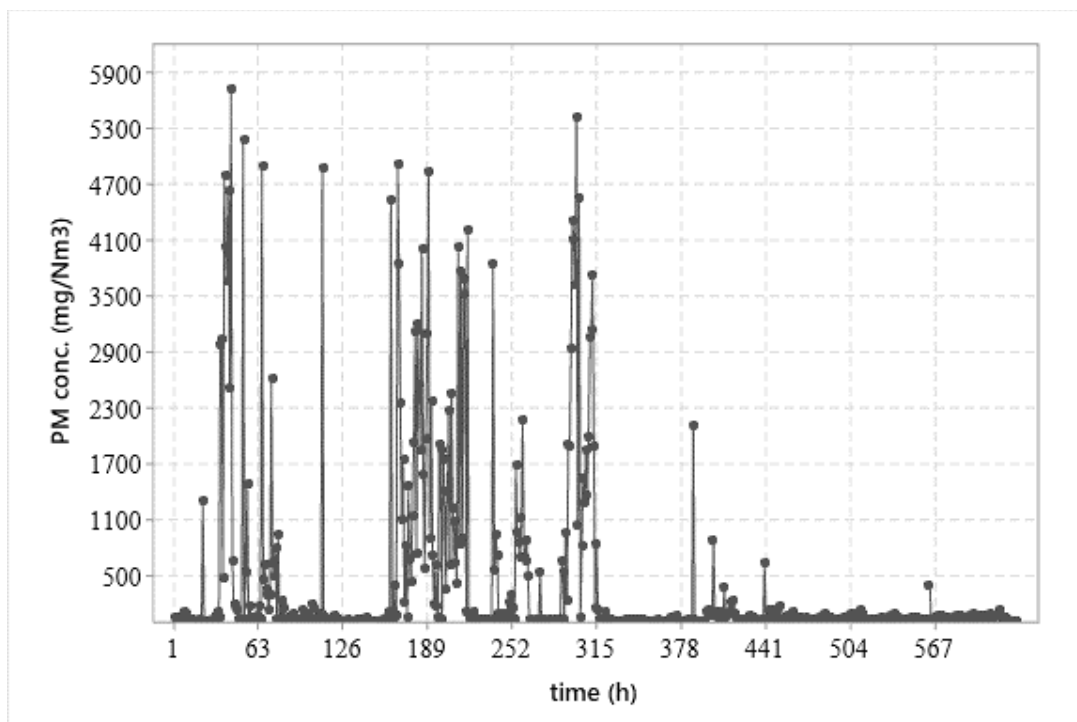
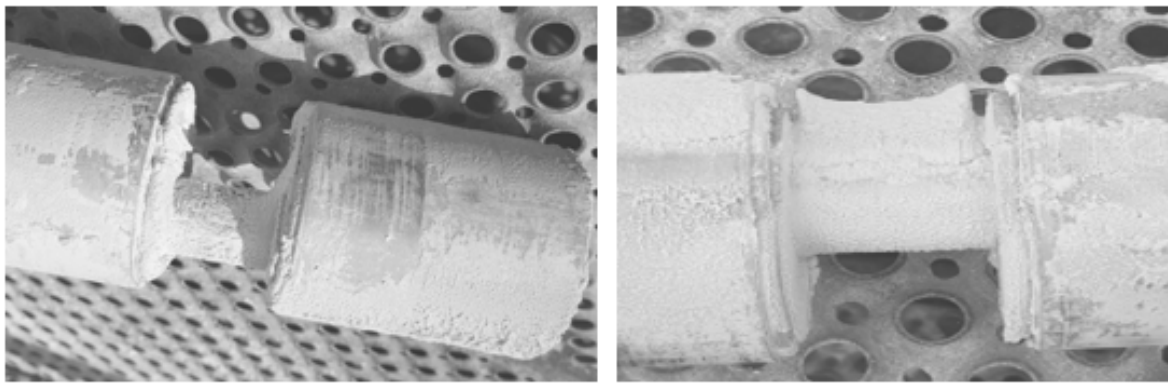


Figure 21 PM concentration read from EDA over 600h in fall



PCME (2018) states the sampling probe on EDA is not affected by product scaling on the surface, so to test this statement, an analysis of the period when both sampling probes were dirty (span test for the OSA less than 80%) was performed.

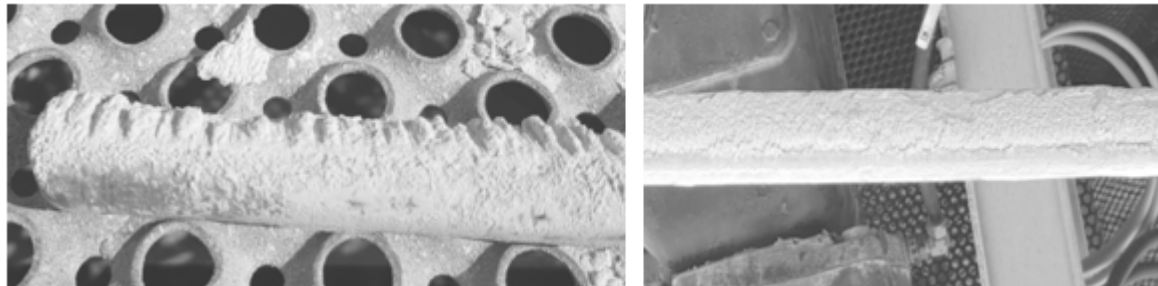
During inspections and cleaning it was observed that the part of the instruments exposed to the process conditions were having layers of material incrustated on their surface as showed on Figure 22 and Figure 23. Both analyzers studied presented the same level of material accumulated on its surface. Based on this fact, the EDA results from the period the span test on the OSA showed values lower than 80% were discarded from the database, due to potential lack of reliability.



(a)

(b)

Figure 22 (a) Laser sensor from OSA day 1 (span 80%). (b) Laser sensor from OSA day 15 (span 71%).



(a)

(b)

Figure 23 (a) Sampling probe from EDA day 1 (self-check 100%). (b) Sampling probe from EDA day 15 (self-check 100%).

### 5.3.3. Saturated Steam Effect on EDA Outputs

In the period showed on Figure 24, the start-up of the plant generated high PM concentration levels for about 30min and both sensors have indicated at. Once the process was under stationary regimen again, EDA still presented peaks occurring every 15 min, while on the OSA no disturbance was noted on the same period.

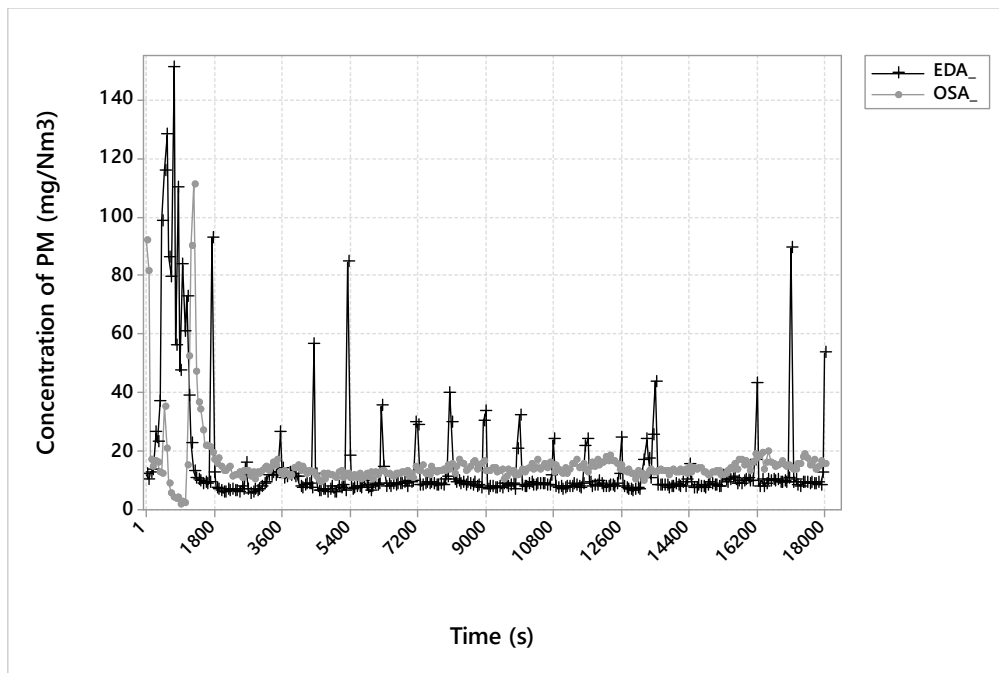


Figure 24 Online analyzers output during start-up of the plant.

The origin of the peaks was investigated further in the process upstream the stack. Going through the control monitoring system in the plant, it has been identified that the only change occurring in the same frequency of the peaks found in Figure 25 was the injection of medium pressure saturated steam to the centrifugal bucket, inside the tower, in order to keep it clean, every 15 min. Colver (1999) describes the use of electrostatic charging in liquids to detect the void fraction of bubbles. Such probes respond to the difference in conductivity of the liquid-gas phases. The author also highlights the polarization effect, which creates a signal of opposite charge, diminishing the current. To confirm this hypothesis the automatic steam injection was stopped for about one hour.

As a result, the trend on Figure 27 shows that the steam injection was the source of disturbances for the EDA. Just one manual steam injection was performed at the beginning of the test and the emission went up to  $70 \text{ mg/Nm}^3$  for about 2 min, but then went back to normal range with average of  $8.5 \text{ mg/Nm}^3$  for the rest of the period.

This observation helps to understand also why the PM concentration peaks found on start-ups of the plant were around of 10 times higher in EDA as in OSA (as per Figure 19 and Figure 21). The presence of steam from the cleaning and change on the gas media composition could have been read as PM concentration from EDA.

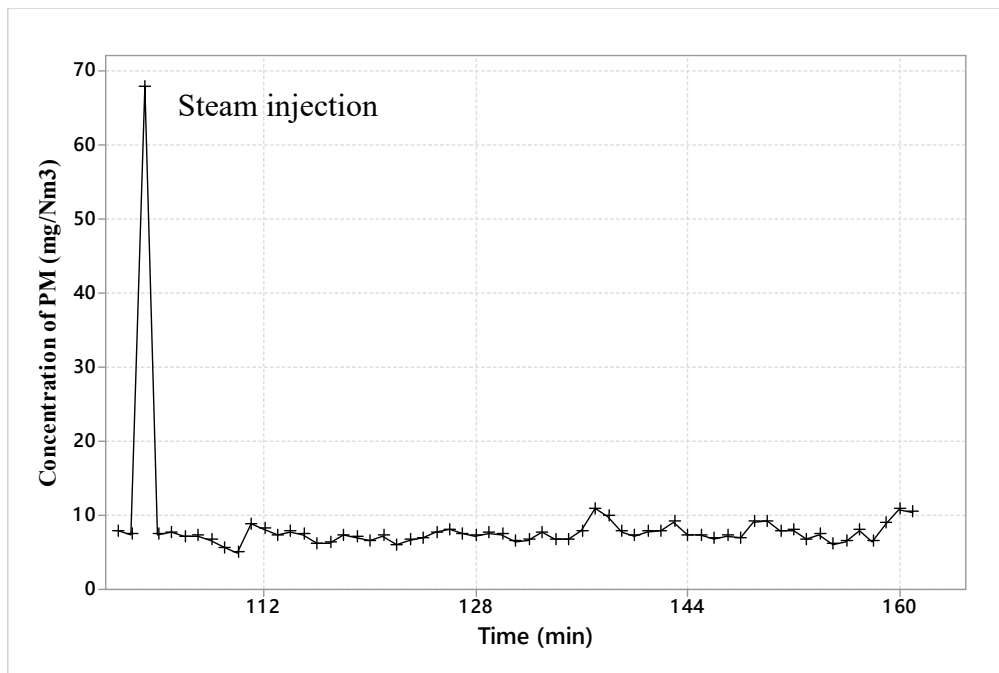


Figure 25 EDA outputs for reducing the steam injection frequency.

Once the source for the disturbance on the EDA reading was found, in the next calibration campaigns the injection of steam was kept as low frequent as possible to avoid further interferences on the data analysis and calibration factors obtained.

#### 5.3.4. Analyzers Responses to Sudden Changes on PM Concentration

The influence of sudden changes on PM concentration was analyzed for a period of 140 h during an event occurring in the industrial plant with simultaneous GS. It can be seen from Figure 26 that EDA followed the sudden increase to PM concentration to the level of 450 mg/Nm<sup>3</sup>. Although OSA shows sudden increase on the same period, the values measured vary only from 2 to 13 mg/Nm<sup>3</sup>. Considering that GS in the period between hour 60 and 120 measured 558mg/ Nm<sup>3</sup> and in the period 125 to 140 measured 49 mg/ Nm<sup>3</sup>, it can be observed that reading from EDA was more consistent.

One potential reason for this phenomenon was found to be the range of operation of EDA (0-500 mg/Nm<sup>3</sup>) while OSA has a smaller operation range (0-300 mg/Nm<sup>3</sup>). Furthermore, the area covered by the laser on OSA is much smaller than the probe surface on the EDA and therefore could be obstructed easier by sudden high amount of dust.

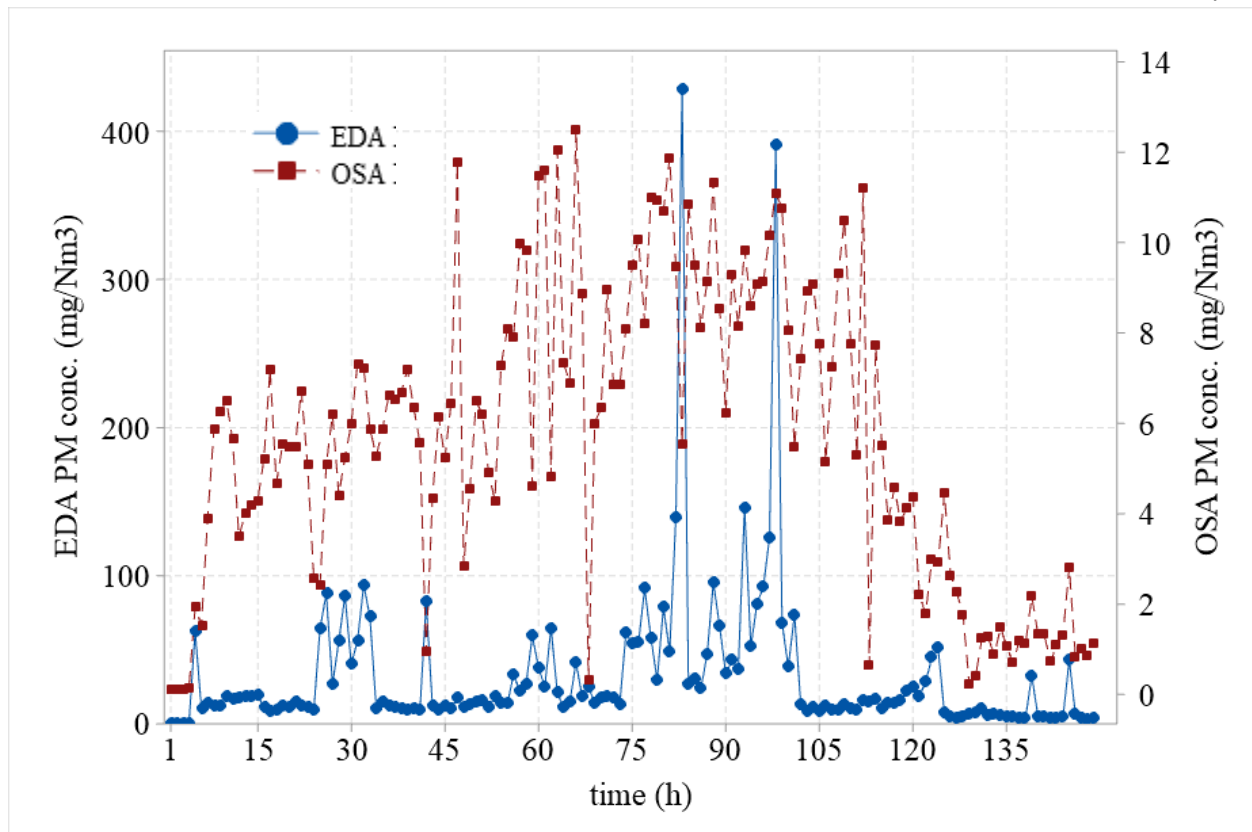


Figure 26 EDA (red squares) and OSA (blue circles) results under sudden high changes on PM concentration.

#### 5.4. CONCLUSIONS

Evaluating the performance and challenges of continuous fine PM concentration measurement in an industrial application it can be concluded that both analyzers can follow variations in the process if they are kept clean, what is easier to be diagnosed on OSA since it shows the need for cleaning through the span test results. In terms of response, for sudden huge changes in PM concentration at the stack the EDA represented better and faster the process behavior while the OSA presented normal output what can be due to the difference between the reading range of the instruments. A limitation observed on the EDA is that it cannot be applied in processes that have constant saturated steam or water presence considering the artificial high emission outputs it shows on those situations. In this specific case here studied, a logic system could exclude the non-realistic results from this short period of cleaning steam injection once there is a defined interval and duration. The build-up of product influences the reading of both analyzers, leading to need for cleaning between 15 to 30 days of operation in fall, what can be reduced with more efficient clening methods once here only compressed instrument air was employed at a flow rate of 60l/s. The calibration factors generated by GS for OSA presented up

to 0.5 standard variation over both seasons and products while EDA was much poorer with up to 4 standard deviation over seasons and 3 standard deviations among products. These findings highlight the challenge of continuous PM concentration monitoring in mineral fertilizer industry for compliance purposes, where the standard is GS, being optical scattering the most promising technique once it follows the process changes over time, under stable operation and provides feedback on the condition of the sensor.

## 6. DEVELOPMENT OF A REGRESSION MODEL TO PREDICT ULTRAFINE PARTICLES EMISSION IN AN INDUSTRIAL PLANT COMBINING METEOROLOGICAL AND PROCESS VARIABLES

Elisangela Krauss\*, Monica Lopes Aguiar

PPGEQ – Department of Chemical Engineering, Federal University of Sao Carlos, Rod. Washington Luis, KM 235, CEP: 13565-905, São Carlos, SP, Brazil

\*corresponding author: krausselisangela@gmail.com

### Abstract

Ultrafine particles are object of main health concern, but its concentration is challenging to be continuous monitored due to presence of semi volatile components under different meteorological conditions around industrial processes. This paper shows the development of an empirical regression model correlating the ultrafine particles concentration measured by two continuous analyzers, electrodynamic (EDA) and optical scatter (OSA) with meteorological and process parameters. The analyzers were installed at stack of an industrial plant and data was collected over 4 seasons. The results showed that EDA have no correlation with process or meteorological parameters (r-squared less than 10%) what can be caused not only by particles not being charged evenly on the stream but also the better accuracy for particles over 10 $\mu$ m, as previous studies had suggested. The OSA ultrafine particles concentration model showed r-squared of 45% and strong correlation with meteorological parameters and raw material feed. The model presented and standard error of 0.21 mg/Nm<sup>3</sup>, which is considered adequate for industry compliance purposes. OSA shows promising application for ultrafine particles monitoring if the influence of particle characteristics under industrial operation is considered and meteorological parameters are included, as already in practice for ultrafine particles monitoring outdoors.

**Keywords:** Continuous dust analyzers; forward scattering; electrodynamic effect; ultrafine particles; regression model; mineral fertilizer

### 6.1. INTRODUCTION

The mineral fertilizer industry produced in 2018 around 62 million tons of ammonium nitrate/ calcium ammonium nitrate (AN/CAN) over the world (IFA, 2019). When producing AN/CAN there is emission of ultrafine particles (UFP) mainly formed in gas phase, no matter

which production process is employed but, when using prilling towers (PT) the issue becomes critical due to the high air flow needed. If it is taken into account that PT is broadly employed in diverse segments as food, hygiene, pharmaceutical and chemical industries among others it is clear that UFP emissions can be a common issue among different industries sectors. UFPs have particle sizes in the range of 100 – 2500 nm and can also be agglomerates of UFPs, nanoparticles or nanoclusters (Fahlman, 2007).

Studies of the size and composition of atmospheric particulate matter (PM) have demonstrated the usefulness of separating them into its fine and coarse components (Wilson, et al., 2002) especially when evaluating the health impact of PM, as worldwide epidemiological studies have shown. The human exposure to respirable PM is correlated with an increase in cardiac and respiratory morbidity and mortality (Dhananjayan, et al., 2019)

Combining the transient nature of UFPs with stricter regulations in place from WHO (Team, 2006) regarding concentration level of called PM<sub>1</sub> (PM with diameter below 1000nm) being reviewed and intended to be published in 2020 the need for accurate continuous monitoring of these type of PM with existing methods and equipment is urgent to be evaluated and validated.

### **6.1.1. Mapping of Potential Parameters in Prilling Fertilizers with AN/CAN**

The approach here employed was to identify which meteorological and process parameters could potentially influence the UFP emission or the reading of those instruments, defining a system which includes inlet and outlet parameters of the prilling tower under study.

The potential variables were defined based on prilling related literature (Séquier, et al., 2014), (Hussain, 2012), (Couper, et al., 2012), (Yuan, et al., 2007), (Partridge, et al., 2005), (Wong, et al., 2004), (Shirley, et al., 1996)) and listed in Table 7. For instance Shirley et al. (1996) have applied quick freezing to prilling of ammonium nitrate, urea, and potassium nitrate to improve cooling, reducing the air flow needed while obtaining the same or increased production rates while Partridge et al. (2005) studied the effect of liquid dynamic viscosity, rotation rate and orifice size in laboratory and pilot scale PT concluding that the increase on the rotation rate generates a decrease of primary and secondary droplets.

Also, Sequier et al. (2014) when prilling molten lipids, have obtained spherical prills when adjusting prilling melt temperature and have observed coalescence of liquid droplet during their fall, what they assumed was caused by turbulence into the air column.

Table 7 Data set employed to build the model

Type of variable	Description of the Variable	Unit
	Date	text
	Time	#
Process Parameters	Liquor to PT	t/h
	Salts to PT	t/h
	Off-spec flow to PT	t/h
	NH <sub>3</sub> gas to PT	kg/h
	Mixer rotation	rpm
	Bucket rotation	rpm
	Melt temperature	°C
	Liquor temperature	°C
Meteorological Parameters	Air temperature	°C
	Relative humidity (RH)	%
	Precipitation	mm/h
	Wind speed	m/s
Output of the Analyzers	OSA	u/m <sup>3</sup>
	EDA	u/m <sup>3</sup>

The flow rate of raw materials fed to the PT was collected from the Distributed Control System (DCS) and included in Table 7, which will be the base for building the UFP model. These flow rates (salts to PT, liquor to PT, off-spec flow to PT and ammonia gas to PT) change over time due to the recipe of fertilizer under production and can affect the emission of UFP.

### 6.1.2. Ultrafine Particle Concentration Methods

There are standard and reliable methods to measure concentration for PM<sub>10</sub> and for PM<sub>2.5</sub> ( $\pm 10\%$  error for PM<sub>2.5</sub>) yet not continuous, developed and validated (Wilson, et al., 2002) but per authors knowledge nothing similar is available for UFP. Studies concerning UFP shows a difference between methods (light scattering and personal gravimetric samplers) at a factor of 2.23, for instance in an in-mine application (Thakur, 2019).

Galvão et al. (2018) when studying trends in analytical techniques applied to particulate matter characterization highlighted the importance of the knowledge of particles properties, sampling even in a controlled environment as the laboratory.

The measurement of semi volatile UFP, for instance, is discussed by Wilson et al. (2002) specially in the case of sulfates and nitrates where the concentration and composition changes due to the process but also to the location and season.

Several industrial plants produce over dozens of different types of fertilizer with frequent changeovers between recipes, sometimes a batch production of less than 24 hours.



This means that the shape, color, mass, density and composition of nutrients e.g. can also change over time what makes continuous monitoring of this UFP challenging.

The commercially available PM analyzers are based mainly on two principles, electrodynamic and optical trap or scatter (Sullivan, et al., 2018). The electrodynamic diffusion charger (EDA) traps charged aerosol particles by balancing the aerosol particle in an electric field. This stable trap is sensitive to changes in mass. The trapping capabilities of the EDA do not depend on particle shape, and thus the EDA should not be restricted to spherical particles as is the OSA trap. On the other hand, OSA trap uses a laser beam passing through the flow creating an optical trap. OSA can trap smaller particles up to hundreds on nanometers.

### 6.1.3. Modelling Techniques for Experimental Data

Modelling experimental data is widely used as presented in Figure 27, however few papers deal with particulate matter. From 6121 research papers from 2010 until 2020, just 8 were found to be related to stationary sources, from those only one is regarding UFP or PM less than  $1\mu\text{m}$  (Elsevier, 2020). These figures show the gap between the stricter regulations by WHO and governmental agencies over the recent years and the level of maturity on this research field.

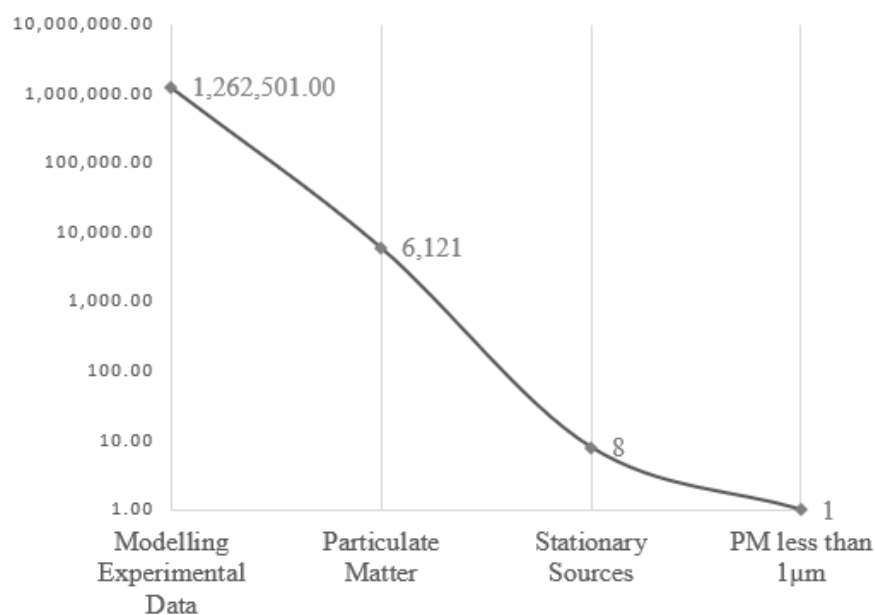


Figure 27 Web search on keywords in Science Direct from 2010 – 2020

Consistent with the technology scenario described, this paper aims to develop an approach to address the challenges found when monitoring continuous UFPs concentration in industrial processes, by developing empirical models based on regression, for two distinct online analyzers installed at stack of a fertilizer industrial plant, correlating the UFP concentration to process and meteorological parameters over four seasons in Europe. Finally,

there will be evaluated if the method current in use for UFP ambient monitoring can be applied to industrial stationary stacks.

## 6.2. MATERIAL AND METHODS

This work was performed at an industrial fertilizer plant, where more than 40 different grades are currently produced. The potential set of candidate variables included both process and meteorological parameters. The particle characterization was performed with ELPI+ and the concentration at the stack monitored with both optical scatter and electrodynamic trap techniques.

The results from four seasons monitoring was examined employing Minitab 19<sup>@</sup>.

### 6.2.1. Industrial Process Set-up

The process is based on reaction from phosphate rock and nitric acid and after some separation steps the called mother liquor is mixed with potassium chloride and ammonia (also some formulas take small amounts of other nutrients source), generating a melt in high temperature (over 140°C) which is pumped to a centrifugal bucket with small holes inside the PT (Hussain, 2012). As showed in Figure 28, the melt droplets fall in the tower and are cooled down by ambient air in counter-current flow. The microspheres go to the bottom of the PT and then to the size classification process, while the UFP is carried to the top of the PT by six fans connected to their respective stack. The analyzers were installed at the same position where gravimetric sampling takes place.

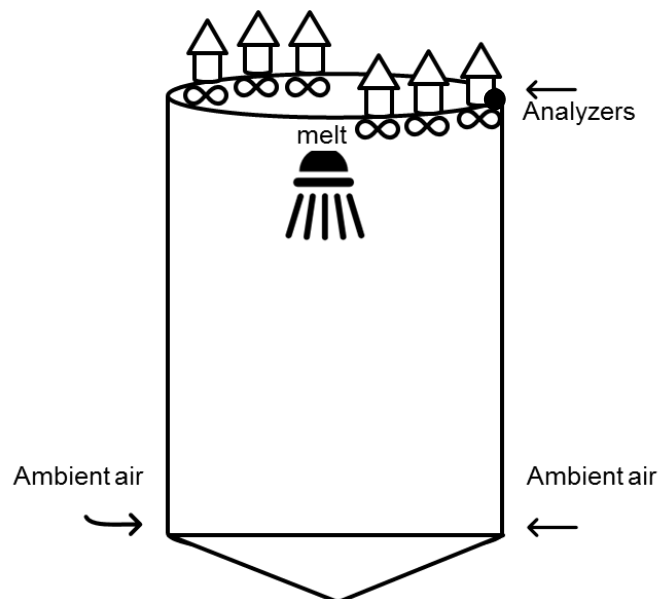


Figure 28 Industrial Prilling Tower (PT) set-up with 6 stacks

### 6.2.2. Equipment Employed to Characterize and Measure Concentration of UFP

In order to characterize the PM emissions from stack, ELPI®+ (Dekati, 2020) was employed, once it can provide online concentration and PSD changes in the continuous process and still keep samples in 14 different stages (particle size range from 10 $\mu$ m to 0.01 $\mu$ m) to be further analyzed to estimate its composition. The aluminum foils were pre-greased to avoid re-entrainment for the next stages.

A design of experiments was performed (second order with middle point) with a grand nine tests each with duration of 13min under same product but different meteorological conditions to evaluate the PSD of the emissions at stack. The concentrations are expressed in mass.

To collect enough material to chemical characterization a test was performed under stable operation until the impactor ELPI+ was full (the pressure drops over the impactor can no longer be kept under 35mbar). The aluminum foils from each of the 14 stages was analyzed with SEM/EDS (scanning electron microscopy / energy dispersive x-ray spectroscopy) and elements as oxygen, nitrogen, carbon, chlorine, silicon and fluorine could be determined. The method was also employed to search for the origin of the PM, for instance if the UFP collected had the same composition as the product or could originate from reactions in gas phase.

Two continuous monitoring sensors from PCME (2018) were installed at stack, being optical scattering analyzer (OSA) model PCME QAL 181 with certification range of 0-15mg/Nm<sup>3</sup> and measurement capability of 0-300mg/Nm<sup>3</sup> and electrodynamic analyzer (EDA) model PCME STACK 980 with certification range of 0-15mg/Nm<sup>3</sup> and measurement capability of 0-500mg/Nm<sup>3</sup>. The certificate range is the range in which the instrument is approved for compliance purposes.

### 6.2.3. Dataset Preparation and Regression Techniques

To develop the model, data from three different sources was collected. The DCS (Distributed Control System) from the plant operation, meteorological data from the closest meteorological station and finally the output from two continuous dust analyzers (OSA and EDA).

Meteorological data such as temperature, wind speed, relativity humidity (RH) and precipitation were collected from the nearest meteorological station (1.2km far from the stack monitored in straight line). The results were available in hour average basis. There were

employed 6,215 complete hourly data sets, representing 344 days from May 1st, 2018 to April 10th, 2019.

For the statistical analysis of data set it was used Minitab® 19 software was used and mainly regression, with models the relationship between categorical or continuous predictors and one response, to include interaction and polynomial terms, or transform the response if needed.

The industrial application investigated was a constraint in terms of which statistical approach could be employed due to sudden changes in process parameters to build potential experiments, what led to the choice of regression model. Potential interactions between parameters can be lost on this approach but the data set collected over 4 seasons can still provide a robust model.

The main statistical indicators considered here will be coefficient S (standard error in the regression) measured in absolute numbers and complementary to that r-squared which is the percentage of response variation explained by a linear model.

The significance of parameters will be given by p-value which one determine the significance of the results, based on the hypothesis of at least 95% of the data set can be explained by the model proposed ( $p\text{-value} \leq 0.05$ ).

A residual is the vertical distance between a data point and the regression line. They will be employed here to analyze how close is the fit of the linear model to the dataset and if their distribution is random above and below the zero line what means there is only error left in the model and all relevant parameters were included.

### **6.3. RESULTS AND DISCUSSIONS**

The results from the particle size and chemical composition of UFP are presented followed by the best regression model found for each dataset correlating process and meteorological parameters to the concentration measured by OSA and EDA.

#### **6.3.1. Characterization of PM Under Study**

From the background available on the transient behavior of fine PM, the first task of the project was to characterize the aerosol under study. The result is presented in Figure 30. The PM has a monodisperse distribution with a median of aerodynamic diameter of 1.23 $\mu\text{m}$  from nine tests performed. The particles smaller than 1.24 $\mu\text{m}$  represent 78% of the mass distribution. When taking into account the number of particles, up to 93% of particles are smaller than 0.75 $\mu\text{m}$  leading to classify them as ultrafine particles (Soysal, et al., 2017).

Soysal et al. (2017) when discussing the challenges of measuring concentration for fine PM highlight that ELPI measures current in real-time but demands the previous knowledge of effective density. In this case, the effective density set on ELPI+ was  $1.36 \text{ g/cm}^3$  for ammonium nitrate compounds (Yin, et al., 2015).

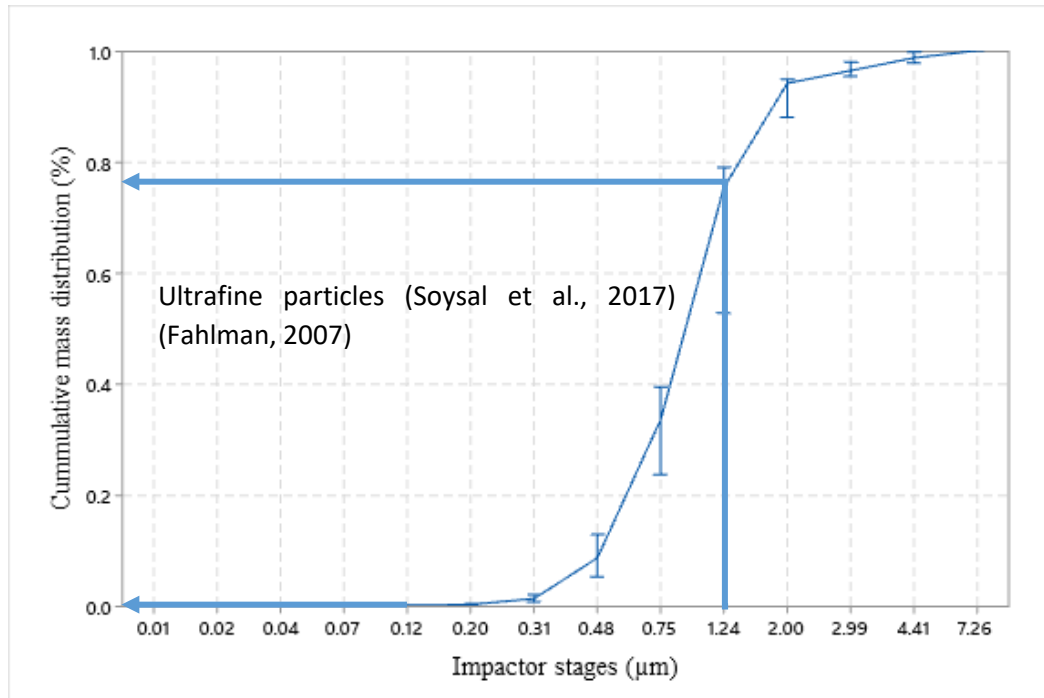


Figure 29 Cumulative particle size distribution of mineral fertilizer aerosol in each impactor stage (95% confidence interval for the mean).

Samples of the PM collected over a long test (5h sampling) were taken to SEM/ EDS in order to determine their composition, although only stage  $1.24\mu\text{m}$  gave significant results. The other stages contained very small amount of sample, even after 5h sampling time, that was not possible to determine its concentration.

Figure 31 (a) shows the foil under study. One of the agglomerates is showed on Figure 31(b) with 180 times magnification and a further increase to 1500 times magnification is presented on Figure 32 which one shows 3 different types of particles, marked as A, B and C. There is a region where the main area is covered by gray particle agglomerates (A). In the center of the image there are some potential single light-gray particles (B) and next to it some white agglomerate (C).

The chemical composition of the UFPs presented on Table 8 suggests that the main component here is ammonium nitrate what is in accordance to the effective density parameter inputted in the ELPI+ (area A). Area B has composition that potentially can be ammonium fluoride ( $\text{FNO}_3$ ) and silicon tetrafluoride ( $\text{SiF}_4$ ) in addition to the carbon, what can be originated

from the grease applied to the foil, to avoid particle re-entrainment, while area C shows the white crystal of ammonium chloride aggregated to a ammonium nitrate particle. In this area, the shape and color are similar to this crystal's description from the literature.

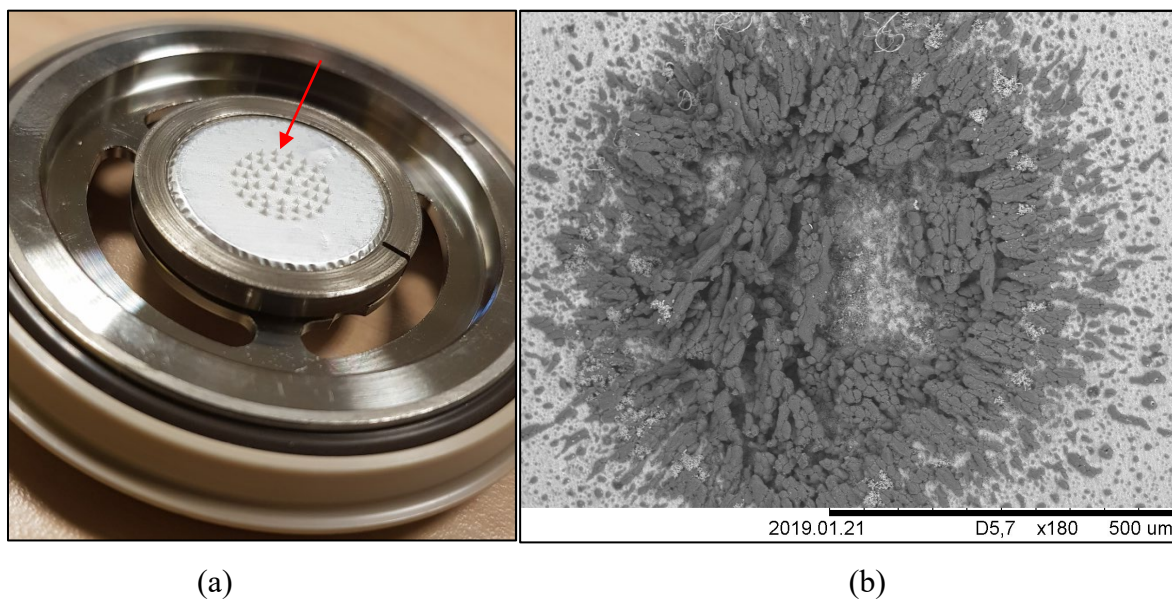


Figure 30 (a) Stage 1.24 $\mu$ m aerodynamic diameter support, aluminum foil, substrate and UFPs. (b) Magnification of 180 times of one of the UFP agglomerates.

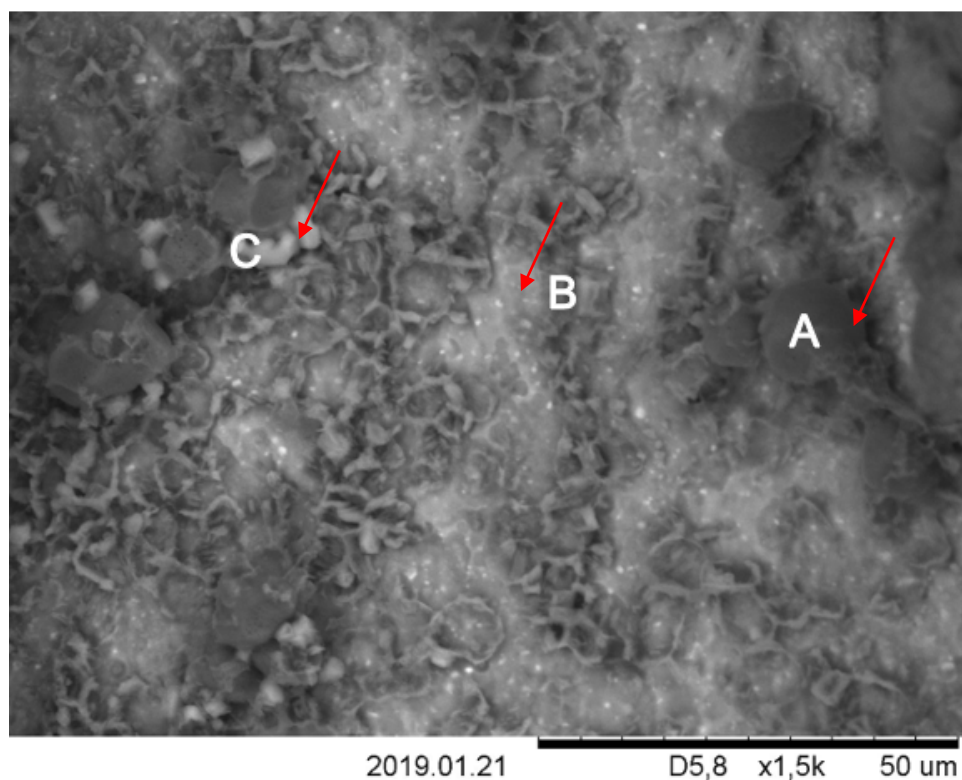


Figure 31 Magnification of 1500 times of UFP agglomerate with particles named as A, B and C.

Aluminum is excluded from the detected elements on Table 8 due to the aluminum foil (substrate). Besides that, no source of Aluminum is used in this plant. Later, the presence of Carbon was found to be due to the grease applied on the aluminum foil to ensure attachment of particles to the foil surface and avoid re-entrainment.

Table 8 Chemical composition of particles from stage 1.24 $\mu$ m

	A	B	C
Oxygen	47%	23%	13%
Nitrogen	36%	0%	33%
Carbon	15%	43%	0%
Chlorine	1%	2%	54%
Silicon	1%	6%	0%
Fluorine	0%	26%	0%

With the knowledge of the product composition under handling in the prilling tower having 21% nitrogen, 11% potassium, 6% phosphorous and 4.4% sulfur, no correlation was found with UFPs composition what leads to conclude that most part of the emissions come from the reactions in gas phase, once no phosphorous neither potassium was found on the chemical mapping of the emissions. Also, ammonium nitrate can evaporate, under equilibrium up to 50% of its mass, in size ranges from 1 to 2.5 $\mu$ m while ammonium sulphate up to 25% of its mass under same conditions (Wilson, et al., 2002), leading to potential large deviations when comparing concentration measured using ELPI+ with gravimetric sampling.

### 6.3.2. EDA UFP Concentration as a Function of Process and Meteorological Parameters

When correlating the process and meteorological parameters with the output of EDA, the best correlation result obtained was when employing Box-Cox transformation. This transformation employs an exponent, lambda, which varies from -5 to 5 and the optimal value is the one which results in the best approximation of a normal distribution curve. The optimal lambda found was equal to -0.40. The best results for transformed response were S at 0.28 mg/m<sup>3</sup> and r-squared of 9.49%. Table 9 shows the model coefficients found. Parameters as liquor and salts flow to PT, mixer rotation, bucket rotation and wind speed are not significant by the criteria here applied (significance level of 5%).

The resulting model can then be written as per Equation 4 including only the significant parameters.

$$-EDA^{(-0.40)} = -1.220 + 0.000680 \text{ NH}_3 \text{ to PT} + 0.001303 \text{ Off-spec flow to PT} + 0.000295 \text{ Liquor temperature} - 0.000123 \text{ Melt temperature} + 0.010916 \text{ Air temperature} + 0.04463 \text{ Precipitation} + 0.003288 \text{ RH\%}$$

Eq. 4

Table 9 Terms included in the EDA PM concentration model with significance level

Term	Coefficient	P-Value
Constant	-1.220	0.208
Liquor to PT	-0.000248	0.333
NH <sub>3</sub> to PT	0.000680	0.013
Salts to PT	-0.000237	0.480
Off-spec flow to PT	0.001303	0.044
Mixer rotation	0.000017	0.728
Bucket rotation	-0.00003	0.975
Liquor temperature	0.000295	0.004
Melt temperature	-0.000123	0.040
Air temperature	0.010916	0.000
Precipitation	0.04463	0.000
Wind speed	0.00135	0.359
RH% (relative Humidity)	0.003288	0.000

The standardized effect of meteorological parameters for EDA PM concentration model accounts for most of significance in the model (Figure 33). The reference line for the case when all the effects are null was found to be 1.96. The air temperature is by far the most significant parameter in the model, followed by RH% and precipitation.

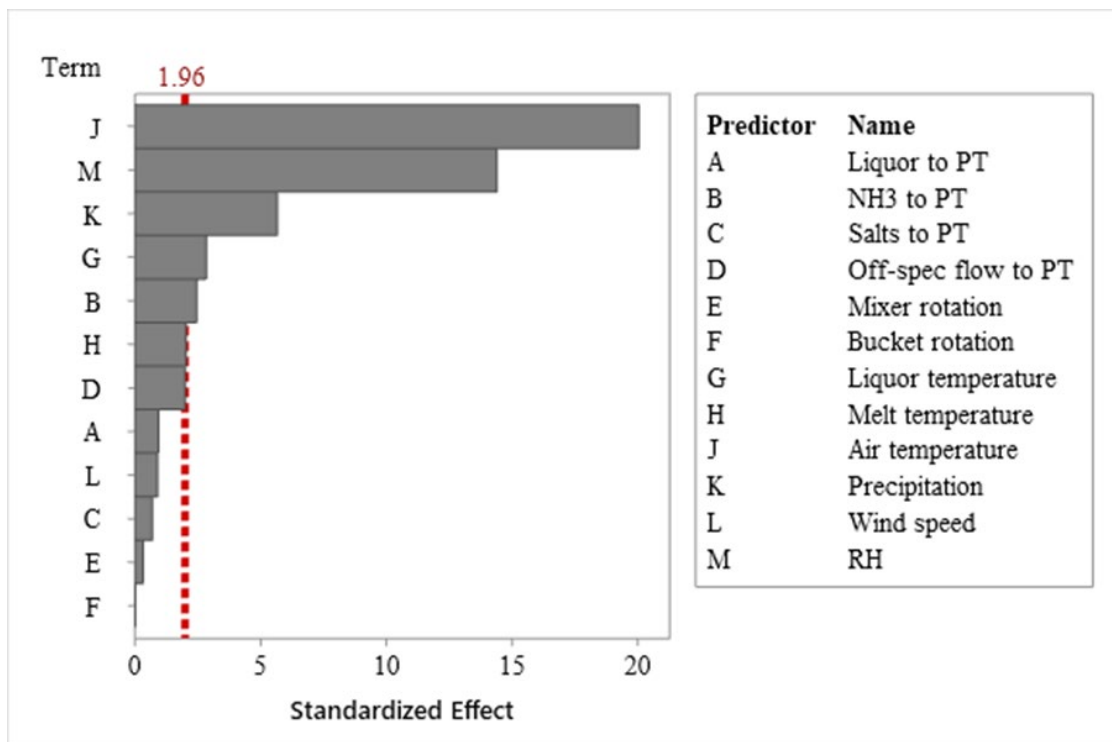


Figure 32 Standardized effect for EDA PM concentration for significance level of 5%



Only two process parameters have significance over the reference line, being liquor temperature and  $\text{NH}_3$  flow, what is not consistent to behavior found by other authors as Sequier et al. (2014), Couper et al. (2012), Yuan et al. (2007), Wong et al. (2004) and Shirley et al. (1996).

Once there is data available for the ambient air from the nearest meteorological station, not in the stack itself, it remains the question on if is RH% influencing or not the output of EDA.

The analysis of residuals (Figure 34) shows the difference between predicted values by the model and measured results. The residuals are basically dispersed in the range of -1 to +1. By employing the calibration factor of  $5.45 \text{ mg/Nm}^3$  to  $\mu\text{m}^3$  (which is the raw reading of the sensor EDA) the concentration variation is between 0 to  $20 \text{ mg/Nm}^3$ , what can indicate that some parameter is missing in the analysis. (Lee, et al., 2008).

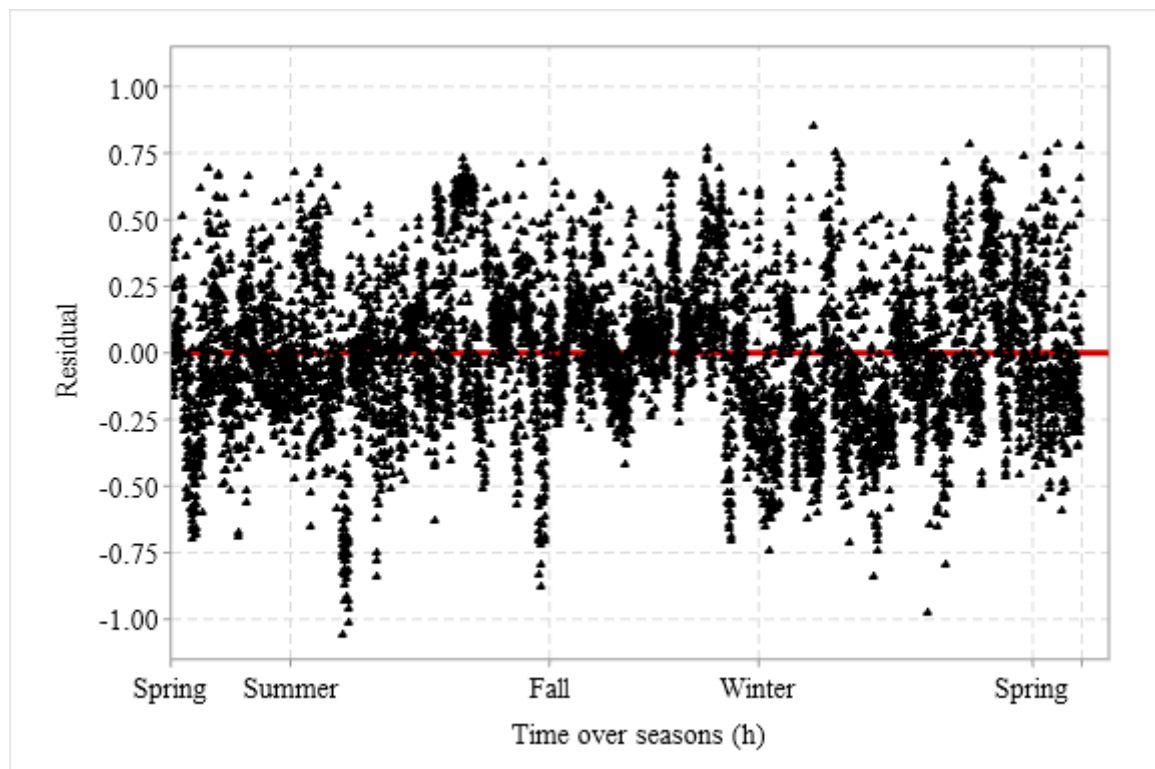


Figure 33 Residuals for EDA UFP concentration model over time

Based on the literature studied when building the model, no potential relevant variable was left aside that could explain such a poor fit of the model besides what was already mentioned for Figure 34 regarding the meteorological parameters monitored from the closest station.

Sullivan et al. (2018) point out that the electric field strength required to stably trap the particle provides an accurate real-time measurement if the charge state is known although tests

for single particles have being performed only on the range greater than 10  $\mu\text{m}$  in diameter. No similar study was found for UFPs by the knowledge of authors.

### 6.3.3. OSA UFP Concentration as a Function of Meteorological and Process Parameters

The best regression model for OSA PM concentration was obtained by Box-Cox transformation with lambda equal to 0 (natural log) where the standard error found was 0.72 (equivalent to 0.22  $\text{mg}/\text{Nm}^3$ ) and r-squared equal to 45.25% what can be considered promising results once in this process under study BAT emission is 5 $\text{mg}/\text{Nm}^3$  (Fertilizers Europe, 2000) and the standard error here found is equivalent to only 4.4% over the whole year monitored.

Also, the inclusion of the constant term in the model ensures that all non-explained effects are considered. When not including the constant term in the model the r-squared for the same data set would be 96.34%, although not realistic. Once no such model has been found in the literature, a comparison was made with authors studying ambient air modelling. Padoan et al. (2017) for example, found a r-squared of 74% when modelling road dust emissions with a much smaller data set while Xu (2018) found 60 to 80% r-squared using dust aerosol optical depth with PM10 results and Sieniutycz & Szwast (2018) with neural networks were able to predict PM10 with 75 to 86% r-squared and Denby et al. (2016) found r-squared of 28% when modelling PM10 in salt road emissions.

The coefficients obtained for OSA PM concentration model as a function of both process and meteorological parameters, are showed in Table 10.

P-value for  $\text{NH}_3$  flow to PT, mixer rotation and precipitation were over 0.05 so they are not considered significant by the criteria here applied and the model can be written as per Equation 5.

$$\begin{aligned} \ln(\text{OSA}) = & 16.69 + 0.007973 \text{ Liquor to PT} - 0.015599 \text{ Salts to PT} \quad \text{Eq. 5} \\ & + 0.00323 \text{ Off-spec flow to PT} - 0.01627 \text{ Bucket rotation} \\ & + 0.000591 \text{ Liquor temperature} + 0.000762 \text{ Melt temperature} \\ & + 0.08369 \text{ Air temperature} + 0.00893 \text{ Wind speed} + 0.007250 \text{ RH\%} \end{aligned}$$

The precipitation can be a contributor factor to RH% which one was significant in the emissions model for OSA, but not on its own, probably because of its irregular distribution over the area, once the weather station is located 1.2km far from the stack monitored. Besides that, the year under analysis presented a dry summer with no precipitation, what can be interpreted in the model as a constant parameter. The same applies to  $\text{NH}_3$  flow to the PT and the mixer rotation, once its little variation over time makes them not relevant for the model.

Table 10 Model coefficients for OSA PM concentration

Term	Coefficient	P-Value
Constant	16.69	0.000
Liquor to PT	0.007973	0.000
NH <sub>3</sub> to PT	-0.000552	0.441
Salts to PT	-0.015599	0.000
Off-spec flow to PT	0.00323	0.057
Mixer rotation	0.000077	0.549
Bucket rotation	-0.01627	0.000
Liquor temperature	0.000591	0.028
Melt temperature	0.000762	0.000
Air temperature	0.08369	0.000
Precipitation	0.0223	0.275
Wind speed	0.00893	0.020
Relative humidity (RH%)	0.007250	0.000

The transformation used to normalize the dataset when building the model seems to be adequate as can be seeing in Figure 35, where the red line is the model and the black triangles represent the residual when applying the model to the experimental results, if considered that this is an industrial application, not a controlled environment.

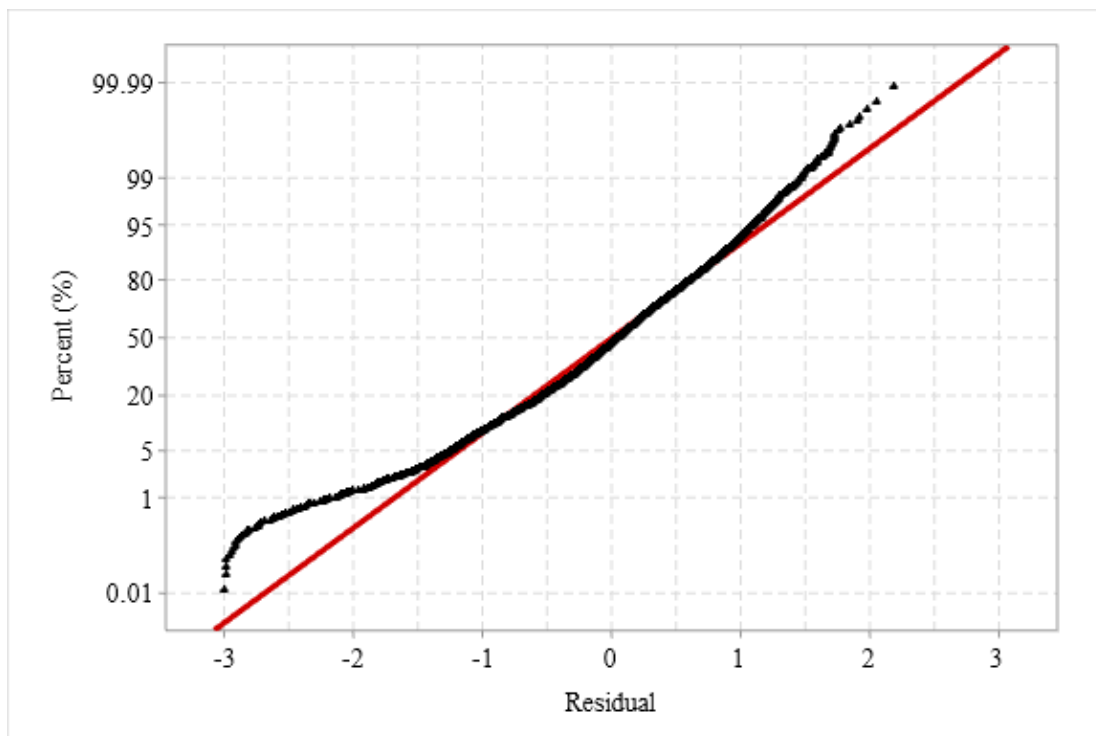


Figure 34 Probability plot of OSA model versus data set

The residuals presented a random distribution (Figure 36) what led to conclude the model has included most relevant parameters in the process, in the whole period, besides during fall and winter where there is a trend to underestimate PM emissions.

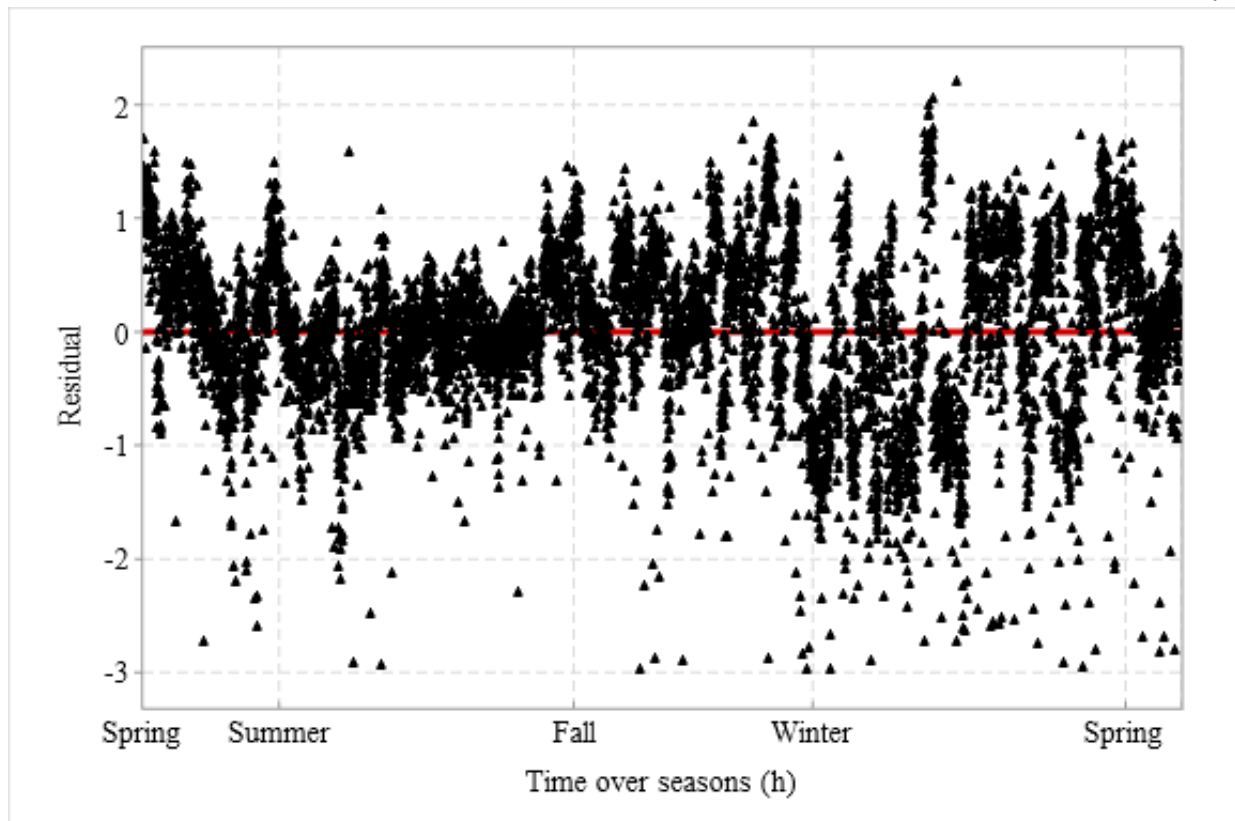


Figure 35 Residuals between OSA model and data sets

The residuals appeared to higher than for EDA (Figure 34) but the magnitude order is different once for OSA the correlation to  $\text{mg}/\text{Nm}^3$  is about 0.3 times while for EDA is 5.45 times.

Winter is a challenge for the model once during this season there is a trend of underpredicting the emissions. This behavior could be due to the gases thermodynamic properties. Winter time in northern Europe present often negative temperatures with low RH% and lower gas viscosity, leading the gas stream to have particles less agglomerated freely moving that could affect the sensor capacity to measure this very small UFPs considering that the wavelength of the optical sensor on OSA is 650nm.

Figure 37 shows that both process and meteorological parameters are included and relevant for the model. The reference line when all effects are null was found to be 1.96. With basically same behavior as found for EDA, the air temperature is by far the most significant parameter on the model, but here also the raw materials flow to the PT are showed as responsible for UFPs concentration showing that the optical sensor was able to measure this contribution.

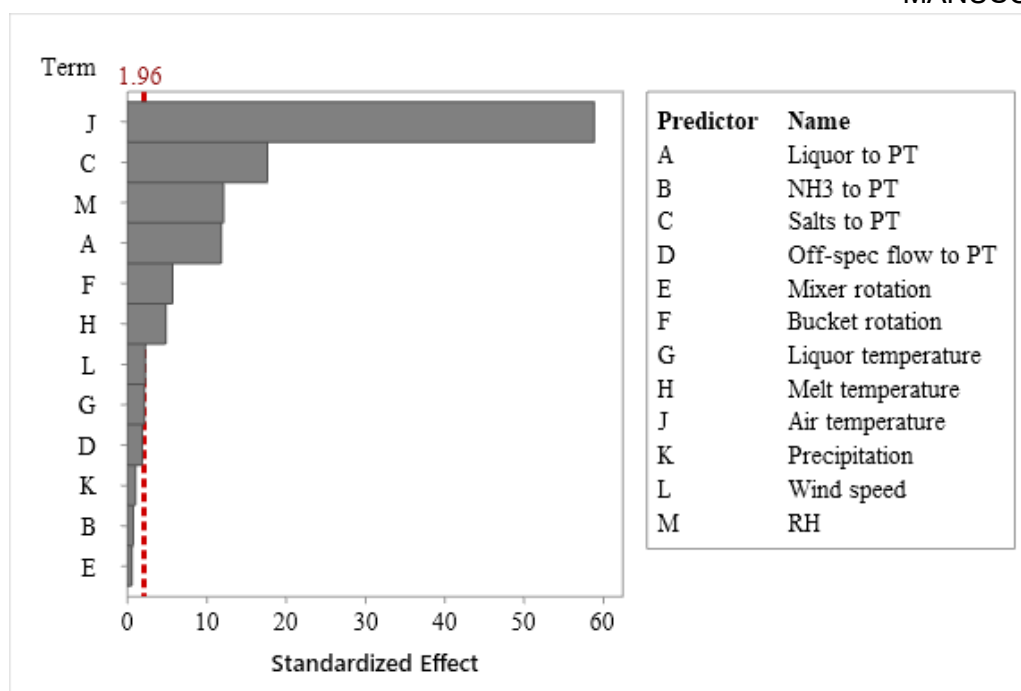


Figure 36 Standardized effects of parameters. Level of significance 5%

Gong et al. (2018) states that optical scattering have developed enough to be applied on understanding UFP changes in the environment they are inserted and Mitchem & Reida (2008) have studied the use of optical sensor to manipulate and characterize single particles in the range of 1 to 10 $\mu$ m.

#### 6.4. CONCLUSIONS

This project found out that the attempt to employ EDA to build a model correlating process and meteorological parameters was not successful, being the best regression model found using transformed response with optimal lambda equal to -40 giving a r-squared equal to 9.49% and standard error of 2 mg/Nm<sup>3</sup>. The most significant parameters in the EDA model were air temperature, RH% and precipitation, all meteorological parameters. The process parameters were at least one-degree order smaller than the meteorological ones.

On the other hand, the model designed employing all potential variables mapped and the OSA output presented a standard error of 0.22mg/Nm<sup>3</sup> and r-squared of 45.25%, equivalent to best models found in literature for ambient air application. The most relevant parameters in the OSA concentration model were air temperature, salts flow to PT, RH% and liquor flow to PT, respectively.

Particulate matter in the process studied was classified as UFPs and it was observed that its composition differs significantly from the product under handling due to reactions in gas

phase producing mainly unstable ammonium nitrate, ammonium chloride, ammonium fluoride and silicon tetrafluoride.

The current official methods employed to evaluate the calibration of continuous PM concentration sensors for stationary sources as gravimetric sampling is limited when dealing with UFPs. The actual concentration levels can be higher due to the instable compounds present so the use of equipment's with principles such ELPI+ should be adopted in addition to gravimetric sampling.

## 7. NEW METHODOLOGY TO MEASURE AND CALIBRATE ULTRAFINE PARTICLES EMISSION IN INDUSTRIAL PRILLING TOWERS

Elisangela Krauss<sup>1\*</sup>, Sander Wijnsma<sup>2</sup>, Monica L. Aguiar<sup>1</sup>

<sup>1</sup>Dept. of Chemical Engineering, University of Sao Carlos, Brazil

<sup>2</sup>Dept. of Chemical Engineering, Norwegian University of Science and Technology, Trondheim, Norway

[\\*krausselisangela@gmail.com](mailto:krausselisangela@gmail.com)

### Abstract

Among the processes that generate emissions of ultrafine particles (UFP) whose are known by their high potential to cause brain diseases when inhaled, the prilling towers have a significant contribution, once those processes use flow rates up to 10 times higher than other dryers. From the monitoring perspective, UFPs are generally instable and volatile (as the case of sulfates and nitrates) making its mass concentration hard to measure, especially if continuous mass monitoring is required. With this background, a controlled experiment was performed in an industrial fertilizer prilling tower to evaluate a potential methodology for continuous UFP monitoring in those environments. The dust emission was measured at stack of the prilling tower by two commercial continuous particulate matter instruments (optical scatter and electrodynamic diffusion charger) and the electrical low-pressure cascade impactor (ELPI), while running a second order design of experiments (DoE) and monitoring both meteorological and process parameters. Linear regression models were built for the three measuring techniques compared, but once raw material flows and meteorological parameters were kept stable, the commercial sensors did not provide accurate results. ELPI analyzer output presented a model with adjusted r-squared of 94.13% and a standard error of 0.02 mg/m<sup>3</sup>. The ELPI shows potential to be used as calibration device to other in-situ continuous dust monitoring when dealing with UFP if the methodology here proposed is applied. The continuous monitoring can be then implemented in the industries and optimization of the parameters performed to reduce the emission of UFP to the environment.

**Keywords:** Design of experiments; ELPI; Ultrafine particles; Industrial fertilizer; Continuous monitoring.

## 7.1. INTRODUCTION

Currently, the high-quality fertilizers are produced by prilling or granulation to get all the nutrients bound together granules or prills with high uniformity degree. This industry segment produced around 62 million tons of fertilizer based on ammonium nitrate (AN) in 2018 (IFA, 2019). The particulate matter (PM) emitted by those plants consists mainly of particles in the range of 0.1 to 2.5 $\mu\text{m}$ , called ultrafine particles (UFP) (Fahlman, 2007).

In the ambient air UFP can be inhaled, get to the lungs and to the blood system, what can cause degenerative brain diseases, as such Alzheimer, Parkinson and Huntington (Maher, et al., 2016) (Win-Shwe & Fujimaki, 2011) to such an extent of concern that the World Health Organization (WHO) works in a new guideline for concentration of particulate matter with a diameter smaller than 1 $\mu\text{m}$  (PM1.0).

In previous research by Krauss & Aguiar (2019) the challenges of continuous monitoring of UFP on industrial prilling towers were evaluated and the authors observed that the calibration of the sensors employing the usual gravimetric sampling (GS) methodology (EPA, 2019) provided inconsistent results over time, due probably to variations associated to transient and volatile UFP present at stack.

Later the authors employed regression models (Chapter 6) to correlate the reading of the continuous monitoring sensors to process and meteorological parameters, as employed for ambient air studies (Kalaiarasan, et al., 2018) (Dias, et al., 2016) (Li, et al., 2017), (Tchepel, et al., 2012), concluding that for optical scattering the raw materials did have some influence on the UFP mass concentration as expected but the main parameter impacting was the air temperature fed to the tower. On the other hand, the electrodynamic principle had output severely affected by relative humidity and presence of droplets in the stream, not qualifying for long term continuous monitoring.

Based on the explained above, the goal of this project was to propose and test a methodology under industrial conditions to continuously measure and calibrate the UFP concentration employing ELPI associated with commercial continuous monitoring sensors.

Knowing beforehand that an industrial process is subject to many variations over time a design of experiments was employed associated with measuring and monitoring of both meteorological and process parameters. At the same time, PM concentration was measured using three different techniques, forward optical scattering (OSA), electrodynamic diffusion charger (EDA) and electrical low-pressure cascade impactor (ELPI).



7.2. MATERIALS AND METHODS

7.3. Process Description

A typical process flow diagram of the NPK prilling process is showed in Figure 38, where the main equipment are evaporators, mixer, prilling bucket, prilling tower (PT) and screening. Here liquid, solid, and gas streams are illustrated using blue, brown, green arrows, respectively and measured/adjusted parameters are circled in red.

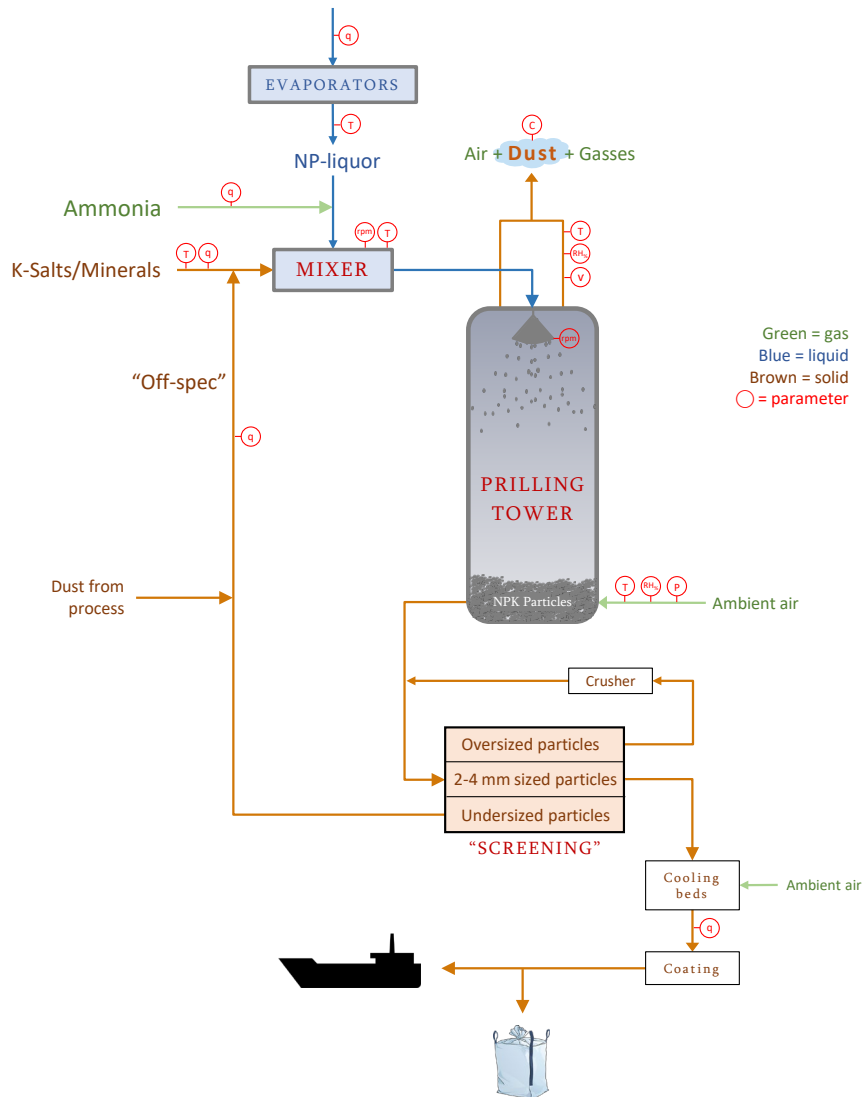


Figure 37 Process flow diagram of NPK prilling process

The raw materials (NP-liquor, ammonia, K-salts/minerals) enter the mixer as a three phase (gas, liquid, and solid) mixture that needs to be intensively agitated to create a homogeneously mixed melt and to prevent solidification. This melt is thereafter sent to a rotating prilling bucket that sprays the liquid melt into the PT. Therefore, the melt solidifies creating an uniform spherical particles with a diameter of 2-4 mm. The falling droplets are

cooled by ambient air in counter-current flow that is dragged by using fans located at the outlet stacks at the top of the tower. After solidification, the prills must be separated by particle size in the screens. The oversized particles are sent to a crusher and then back to the screening while the undersize particles (called off-spec) are sent back to the mixer together with dust collected from bag filters of other process equipment (Fertilizers Europe, 2000).

The particulate matter (PM) emitted from the stack is mainly composed by particles that are dragged up by the upward velocity inside the stack (diameter of 1700mm) and are mainly ammonium nitrate ( $\text{NH}_4\text{NO}_3$ ) that is produced from a side reaction in gas phase between the acidic melt and the ammonia that is added in the mixer.

### 7.4. Proposed Methodology

The methodology proposed here will be tested following the steps described in Figure 39. For the characterization of PM, in this application the PSD of the UFP will be defined based on ELPI measurements while the estimate chemical composition using SEM/EDS (scanning electron microscopy energy dispersive x-ray spectroscopy). This step was done previously in Chapter 6.

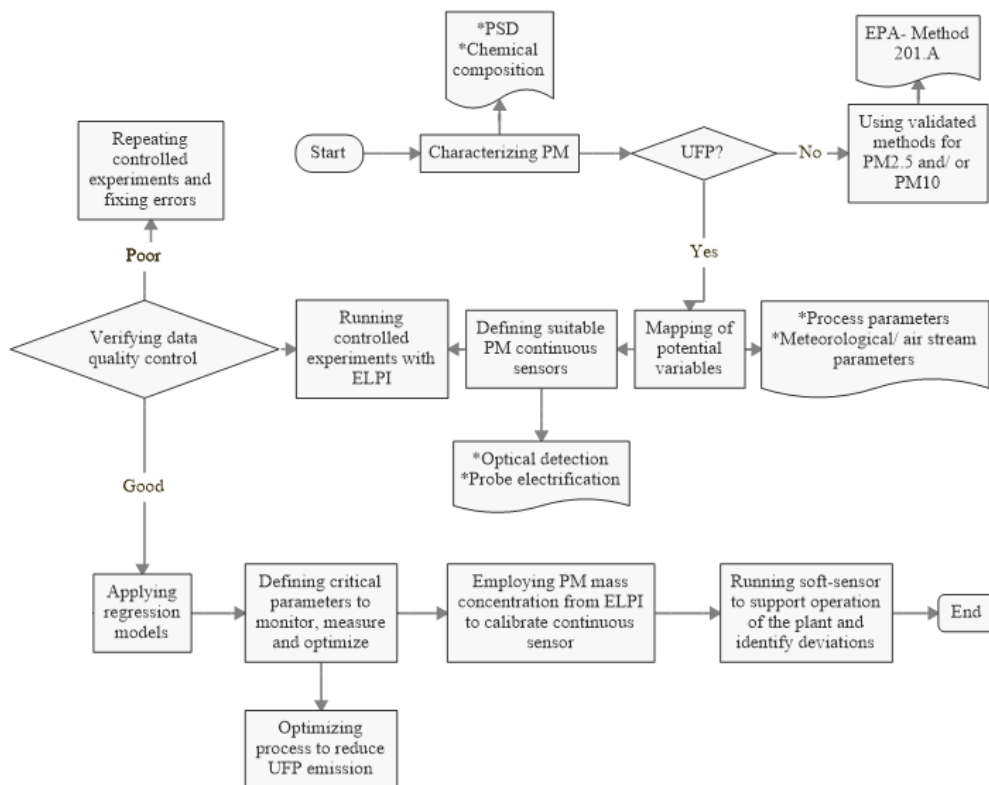


Figure 38 Proposed Methodology to Continuous Measure UFP in PT

The mapping of potential process and meteorological variables affecting the generation and change of the UFP composition was performed using the concept of volume of control generating the list showed on Table 11 where the process parameters were collected from the distributed control system of the plant (DCS). The melt containing nitrogen and phosphorus is here called NP-liquor.

Table 11 Parameters mapped from the volume of control

Type of parameter	Parameter description	Unit	Source
	Date	text	DCS
	Time	text	DCS
Process parameters	Off-spec flowrate	t/h	DCS
	NP-liquor temperature	°C	DCS
	Flowrate of salts	t/h	DCS
	Flowrate of NP-liquor	m <sup>3</sup> /h	DCS
	Flowrate of NH <sub>3</sub>	kg/h	DCS
	Flowrate of product	t/h	DCS
	Temperature of salts	°C	DCS
	Temperature of mixer	°C	DCS
	Mixer rotation	rpm	DCS
	Bucket rotation	rpm	DCS
	Inlet temperature	°C	DCS
Manually sampled parameters	Inlet relative humidity	%	Testo 440
	Inlet temperature	°C	Testo 440
	Stack relative humidity	%	Testo 440
	Stack temperature	°C	Testo 440
	Stack velocity	m/s	Kimo 210
Meteorological parameters	Barometric pressure	hPa	Druck 705
	Air temperature	°C	Meteor. Station
	Relative humidity	%	Meteor. Station
	Precipitation	mm	Meteor. Station
	Wind speed	m/s	Meteor. Station
Output of dust analyzers	ELPI	mg/m <sup>3</sup>	Instrument
	OSA*	mg/m <sup>3</sup>	Instrument
	EDA*	mg/m <sup>3</sup>	Instrument

\* The output of the OSA and EDA dust analyzers was used as raw data, without applying any calibration factor.

Parameters as ambient temperature and relative humidity (RH) were manually measured using Testo 440 (probe head of 290mm long with diameter of 12mm and measuring range was from 0 to 100% RH, ±2% RH accuracy and -20 to +70°C, ±0.5°C accuracy), while velocity inside the stack was manually measured with Kimo 210 (range from 2 to 100m/s, accuracy of ±0.2 m/s) and pressure with Druck 705 (range of -200 to 200 mbar, accuracy of ±0.1%) where the average velocity over the whole diameter of the stack was measured at 8 points. These manual measurements were done at the beginning of each experiment.

The PM continuous monitoring instruments employed were OSA model PCME QAL 181, which one had a certification range of 0-15mg/Nm<sup>3</sup> and measurement capability of 0-300mg/Nm<sup>3</sup> and EDA model PCME STACK 980 which had a certification range of 0-15mg/Nm<sup>3</sup> and measurement capability of 0-500mg/Nm<sup>3</sup>.

The second order design of experiments was performed using Minitab 19<sup>®</sup>. The type of factorial design chosen was a full factorial design with a low, medium and high value of the two adjusted process parameters. One center point and two replicates were chosen to improve the statistical significance of the results obtained.

For the second order design of experiment was needed to define two parameters to be adjusted in the process to see the influence of those on the dust emissions while keeping the already known effects of raw materials and ambient air temperature as stable as the industrial application allowed (as concluded from Chapter 6). The criteria for parameters selection was that no deviation in productivity levels or product quality was caused by the experiment, the candidate parameter must had a wide enough operability range to see the effect of those changes in the process and finally, the parameters needed to be adjusted relatively fast from one run to the next.

Based on the criteria mentioned, from the flow rate parameters available the only candidate parameter was the off-spec flowrate while from the remaining list from Table 11 only the NP-liquor temperature met the criteria. To adjust the off-spec flowrate and NP-liquor temperature, it was defined the operational range (minimum and maximum) of those two parameters. Therefore, a check was done in the prescribed operating range for the product under analysis and consultation to the operational plant team.

The standardized values for the adjusted parameters were 5.15 to 7.15 t/h of off-spec flowrate and 89 to 91.5°C for the NP-liquor temperature. The middle point was calculated based on arithmetic average.

The resulting design of experiment obtained from Minitab19<sup>®</sup> is illustrated in Table 12. The design was duplicated under same product composition but in different days, both in summertime. A period of 13 minutes of data collection was registered once the plant was considered operating under each setup of parameters. All the data was recorded in a minute-weighted average besides meteorological parameters from the near station which ones were recorded and made available once an hour.

The electrical low-pressure impactor (ELPI) plus from Dekati (2020) was used to measure the particle size distributions (PSD) and mass concentrations in the size range of 6 nm-

10 $\mu$ m coupled to a co-polymer particle dryer (DD-600) and nozzle for isokinetic of 10 l/min. The sampling point was located 12 diameters over the PT top and 3 diameters below the gas stream exits to the atmosphere.

Table 12 Design of Experiment from Minitab19®

Standard Order	Run order	Off-spec flowrate [t/h]	NP-liquor temperature [°C]
8	1	7.15	91.5
4	2	7.15	91.5
3	3	5.15	91.5
5	4	5.15	89
2	5	7.15	89
1	6	5.15	89
9	7	6.15	90.25
6	8	7.15	89
7	9	5.15	91.5

The data quality check was performed using Minitab19® employing normality tests, outliers test and test for equal variances. Furthermore, the same software was employed to build the linear regression models, using transformed response when the resulting model provided a better fit (considering standard error and r-squared).

## 7.5. RESULTS AND DISCUSSION

Here the results obtained from the application of the methodology are presented and discussed. The steps to evaluate the quality of the data collected are described in details to explain which set of variables was included on the model.

### 7.5.1. Data Quality Control

#### 7.5.1.1 Checking for outliers in the parameters set

Figure 40 shows the variation of the off-spec flow rate over the 18 runs performed. The deviation from the setpoint (given by red values) is higher for the high off-spec flowrate setpoint of 7.15 t/h compared to the lower setpoint of 5.15 t/h, what indicates that running under lower flow of off-spec gives more stability to the operation. To achieve this is needed to apply the lean manufacturing concepts to reduce generation of off-spec in the process (Ellis, 2020) so, the lower flow rates are feasible. Besides that, there is a deviation per experiment, due to the

operator in-charge as can be seeing among experiments #1 with smaller range while #2 has a broader operating range. The same behavior can be seeing from experiments 10 and 11.

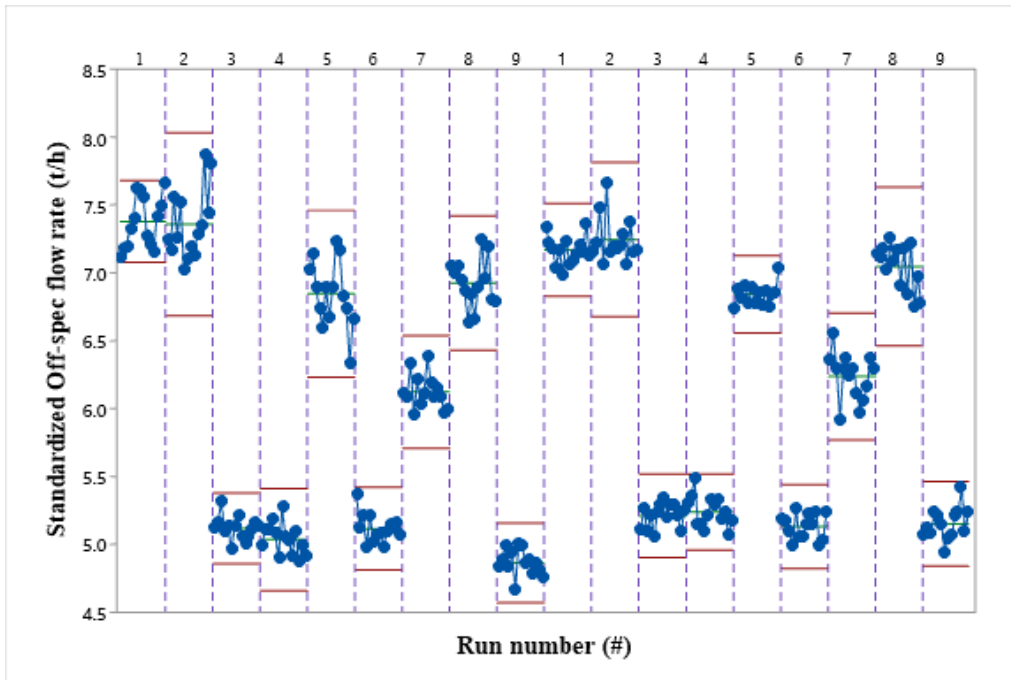


Figure 39 Standardized off-spec flowrate per run (9 runs each campaign) for the two campaigns performed

Figure 41 illustrates that the deviation from the set point of the NP-liquor temperature (given by red values) for each experiment it is much smaller than the deviation for the off-spec flowrate (Figure 40).

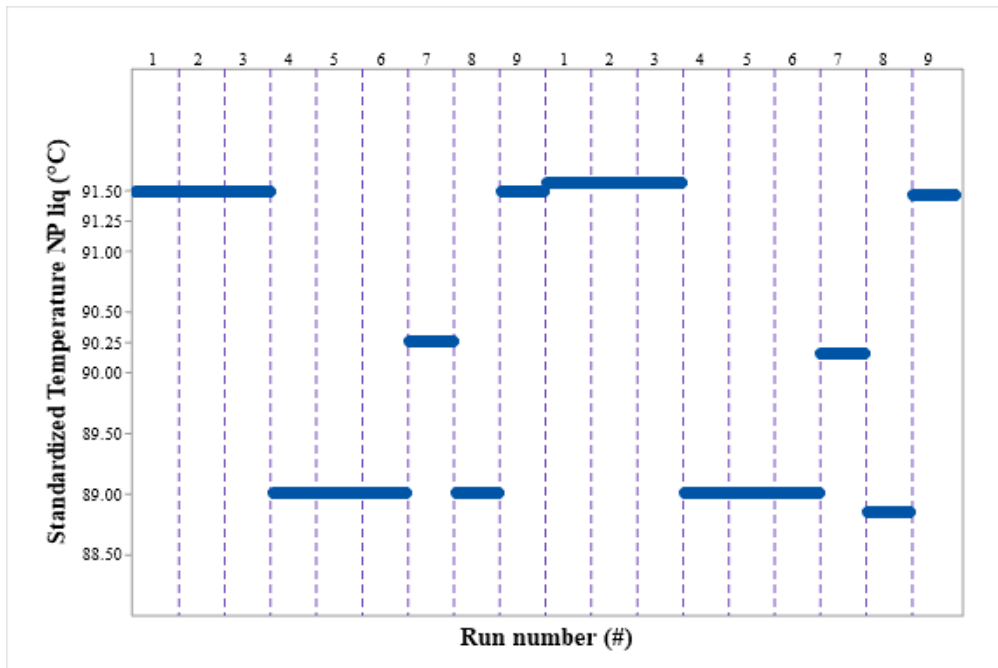


Figure 40 Standardized NP-liquor temperature per run (9 runs each campaign) for the two campaigns performed

All setpoints for the NP-liquor temperature, low/medium/high, were easily reached and kept around the setpoint. This indicates that the NP-liquor temperature could potentially be used for modelling and optimization of dust emissions if required.

The outliers test performed for the monitored parameters was performed and besides in some of the runs, the mixer temperature and mixer speed presented outliers, it was indeed operating conditions of the plant, so these data sets were kept for further modelling. Also for the K-salts temperature and bucket speed, there were points that indicated that the process conditions were stable and kept for the duration of the experiment, what means that they were a different process condition employed.

### 7.5.1.2 Test for normal distribution

To evaluate normality of the raw material flows, a ratio between each flow to the product flow at the boundary of the control volume was calculated and the results showed in Figure 41, where the blue data set refers to the K-salts flow rate, the green data set to the NP-liquor flow and red data set to the NH<sub>3</sub> flow rate. Most part of data fits a normal distribution with an exception for the lower flow rate ratios, responsible for about 10% of data set, originated during the last two experiments where a product flow scale was calibrated during operation and the recorded value on the DCS was based on mass balance not actual weight.

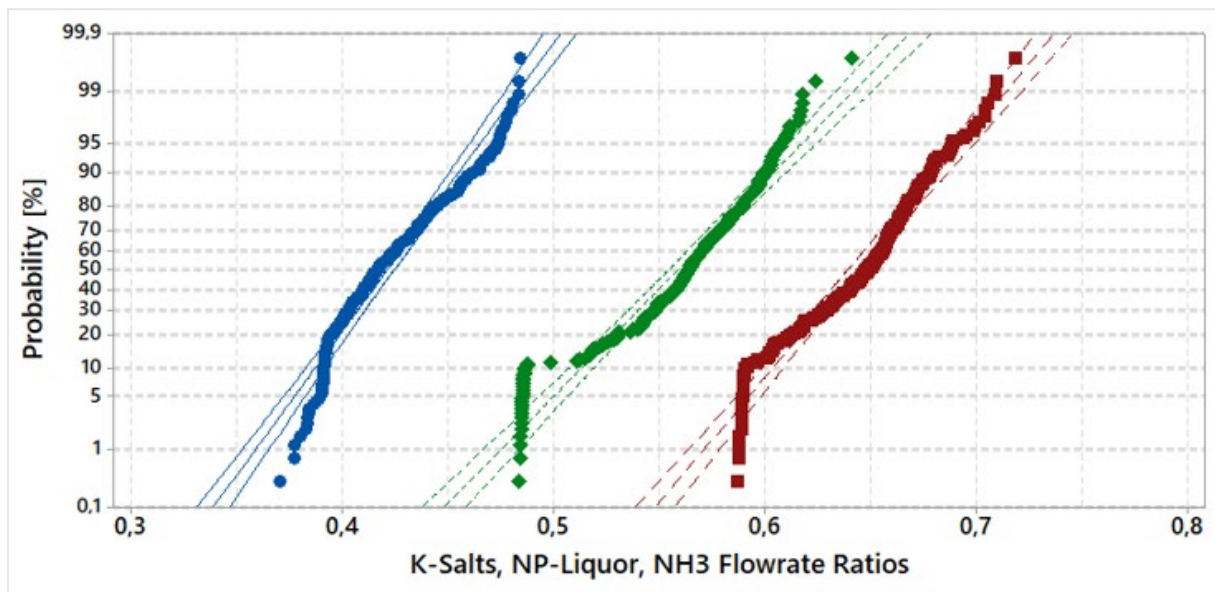


Figure 41 Probability plot for the flowrate ratios of raw materials to the final product

For the flowrate ratio of K-Salts (in blue), the deviation was caused between experiments 5 and 9 of experimental set of runs #1 which is the period after calibration of the salt silo weighing system.

### 7.5.1.3 Potential use of meteorological station data

A potential use of data from the nearest meteorological station was evaluated. The results for the temperature can be seen on the test for equal variances showed in Figure 43. The air temperature measured at nearest meteorological station is statistically different than the one measured at inlet of PT once the standard variation ranges represented by the external boxes do not overlap. The standard deviation on the data collected from the meteorological station presented a standard deviation of  $1.49^{\circ}\text{C}$  while from the plant the standard deviation of  $1.75^{\circ}\text{C}$ . It is an expected result once the data from the meteorological station is available based on hourly averaged data.

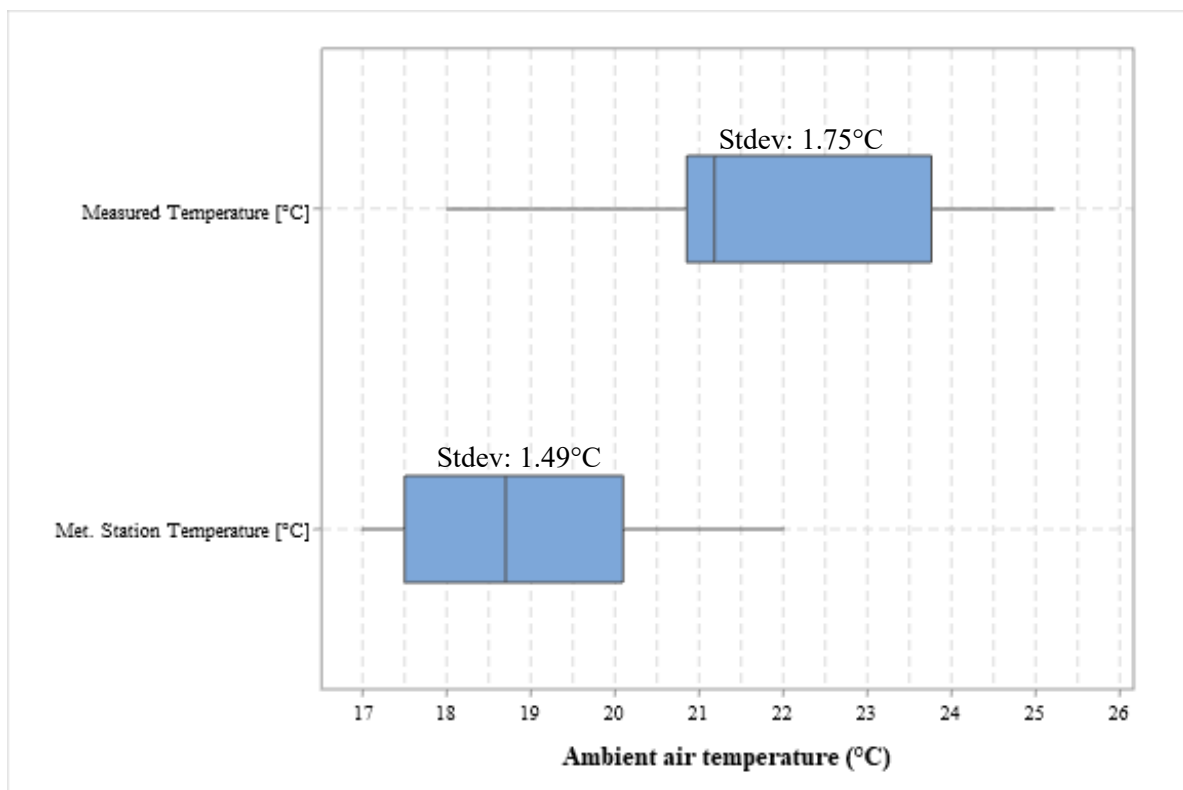


Figure 42 Test for equal variances on air temperature considering normal distribution with confidence level of 97.5%

The same tests were performed for relative humidity and the results are presented in Figure 44. The hypothesis here tested was at the RH measured at inlet of PT was statistically equivalent to the one measured at the meteorological station but the result showed that they are not equivalent. Besides the position of the box shows that they have ranges that overlap each other, the median for the meteorological station was 45% while for the inlet of the tower was 40%.

When comparing the confidence intervals for it can be seen that for the meteorological station RH the result was 8 to 10 intervals while for the inlet of PT was 7 to 8 intervals. Once



again, the RH data from the nearest station it is significantly different from the data measured at the plant, even being the station just 1.2km away from the PT. In the statistical analysis it is shown that the results collected from the station during run #8 of second campaign are outliers but they were kept in the database once they were actual results from the nearest station.

Still on Figure 44 the stack RH is displayed to evaluate if it has the same range variation as outside although the results show that the variation inside the stack is smaller than outside with confidence intervals from 2.8 to 3.4 intervals. Based on those figures, the first choice should be measuring the RH inside the stack to correlate it with the UFP concentration measured at stack by the online sensors. If that is not possible so the RH should be measured at inlet of the PT.

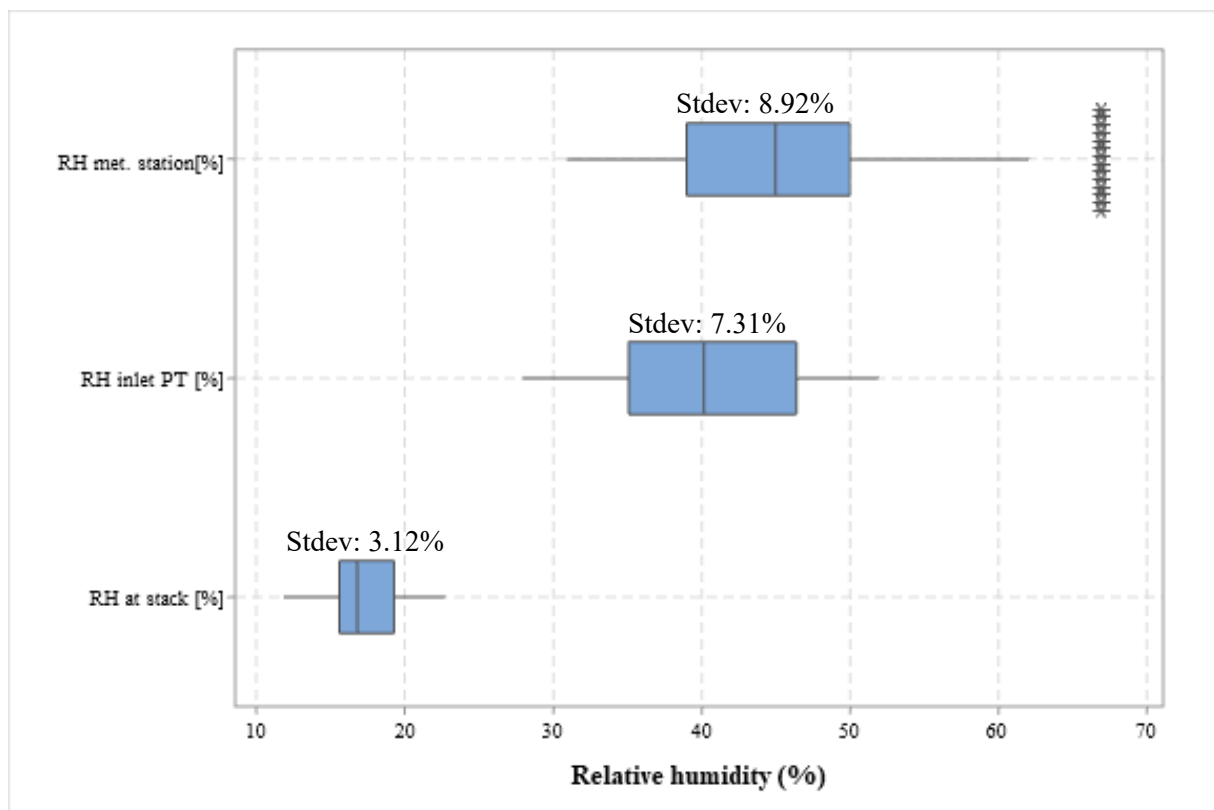


Figure 43 Test for equal variances on relative humidity with confidence level of 98.3% considering normal distribution

### 7.5.2. Linear Regression Models Generated

The linear regression models obtained for the three dust analyzers are therefore based on specific 13 minutes operation periods and parameters from the process and manual measurements. A summary of the regression models from Minitab® is given in Table 13. The r-squared determines how well the regression model fits the database analyzed, while adjusting

for the number of predictors in the model relative to the number of observations, being able to compare models that have different numbers of predictors.

From Table 13 the regression models obtained for the OSA/EDA dust analyzers give a low value for r-squared and a high standard error. On the other hand, the r-squared obtained from the ELPI model was 94.13% and has a standard error of only 0.02 mg/m<sup>3</sup>.

Table 13 Summary of quality parameters generated by the regression models from ELPI/ OSA/ EDA

<b>Instrument</b>	<b>R-squared (%)</b>	<b>Standard error (S) mg/m<sup>3</sup></b>
OSA	10.75	0.61
EDA	64.58	0.16
ELPI	94.13	0.02

### 7.5.2.1 ELPI PM concentration model

The LRM built with ELPI data presented a 94.13% of measured data fitted to the model and small standard error (0.02 in an average emission in this specific plant of 15mg/Nm<sup>3</sup>) what shows that the equipment was able to measure the UFP emission variation when the process parameters have just slightly changed, once the conditions were controlled in terms of season and product type.

From the p-values given in Table 14, it can be seeing that NH<sub>3</sub> flow rate, mixer temperature, wind speed, air temperature and RH% does not have enough significance on the ELPI output, once here the acceptance criteria defined is so that significance level of each parameter has to be over 95%, incurring in p-value smaller than 0.05). The air stream parameters were not identified as significant in the model what can be due to the sample being extracted and dried before analyzing it so the ELPI setup was able to avoid the impact of the air stream conditions.

The significant parameters from this controlled experiment are the off-spec flowrate and the temperature of NP-liquor, pointing that the choice of adjustable parameters was adequate. Besides that, the flow rate of NP-liquor, temperature and flow of K-salts as well as mixer and bucket rotation speed were included in the model due to their significance level.

This suggests that under controlled situation, small changes to those parameters can have strong effect on the mixer temperature. This effect is related to the liquid viscosity change as explained by Partridge et al. (2005) and Wong et al. (2004).

Table 14 ELPI regression model coefficients and significance

Term	Coefficient	P-Value
Constant	-5.94	0.00
Flowrate Off-spec	0.01	0.00
Temp. NP-liq.	0.02	0.00
Flowrate K-Salts	-0.02	0.00
Flowrate NP-liq.	0.01	0.01
Flowrate NH <sub>3</sub>	0.01	0.14
Temp. K-Salts	0.08	0.00
Temp. Mixer	-0.01	0.67
Bucket speed	0.03	0.00
Mixer speed	-0.01	0.00
Air Temperature	0.01	0.05
Wind speed	0.00	0.88
Relative Humidity	-0.06	0.54

The model equation can be written as Equation 6 below, eliminating the terms with low significance level from the Table 14.

$$\begin{aligned}
 -ELPI^{(-0.13749)} = & -5.94 + 0.01 * \text{Flowrate Off-spec} + 0.02 * \text{Temp. NP-liq.} & \text{Eq.6} \\
 & - 0.02 * \text{Flowrate K-Salts} + 0.08 * \text{Temp. K-Salts} + 0.03 * \text{Bucket speed} \\
 & - 0.01 * \text{Mixer speed} + 0.01 * \text{Flow rate of NP-Liq.}
 \end{aligned}$$

Figure 45 shows the normal probability plot where the majority of the data sets follow the linear regression model (red straight line). The points with high deviation from the predicted values are discussed with data from Figure 46, where the residuals over the sequence of runs is presented.

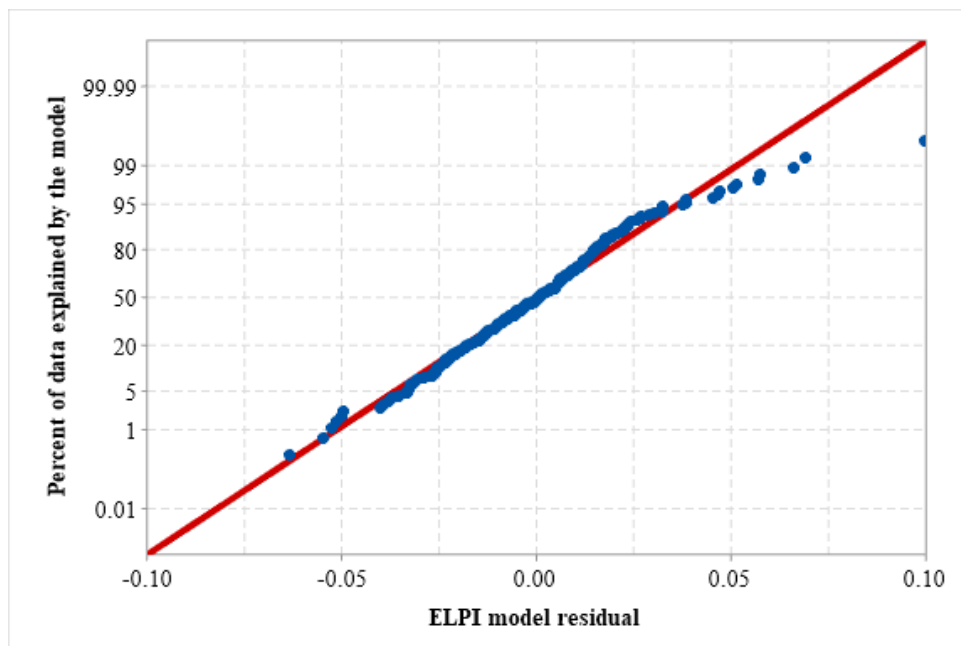


Figure 44 ELPI linear regression model

The model has predicted lower emission than the experimental value obtained for experiment #4, in both runs. This can be due to parameter standardized temperature of K-salts which have reduced from 19°C to 18°C from first run #4 to the second so the model have considered this parameter as significant but the spot variation was over the expected range, what could be due to calibration problems with the temperature probe or a change performed at the salts dryer not monitored in the set of parameters defined.

Between runs #4 and #5, on the second set, the model has presented a residual twice the magnitude order than the other runs, over 0.05mg/m<sup>3</sup>. While run #4 was affected by the K-salts temperature, run #5 was performed with high flow of off-spec and low NP-liquor temperature leading to low mixer temperature. At this moment the melt started to solidify inside the mixer. While ideally the UFP emission has decreased considerably, at beginning of run #5 the process became instable and the emission has increased being followed by a required stop to clean the mixer and bucket holes. This confirms that the ranges for the adjustable parameters were stretched enough.

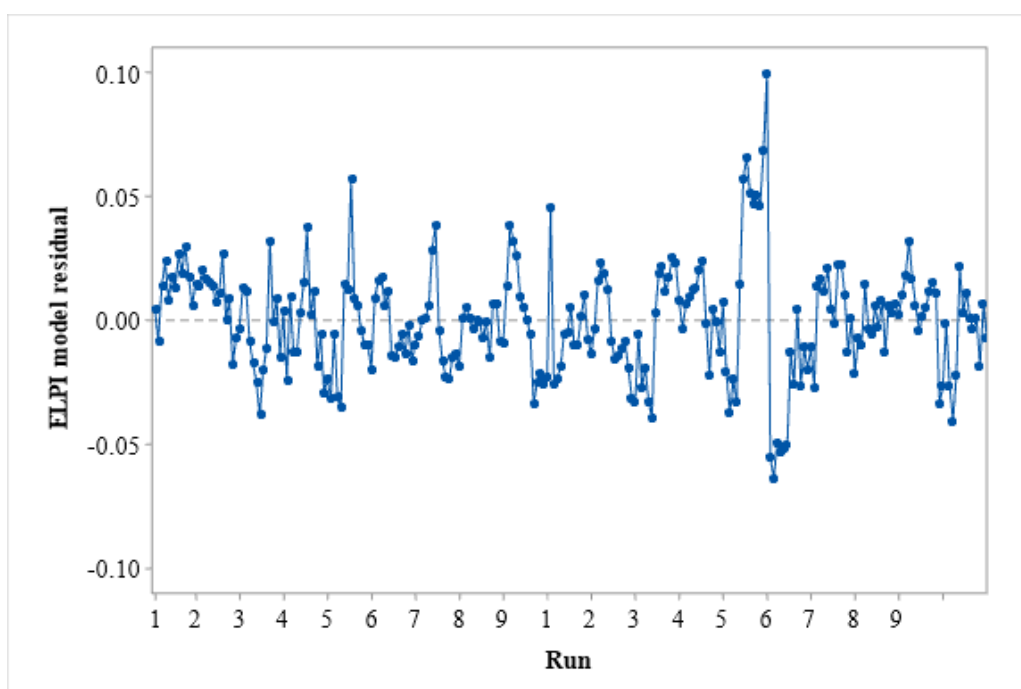


Figure 45 Residuals over time for ELPI regression model (18 experiments data set)

From these findings there is potential to get the calibration factors from ELPI to the continuous sensors, instead using GS, once it has being showed in research from Wilson et al. (2002) and Giechaskiel et al. (2014) that the losses due to presence of nitrates and sulfates can be up to 45% when applying gravimetric sampling.

There is although a remark to be done regarding the use of ELPI for mass concentrations, the estimation/ measurement of effective density. In this work, the effective density set to ELPI was  $1 \text{ g/cm}^3$ , as default recommendation by the equipment supplier (Dekati, 2020). Extensive measurements have found for AN combined with ammonium sulfate the effective density can vary from  $1.36$  to  $1.55 \text{ g/cm}^3$  depending on the PSD (Yin, et al., 2015). If taken into account the conversion from aerodynamic diameter to stokes diameter (as standard from the environmental agencies), applying the conversion equation from Allen & Somerscales (1982) the difference obtained represents 15 to 20%, meaning that the average aerodynamic diameter here measured, when converted to stokes diameter is equal to  $1 \mu\text{m}$ , smaller than the figures here showed.

### 7.5.2.2 Commercial *in-situ* sensors concentration model

Previous work presented in Chapter 6 have shown that PM concentration from both OSA/EDA are influenced by raw materials flow rates and air stream parameters to a certain extent. Once those were kept as stable as possible in this controlled experiment it is expected that no strong correlation is found with those parameters in the modelling process. There is although a remaining question regarding the stream/ meteorological parameters which ones now are measured at the PT air inlet, not employing average hour data from the nearest station, as the experiments conducted in Chapter 6.

The Table 15 shows the level of significance obtained with the best LRM fit for both commercial *in-situ* sensors. Only flowrate of K-Salts and mixer speed were parameters considered significant for OSA output what can be attributed to the resolution of the equipment, both because it has a very small opening where the particles are in contact with the laser either because the laser wavelength has a limitation for particles with diameter smaller than  $560\text{nm}$  (Babick, 2020), (PCME, 2018). On these runs the PSD measured was from 20 to 40% of particles smaller than  $600\text{nm}$  in mass distributions. If the distribution is taken in terms of number of particles the PSD is equivalent to around 70 up to to 90% particles smaller than  $600\text{nm}$ .

On the other hand, the model obtained for EDA, had a positive agreement with humidity, as Table 15 shows, so potentially humidity or droplets could be affecting the reading of the instrument, what has being observed previously on Chapter 6. The humidity had a coefficient 4.5 times higher than the second most relevant parameter that is the flow rate of  $\text{NH}_3$  fed to the mixer. Both flow rate of NP-liq. and temperature of the mixer were not significant.

Table 15 OSA/EDA PM concentration model coefficients

Term	Coefficients		P-Value	
	OSA	EDA	OSA	EDA
Constant	-172	16.23	0.08	0.05
Flowrate Off-spec	-0.24	0.04	0.34	0.04
Temp. NP-liq.	0.01	-0.11	0.96	0.00
Flowrate K-Salts	0.89	0.21	0.01	0.00
Flowrate NP-liq.	0.10	0.051	0.81	0.12
Flowrate NH <sub>3</sub>	-0.29	0.57	0.72	0.00
Temp. K-Salts	-0.53	0.17	0.34	0.00
Temp. Mixer	-0.11	-0.04	0.74	0.19
Bucket speed	0.15	-0.29	0.70	0.00
Mixer speed	0.35	0.05	0.04	0.00
Air Temperature	-0.35	-0.07	0.37	0.02
Wind speed	-0.62	-0.38	0.23	0.00
Humidity	-3.38	2.55	0.69	0.00

The residuals for OSA model are showed in Figure 47 over the two sets of experiments (#1 to #9, both runs) and besides having a low r-squared (10.75%), it can be observed that on experiment #5 OSA also presented a low measured UFP concentration, the same behavior observed for data from ELPI (Figure 46). In this case, the OSA was able to see the reduction of the emission, but once the process was unstable, when running under the same conditions for experiment #6, the resulting UFP concentration has increased and the sensor did not follow the change.

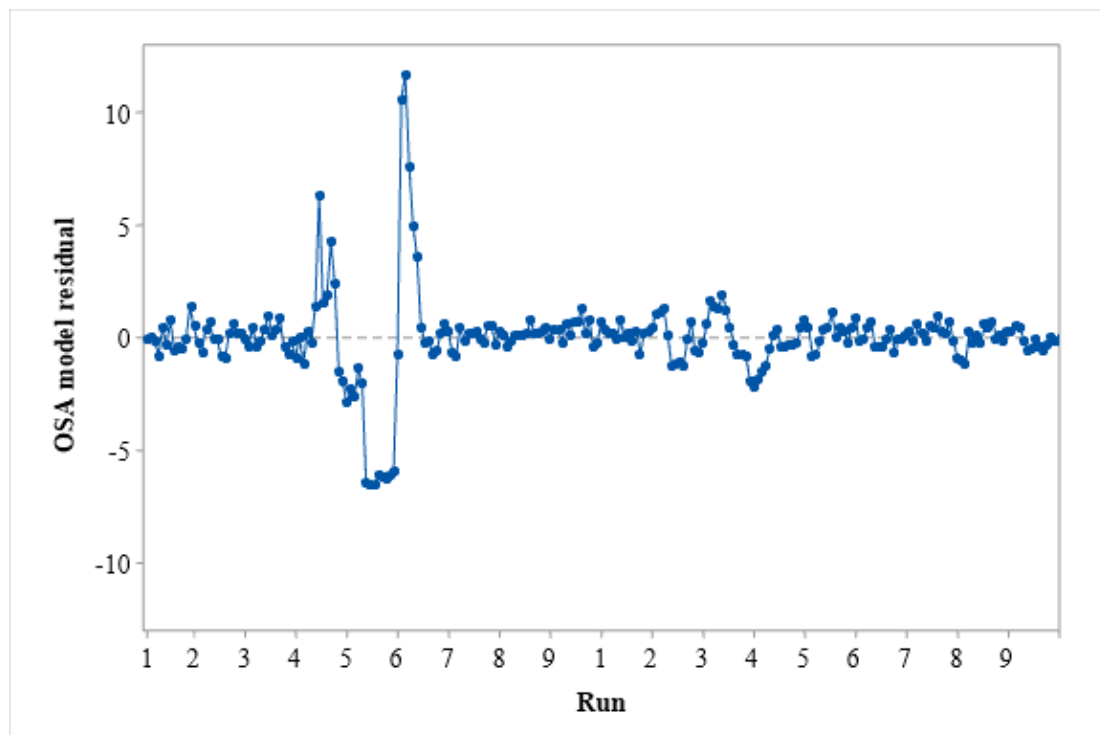


Figure 46 OSA linear regression model residuals

The model obtained with EDA presented a r-squared of 64.58% with a standard error of  $0.16 \text{ mg/m}^3$ . If it is applied a calibration factor of 6.25 as Krauss & Aguiar (2019) have found, this becomes  $1 \text{ mg/Nm}^3$  or 20% of the BAT level of  $5 \text{ mg/Nm}^3$  (Fertilizers Europe, 2000). The residuals presented in Figure 48 shows peaks on experiments #1 and #3, which can be due to wind speeds of about  $4 \text{ m/s}$  in the first set of experiments while for the second set the wind speed was  $1.5 \text{ m/s}$ , with all the others monitored parameters stable. The same behavior is observed on run #8, second set of experiments, where the model again underestimates the UFP concentration. The only parameter diverging from the first to the second set of experiments was the relative humidity. The second run #8 was performed under relative humidity of 67% while on the first set of experiments the relative humidity was 43%.

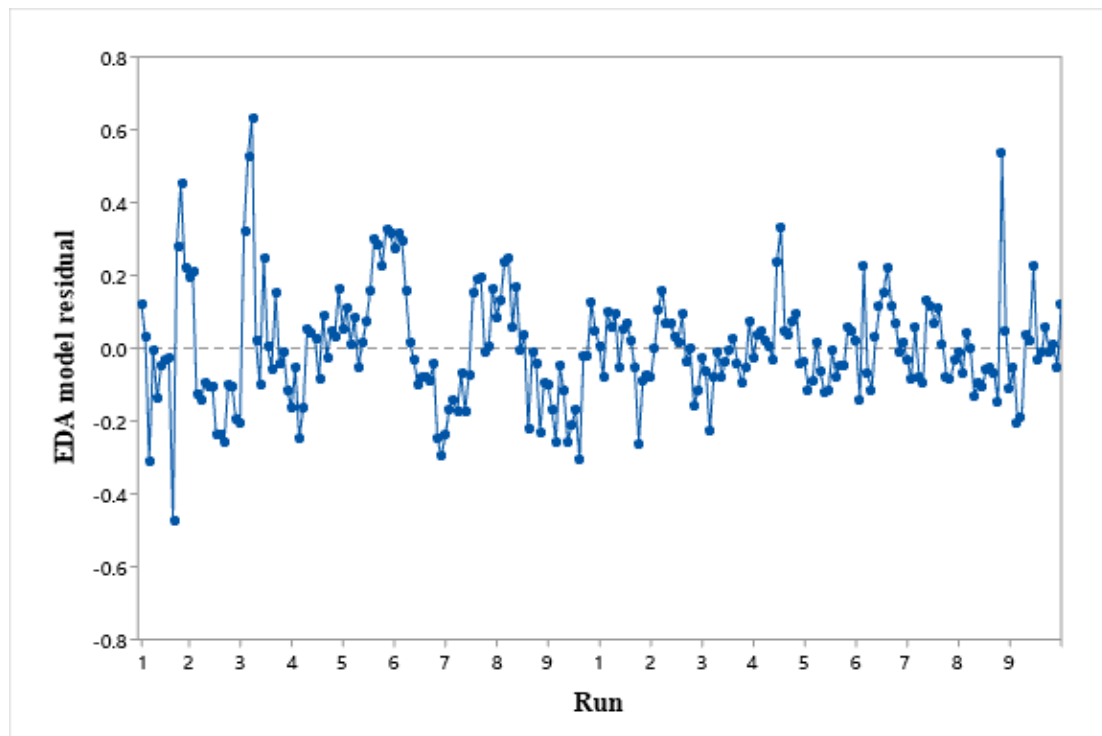


Figure 47 EDA model residuals over the experiments

From the data collected and analyzed, it appears that the EDA have a higher sensitivity to changes in the air stream during the experiments than OSA, what is somehow observed in Chapter 6. The model from EDA delivered a better model than OSA when conditions as flow rates and season are kept stable, although the effect of the humidity on the sensor output has to be studied further if it is intended to install this technique for continuous monitoring once there is potential to provide false positive indication of the PM concentration.

### 7.5.3. Application of the model to recommend actions to reduce dust emission

Based on the data obtained from the controlled experiment, the ELPI output and the significant variables found in the model it is possible to evaluate the process to reduce the UFP emission. This is illustrated by Figure 49 where both off-spec flowrate and temperature of NP liquor are combined to provide areas where different levels of PM concentration are reached. The dark blue area represents the operational window to achieve emissions less than  $2\text{mg}/\text{m}^3$ , the blue area 2 to  $4\text{mg}/\text{m}^3$  and the light blue area, 4 to  $6\text{mg}/\text{m}^3$ . It can be seen that the operating range to have medium-low dust emissions ( $< 6\text{mg}/\text{m}^3$ ) is broad while the operating range to have the low dust emission ( $< 4\text{mg}/\text{m}^3$ ) is narrow and can easily start safety problems in the form of blockage of the system and further an increase in dust emission.

The lowest dust emission is obtained when the operating conditions for standardized data are low NP-liquor temperature (less than  $89^\circ\text{C}$ ) and high off-spec flowrate (6.7 to  $7.5\text{t}/\text{h}$ ). The reason found is the change on the melt viscosity, affecting the surface tension properties of the melt and preventing the generation of the secondary droplets (that are much smaller than the prills) as concluded by Partridge et al. (2005) when modelling the break-up of curved liquid jets in PT and Wong et al. (2004) when modelling drop size distributions created from spiralling liquid jets.

The combination of these two parameter setpoints although will result in a strong reduction of the mixer temperature (off-spec is cooling medium, NP-liquor is heating medium) which, as was observed, can easily solidify the melt and obstruct the mixer outlet. Once the melt starts to solidify inside the mixer it is observed that the dust emission increases, so this combination of setpoints needs to be prevented.

It is a very narrow area where levels of PM concentration can be kept below  $2\text{mg}/\text{Nm}^3$  but from the other hand, it is possible to run in the whole range of temperatures and still reach PM concentrations less than  $6\text{mg}/\text{Nm}^3$  what is close to the best available technique in the AN based fertilizer plants (Fertilizers Europe, 2000). Off-spec flow rates should be kept below  $6.2\text{t}/\text{h}$  to ensure optimal operation. Besides out of the scope of this work it is known that lower levels of reprocessing material are desirable in process that aim to reduce waste according to Lean manufacturing principles (Ellis, 2020).



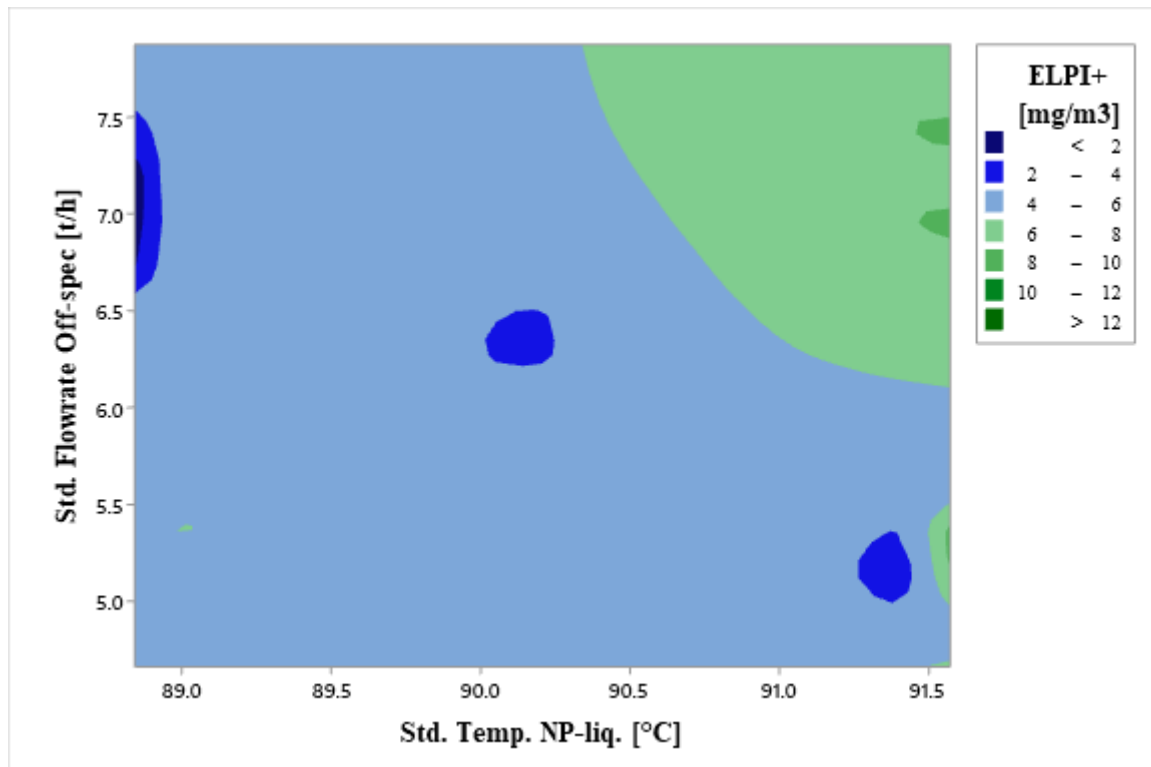


Figure 48 ELPI measurement vs off-spec flowrate and NP-liquor temperature

The blue circles inside the main light blue area can potentially be “sweet spots” (most optimized operational conditions) although the range is so small that could be hard to keep the process under those conditions, especially if considered that conveyor belt scales employed in this process do not have enough accuracy to measure between 6.2 to 6.5t/h, as discussed on item 7.5.1.

Once the ELPI model have identified also other significant monitored parameters, it is possible to evaluate scenarios to reduce the emissions by adjusting those as showed on Figure 50. The color-coding follows the same standard as Figure 49. It can be seeing that for the bucket speed there are 2 “sweet spots” where emission levels below  $2\text{mg/m}^3$  can be reached if the K salts temperature is kept on the lowest range (17 to  $17.8^\circ\text{C}$ ).

The results from this controlled experiment have a good agreement with the literature (Couper, et al., 2012) (Yuan, et al., 2007) once higher rotation speed from the prilling buckets can lead to production of micro-spheres and then, instead of falling and cooling down they can be dragged by the fans out of the stack. This behavior was also observed in recent simulations done by Saleh et al. (2016). It is although, less clear how the salts temperature affect emission.

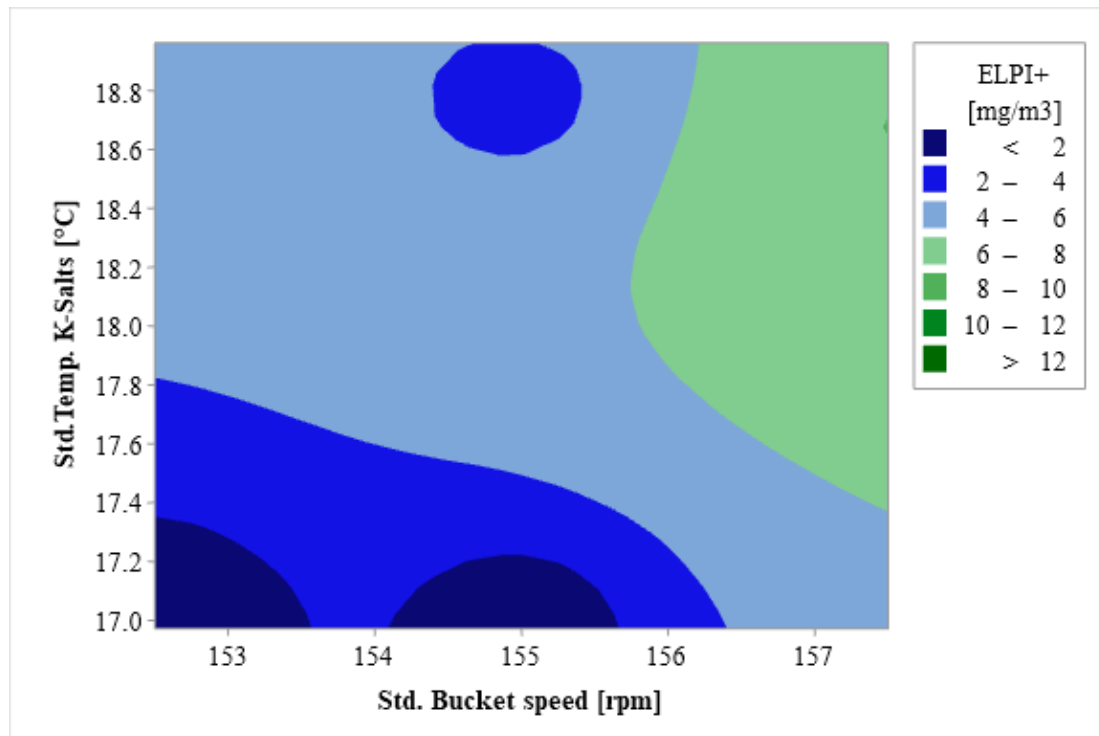


Figure 49 ELPI PM concentration vs K-salts temperature and bucket speed

Higher mixer temperatures have been correlated to increased emissions before, due to the melt viscosity as previously discussed but the model here developed have discarded the mixer temperature due to the low significance. A potential cause could be that the inlet streams to the mixer are taken into the model and the remaining effect of the mixer itself, which one does not lose or gain temperature is annulated.

The last two sets of significant parameters are mixer speed and flowrate of K-salts, being the last one dependent on the product type so, there is no physical consistency on optimizing it, specially because there was calibration performed to this stream between the runs.

## 7.6. CONCLUSION

The main goal of testing a methodology for continuous monitoring of UFP in the industrial fertilizer prilling tower was achieved once following the steps was possible to build a transformed linear regression model for ELPI with 94.13% r-squared and a standard error of 0.02 mg/m<sup>3</sup>. This accuracy if compared to best available techniques for fertilizer prilling is equal to 0.4% (Fertilizers Europe, 2000). In this sense, the ELPI can be used to calculate calibration factors for OSA/EDA analyzers to make online UFP monitoring feasible in this field.

The results obtained can be due to the fact that ELPI analyzer is an extractive technique while the OSA/EDA tested were in-situ measurements. Also, ELPI proved to be very accurate in measuring both the particle size distribution and dust concentration besides detecting changes that are an order of magnitude smaller than that of the OSA/EDA dust analyzers. This feature was used to find optimal sets of operational parameters where the emission of PM could be kept below  $6\text{mg}/\text{Nm}^3$ .

It was investigated the possibility of using data from the nearest meteorological station in the model, instead of at the air stream inlet, but the test for equal variances proved that this is not possible, once neither the ranges nor the mean was the same between the data sets. So, it is needed to install temperature, velocity and relative humidity measurement devices at the inlet of the air stream.

This study has focused on PM mass concentration for UFP and use of commercial sensors, but with ELPI there is opportunity to employ the number concentrations and use the results to optimize the process. In this sense, the issue with the determination of a reliable effective density is eliminated.

## **8. GENERAL CONCLUSIONS AND RECOMMENDATION FOR FUTURE WORKS**

This research project aimed to develop a methodology for continuous monitoring of ultrafine particles emissions in industrial stacks as its main goal. The methodology was proposed, tested and validated for monitoring ultrafine particles in industrial stacks, under the range of measurement of ELPI (6nm to 10 $\mu$ m).

In terms of performance of commercial sensors it can be concluded that both analyzers can follow variations in the process if they are kept clean, what is easier to be diagnosed on OSA since it shows the need for cleaning through the span test results (span less than 75% here employed). In terms of response for sudden huge changes in PM concentration at the stack, the EDA represented better and faster the process behavior while the OSA presented normal output what can be due to the difference of the reading range of the instruments (0-500 mg/Nm<sup>3</sup> for EDA and 0-300mg/Nm<sup>3</sup> for OSA).

The build-up of product influences the reading of both analyzers, requiring cleaning every 15 days of operation in fall to up to three months on winter.

The calibration factors generated by GS for OSA presented up to 0.5 standard variation over both seasons and products while EDA was much poorer with up to 4 standard deviation over seasons and 3 standard deviations among products.

This project found out that the attempt to employ EDA to build a model correlating process and meteorological parameters was not successful, being the best regression model giving a r-squared equal to 9.49% and standard error of 2 mg/Nm<sup>3</sup>.

On the other hand, the model designed employing all potential variables mapped and the OSA output presented a standard error of 0.22mg/Nm<sup>3</sup> and r-squared of 45.25%, equivalent to best models found in literature for ambient air application, once there is no such a study from stationary source, by the knowledge of the authors. The most relevant parameters in the OSA concentration model were air temperature, salts flow to PT, RH% and liquor flow to PT, respectively. These highlight the challenges of continuous PM concentration monitoring in mineral fertilizer industry for compliance purposes, where the standard is GS, being optical scattering the most promising technique.

Particulate matter in the process studied was classified as UFPs (90% of PM below diameter of 1 $\mu$ m) and it was observed that its composition differs significantly from the product

under handling due to reactions in gas phase producing mainly instable ammonium nitrate, ammonium chloride, ammonium fluoride and silicon tetrafluoride.

The controlled experiment run where season and product type were kept as stable as the industrial operation allowed, showed that OSA did not provide a regression model (r-squared less than 11%), what shows that the sensor does not have sensitivity to such small variations but also is not affected by other sources of noise from the air stream. On the other hand, EDA provided a model with 64.58% r-squared where still stream parameters have the higher coefficients as the case of relative humidity that had a coefficient 4.5 times higher than the second significant term in the model.

ELPI was able to follow the process changes with reliability, once the model build had a r-squared of 94.13% and standard error of 0.02mg/m<sup>3</sup> (equivalent to 0.4% of BAT levels in the segment evaluated). The most significant parameters were those selected from the design of experiments, off-spec flow rate and temperature of NP liq. but also small changes on the bucket and mixer speed, temperature and flow rate of K-salts were included in the model. Finally an example of how to optimize the process reducing the UFP emission to the environment was presented, from which can be concluded that the plant is able to run in a relative wide range of parameters and still reach BAT standards (Fertilizers Europe, 2000).

All the efforts to reduce air pollution should be prioritized, particularly the UFP, once it is proved that they are associated to increased serious health problems. In this context this research project contributes to the development of accurate measurements of UFP through continuous monitoring, allowing the optimization of the process to reduce the concentration of UFP to the environment. Besides that, by applying the methodology it is possible to provide reliable information to the environmental agencies, who can drive initiatives to improve the air quality.

Once the build-up of product influences the reading of the *in-situ* OSA, a potential solution to avoid intensive inspection and maintenance can be reached by testing of optical forward scattering cross-stack technology.

A potential application for EDA could be the use as a start-up and shutdown instrument, once it is sensitive to sudden high concentrations of PM and it is an affordable instrument while optical scattering can be used under operating conditions.

While ELPI has detected small changes in the process, has measured the concentration of UFP and was not influenced by the stream parameters, it is recommended to use it to calculate the calibration factors for OSA analyzer. So, accurate online UFP monitoring can become

feasible for prilling towers. In this specific case, the calibration factor needs to be found for each product type. The model can also be used to design a so-called soft sensor, detecting changes in the process affecting emissions with potential use for reporting online PM concentration to authorities.

The suitability of this proposed methodology getting approval by the environmental authorities could be reached by testing it simultaneously with gravimetric sampling to define, for instance a adjust factor, if that is required. Besides that, the ELPI has a feature that allows weighing each stage to calculate the mass concentration, so this data could be compared to the results from GS. It is although important to mention that different sources of errors would be associated, as the handling of such small sample and the precision of scales.

Once this study has focused on PM mass concentration for UFP from ELPI, there was included a potential error source, the determination of a reliable effective density. This effect can be eliminated if the ELPI is used to optimize the process because in this approach, the number concentrations could be employed.

## 9. BIBLIOGRAPHIC REFERENCES

Abreu, G. C. et al., 2007. Visibility control of main stack plume at CST sinter plant: a scientific approach. *Revue De Metallurgie-cahiers D Informations Techniques*, , 104(9), pp. 380-383

Alizadeh, A. & Omrani, H., 2019. An integrated multi response Taguchi- neural network-robust data envelopment analysis model for CO2 laser cutting. *Measurement*, Volume 131, pp. 69-78.

Allegrini, F. & Olivieri, A. C., 2020. Chemometrics and Statistics: Neural Networks. In: *Encyclopedia of Analytical Science*. third ed. s.l.:s.n., pp. 487-498.

Arffman, A. et al., 2014. High-resolution low-pressure cascade impactor. *Journal of Aerosol Science*, Volume 78, pp. 97-109.

Allen, T. & Somerscales, E. F. C., 1982. Particle Size Measurement (Third Edition). *Journal of Engineering Materials and Technology-transactions of The Asme*, , 104(2), pp. 155-155.

Arffman, A. et al., 2014. High-resolution low-pressure cascade impactor. *Journal of Aerosol Science*, Volume 78, pp. 97-109.

B. D., F., 2007. *Materials Chemistry*. s.l.:Springer.

Babick, F., 2020. *Dynamic light scattering (DLS)*. [Online] Available at: <https://sciencedirect.com/science/article/pii/B9780128141823000109> [Accessed 16 7 2020].

Balamurugan, K. et al., 2019. Predicting correlations in abrasive waterjet cutting parameters of Lanthanum phosphate/Yttria composite by response surface methodology. *Measurement*, Volume 131, pp. 309-318.

Benyounis, K. Y., 2019. Procedure of Conducting an Experiment Using Response Surface Methodology. In: *Reference Module in Materials Science and Materials Engineering*. s.l.:s.n., pp. 1-9.

Boulila, A. et al., 2019. Optimization of manufacturing complex-shaped gas turbine blades. *Measurement*, Volume 135, pp. 768-781.

Brachert, L., Mertens, J., Khakharia, P. & Schaber, K., 2014. The challenge of measuring sulfuric acid aerosols: number concentration and size evaluation using a condensation particle counter (CPC) and an electrical low pressure impactor (ELPI+). *Journal of Aerosol Science*, Volume 67, pp. 21-27.

Bras, W. & Hammel, M., 2019. Scattering Methods and their Application in Colloid and Interface Science. By Otto Glatter. Elsevier, 2018. Paperback pp. 404. Price USD 225. Paperback (ISBN 9780128135808), ebook (ISBN 9780128135815).. *Journal of Applied Crystallography*, 52(1), pp. 243-244.

Bréchet, T. & Tulkens, H., 2009. Beyond BAT: Selecting optimal combinations of available techniques, with an example from the limestone industry. *Journal of Environmental Management*, 90(5), pp. 1790-1801.

Chandra, S. & Bhattacharya, J., 2019. Influence of temperature and duration of pyrolysis on the property heterogeneity of rice straw biochar and optimization of pyrolysis conditions for its application in soils. *Journal of Cleaner Production*, Volume 215, pp. 1123-1139.

Chen, D. et al., 2019. The impact of ship emissions on PM<sub>2.5</sub> and the deposition of nitrogen and sulfur in Yangtze River Delta, China. *Science of the Total Environment*, pp. 1609-1619.

Colver, G. M., 1999. Electrostatic Measurements. In: *Instrumentation for fluid-particle flow*. s.l.:Noyes Publications. Published by Elsevier Inc., pp. 47-111.

COM, 2007. *Best Available Techniques (BAT) Reference Document for the Manufacture of large volume chemicals: ammonia*, s.l.: JRC IPTS EIPPCB.

Couper, J. R., Penney, W. R., Fair, J. R. & Walas, S. M., 2012. Dryers and Cooling Towers. I: *Chemical Process Equipment*. 3rd red. s.l.:s.n., pp. 223-275.

Couper, J. R., Penney, W. R., Fair, J. R. & Walas, S. M., 2012. Dryers and Cooling Towers. In: *Chemical Process Equipment*. 3rd ed. s.l.:s.n., pp. 223-275.

Dekati, 2011. *ELPI+ User Manual*, Tampere: Dekati.

Dekati, 2020. *Dekati Ltd.* [Online] Available at: <https://www.dekati.com/products/elpi/> [Accessed 17 01 2020].

Denby, B. et al., 2016. Road salt emissions: A comparison of measurements and modelling using the NORTRIP road dust emission model. *Atmospheric Environment*, Volume 141, pp. 508-522.

Dhananjayan, V., Ravichandran, B., Sen, S. & Panjakumar, K., 2019. *Source, effect, and risk assessment of nanoparticles with special reference to occupational exposure*. [Online] Available at: <https://sciencedirect.com/science/article/pii/B9780128162002000049> [Accessed 6 12 2019].

Dias, D., Tchepel, O. & Antunes, A. P., 2016. Integrated modelling approach for the evaluation of low emission zones.. *Journal of Environmental Management*, Volume 177, pp. 253-263.

- Dong, Y., Hays, M. D., Smith, N. D. & Kinsey, J. S., 2004. Inverting cascade impactor data for size-resolved characterization of fine particulate source emissions. *Journal of Aerosol Science*, 35(12), pp. 1497-1512.
- Ehrlich, C. et al., 2007. PM10, PM2.5 and PM1.0—Emissions from industrial plants—Results from measurement programmes in Germany. *Atmospheric environment*, Volume 41, pp. 6236-6254.
- Ellis, G., 2020. Chapter 4 - The lean equation. In: *Improve: The Next Generation of Continuous Improvement for Knowledge Work*. s.l.:Elsevier, pp. 51-63.
- Elsevier, B. V., 2020. *Science Direct*. [Online] Available at: <https://www.sciencedirect.com/>
- England, G. C. et al., 2013. *Effects of Target Emissions Reductions on Steel Mill Sinter Plant Stack Plume Visibility*. Chicago, A&MWA's 106th annual Conference & Exhibition.
- England, G. C. et al., 2000. Characterizing PM2.5 emission profiles for stationary sources: comparison of traditional and dilution sampling techniques. *Fuel Processing Technology*, p. 177/188.
- EPA, 2016. *Revisions to Test Methods, Performance Specifications, and Testing Regulations for Air Emission Sources*. [Online] Available at: <https://www.govinfo.gov/content/pkg/FR-2016-08-30/pdf/2016-19642.pdf>
- EPA, 2018. [http://www.ecfr.gov/cgi-bin/text-idx?c=ecfr&tpl=/ecfrbrowse/Title40/40cfr60\\_main\\_02.tpl](http://www.ecfr.gov/cgi-bin/text-idx?c=ecfr&tpl=/ecfrbrowse/Title40/40cfr60_main_02.tpl). [Online] Available at: [http://www.ecfr.gov/cgi-bin/text-idx?c=ecfr&tpl=/ecfrbrowse/Title40/40cfr60\\_main\\_02.tpl](http://www.ecfr.gov/cgi-bin/text-idx?c=ecfr&tpl=/ecfrbrowse/Title40/40cfr60_main_02.tpl) [Accessed 10 October 2018].
- EPA, 2019. *Method 5 -Determination of Particulate Matter Emissions*. [Online] Available at: [https://www.epa.gov/sites/production/files/2019-08/documents/method\\_5\\_0.pdf](https://www.epa.gov/sites/production/files/2019-08/documents/method_5_0.pdf)
- Fahlman, B. D., 2007. *Materials Chemistry*. s.l.:Springer.
- Fernández-López, J. A., Angosto, J. M., Roca, M. J. & Miñarro, M. D., 2019. Taguchi design-based enhancement of heavy metals bioremoval by agroindustrial waste biomass from artichoke. *Science of The Total Environment*, Volume 653, pp. 55-63.
- Fertilizers Europe, 2000. *PRODUCTION OF NPK FERTILIZERS by the NITROPHOSPHATE ROUTE*, Brussels: s.n.
- Galvão, E. S. et al., 2018. Trends in analytical techniques applied to particulate matter characterization: A critical review of fundamentals and applications.. *Chemosphere*, Volume 199, pp. 546-568.
- Ghimire, S., Deo, R. C., Downs, N. & Raj, N., 2019. Global solar radiation prediction by ANN integrated with European Centre for medium range weather forecast fields in solar rich cities of Queensland Australia. *Journal of Cleaner Production*, Volume 216, pp. 288-310.
- Giechaskiel, B. et al., 2014. Review of motor vehicle particulate emissions sampling and measurement: From smoke and filter mass to particle number. *Journal of Aerosol Science*, Volume 67, pp. 48-86.



- Glatter, O., 2018. *Light Scattering From Large Particles: Lorenz–Mie Theory*. [Online] Available at: <https://sciencedirect.com/science/article/pii/B9780128135808000109> [Accessed 16 7 2020].
- Gong, Z., Pan, Y.-L., Videen, G. & Wang, C., 2018. Optical trapping and manipulation of single particles in air: Principles, technical details, and applications. *Journal of Quantitative Spectroscopy & Radiative Transfer*, Volume 214, pp. 94-119.
- González-Soto, N. et al., 2019. Impacts of dietary exposure to different sized polystyrene microplastics alone and with sorbed benzo[a]pyrene on biomarkers and whole organism responses in mussels *Mytilus galloprovincialis*. *Science of The Total Environment*, Volume 684, pp. 548-566.
- Govaerts, B. et al., 2020. The Essentials on Linear Regression, ANOVA, General Linear and Linear. In: *Comprehensive Chemometrics*. Second ed. s.l.:2020 Elsevier B.V., pp. 431-463.
- Harrison, R. M. & McCartney, H. A., 1979. Some measurements of ambient air pollution arising from the manufacture of nitric acid and ammonium nitrate fertilizer. *Atmospheric environment*, pp. 1105-1.
- Heydari, M., Ghoreishi, S. M. & Khoobi, A., 2019. Novel electrochemical procedure for sensitive determination of Sudan II based on nanostructured modified electrode and multivariate optimization. *Measurement*, Volume 142, pp. 105-112.
- Hoeflinger, W. & Laminger, T., 2017. PM2.5 or respirable dust measurement and their use for assessment of dust separators. *Journal of The Taiwan Institute of Chemical Engineers*, Volume 94, pp. 53-61.
- Hussain, I., 2012. *The operating experience of a nithophosphate plant*. s.l., SciVerse ScienceDirect, pp. 172-177.
- IFA, I. F. A., 2019. *Nitrogen Products*. [Online] Available at: <https://www.ifastat.org/supply/Nitrogen%20Products/AN%20and%20CAN>
- Ji, Z. et al., 2017. Characteristics of PM2.5 from iron ore sintering process: Influences of. *Journal of Cleaner Production*, pp. 12-22.
- Kahraman, M. F., Kahraman, M. F. & Ozturk, S., 2019. Experimental Study of Newly Structural Design Grinding Wheel Considering Response Surface Optimization and Monte Carlo Simulation. *Measurement*, Volume 147, p. 106825.
- Kalaiarasan, G., Balakrishnan, R. M., Sethunath, N. A. & Manoharan, S., 2018. Source apportionment studies on particulate matter (PM 10 and PM 2.5 ) in ambient air of urban Mangalore, India. *Journal of Environmental Management*, Volume 217, pp. 815-824.
- Kavimani, V., Prakash, K. S. & Thankachan, T., 2019. Multi-objective optimization in WEDM process of graphene – SiC-magnesium composite through hybrid techniques. *Measurement*, Volume 145, pp. 335-349.
- Keskinen, J., Pietarinen, K. & Lehtimäki, M., 1992. Electrical low pressure impactor. *Journal of Aerosol Science*, 23(4), pp. 353-360.
- Koval, S., Krähenbühl, G., Warren, K. & O'Brien, G., 2018. Optical microscopy as a new approach for characterising dust particulates in urban environment. *Journal of Environmental Management*, Volume 223, pp. 196-202.

- Krauss, E. & Aguiar, M. L., 2019. *Performance of two online particulate matter measurement principles in a fertilizer industrial plant*. Cologne, s.n.
- Lee, A. K. Y., Ling, T. Y. & Chan, C. K., 2008. Understanding hygroscopic growth and phase transformation of aerosols using single particle Raman spectroscopy in an electrodynamic balance. *Faraday Discussions*, Volume 137, pp. 245-263.
- Lee, Y. et al., 2019. Efficient and simultaneous cleaner production of biodiesel and glycerol carbonate in solvent-free system via statistical optimization. *Journal of Cleaner Production*, Volume 218, pp. 985-992.
- Lingling, L. et al., 2017. Experimental study on particle removal with gas-liquid cross-flow array system. *Separation and Purification Technology*, Volume 174, pp. 194-202.
- Liou, K. N., 2007. Light Scattering by Atmospheric Particulates. In: K. N. Liou, ed. *An introduction to atmospheric radiation*. s.l.:s.n., pp. 169-256.
- Li, Y. et al., 2017. Monitoring and source apportionment of trace elements in PM<sub>2.5</sub>: Implications for local air quality management. *Journal of Environmental Management*, Volume 196, pp. 16-25.
- Maher, B. A. et al., 2016. Magnetite pollution nanoparticles in the human brain. *PNAS*, 113(39), p. 10797–10801.
- Martins, N. R. & Carrilho da Graca, G., 2018. Impact of PM<sub>2.5</sub> in indoor urban environments: a review. *Sustainable Cities and Society*.
- Mertens, J. et al., 2014. ELPI+ measurements of aerosol growth in an amine absorption column. *International Journal of Greenhouse Gas Control*, Volume 23, pp. 44-50.
- Minitab, 2019. *Minitab 18 Support*. [Online] Available at: <https://support.minitab.com/en-us/minitab/18/>
- Mitchem, L. & Reida, J. P., 2008. Optical manipulation and characterisation of aerosol particles using a single-beam gradient force optical trap. *Chemical Society Reviews*, Volume 37, pp. 756-769.
- Mohankumar, S. & Senthilkumar, P., 2017. Particulate matter formation and its control methodologies for diesel engine: A comprehensive review. *Renewable & Sustainable Energy Reviews*, Volume 80, pp. 1227-1238.
- Mohtashami, R. & Shang, J. Q., 2019. Treatment of automotive paint wastewater in continuous-flow electroflotation reactor. *Journal of Cleaner Production*, Volume 218, pp. 335-346.
- Moser, P. et al., 2017. Solid Particles as Nuclei for Aerosol Formation and Cause of Emissions – Results from the Post-combustion Capture Pilot Plant at Niederaussem. *Energy Procedia*, Volume 114, pp. 1000-1016.
- Muaz, M. & Choudhury, S., 2019. Experimental investigations and multi-objective optimization of MQL-assisted milling process for finishing of AISI 4340 steel. *Measurement*, Volume 138, pp. 557-569.
- Mulholland, G. W., Pui, D. Y. H., Kapadia, A. & Liu, B. Y. H., 1980. Aerosol number and mass concentration measurements: A comparison of the electrical aerosol analyzer with other measurement techniques. *Journal of Colloid and Interface Science*, 77(1), pp. 57-67.
- Muller, K. et al., 2012. Ultrafine and fine particles in the atmosphere - sampling, Chemical Characterization and Sources. *Chemie Ingenieur Technik*, 84(7), pp. 1130-1136.

- Muller, K. et al., 2012. Ultrafine and fine particles in the atmosphere - sampling, chemical characterization and sources. *Chemie Ingenieur Technik*, pp. 1130-1136.
- Ozturk, S., Kahraman, M. F. & Kahraman, M. F., 2019. Modeling and optimization of machining parameters during grinding of flat glass using response surface methodology and probabilistic uncertainty analysis based on Monte Carlo simulation. *Measurement*, Volume 145, pp. 274-291.
- Padoan, E., Ajmone-Marsan, F., Querol, X. & Amato, F., 2017. An empirical model to predict road dust emissions based on pavement and traffic characteristics. *Environmental Pollution*, Volume 237, pp. 713-720.
- Palas, G., 2020. *Palas - aerosol measurement*. [Online] Available at: <https://www.palas.de/en/product/tag?tag=Aerosol%20measurement>
- Parida, A. K. & Maity, K., 2019. Modeling of machining parameters affecting flank wear and surface roughness in hot turning of Monel-400 using response surface methodology (RSM). *Measurement*, Volume 137, pp. 375-381.
- Partridge, L. et al., 2005. Experimental and Theoretical Description of the Break-up of Curved Liquid Jets in the Prilling Process. *Chemical Engineering Research & Design*, 83(11), pp. 1267-1275.
- PCME, 2018. *PCME Ltd*. [Online] Available at: <https://www.pcme.com> [Accessed 12 10 2018].
- PCME, 2019. *Electrodynamic Analyser (EDA) - particulate measurement system brochure*, Saint Ives: Envea UK.
- PCME, 2019. *Optical Scatter Analyser (OSA) - particulate measurement system brochure*, Saint Ives: Envea UK.
- Perepelyuk, M., Maher, C., Lakshmikuttyamma, A. & Shoyele, S. A., 2016. Aptamer-hybrid nanoparticle bioconjugate efficiently delivers miRNA-29b to non-small-cell lung cancer cells and inhibits growth by downregulating essential oncoproteins. *International Journal of Nanomedicine*, Volume 11, pp. 3533-3544.
- Presotto, L., Bellasio, R. & Bianconi, R., 2005. Assessment of the visibility impact of a plume emitted by a desulphuration plant. *Atmospheric Environment*, , 39(4), pp. 719-737.
- Ramesh, K., Baranitharan, P. & Sakthivel, R., 2019. Investigation of the stability on boring tool attached with double impact dampers using Taguchi based Grey analysis and cutting tool temperature investigation through FLUKE-Thermal imager. *Measurement*, Volume 131, pp. 143-155.
- Roberts, D. L., 2009. Theory of Multi-Nozzle Impactor Stages and the Interpretation of Stage Mensuration Data. *Aerosol Science and Technology*, 43(11), pp. 1119-1129.
- Saleem, S. et al., 2019. Investigating the effects of design and management factors on DBPs levels in indoor aquatic centres. *Science of The Total Environment*, Volume 651, pp. 775-786.
- Saleh, S. N. & Barghi, S., 2016. Reduction of fine particle emission from a prillingtower using CFD simulation. *Chemical Engineering Research and Design*, pp. 171-179.
- Sarabia, L. A., Ortiz, M. C. & Sanchez, M. S., 2020. Response Surface Methodology. In: S. D. Brown, R. Tauler & B. Walczak, eds. s.l.:2020 Elsevier B.V, pp. 287-326.

Séquier, F. et al., 2014. Critical parameters involved in producing microspheres by prilling of molten lipids: from theoretical prediction of particle size to practice.. *European Journal of Pharmaceutics and Biopharmaceutics*, 87(3), pp. 530-540.

Shirley, A. R., Forsythe, P. A., Giles, W. M. & Phillips, J. A. F., 1996. *Process for the reducing emissions during prilling of material such as ammonium nitrate*. United States, Patent No. 5514307.

Sick, A., 2020. *Sick AG Product Portfolio*. [Online] Available at: <https://www.sick.com/ag/en/c/products#g54727>

Sieniutycz, S. & Szwast, Z., 2018. *Neural Networks for Emission Prediction of Dust Pollutants*. [Online]

Available at: <https://sciencedirect.com/science/article/pii/B9780128135822000033> [Accessed 4 6 2019].

Singh, A. et al., 2019. Evaluation and analysis of occupational ride comfort in rotary soil tillage operation. *Measurement*, Volume 131, pp. 19-27.

Sivaiah, P. & Chakradhar, D., 2019. Modeling and optimization of sustainable manufacturing process in machining of 17-4 PH stainless steel. *Measurement*, Volume 134, pp. 142-152.

Soysal, U. et al., 2017. Aerosol mass concentration measurements: Recent advancements. Volume 114, pp. 42-54.

Su, C.-H., Nguyen, H. C., Bui, T. L. & Huang, D.-L., 2019. Enzyme-assisted extraction of insect fat for biodiesel production. *Journal of Cleaner Production*, Volume 223, pp. 436-444.

Sullivan, R. C., Gorkowski, K. & Jahn, L., 2018. Characterization of Individual Aerosol Particles. In: *Physical Chemistry of GaseLiquid Interfaces*. s.l.:Elsevier Inc..

Sun, Z. et al., 2019. Sulfate–nitrate–ammonium as double salts in PM<sub>2.5</sub>: Direct observations. *Science of the Total Environment*, pp. 204-209.

Tchepel, O. et al., 2012. Emission modelling of hazardous air pollutants from road transport at urban scale. *Transport*, 27(3), pp. 299-306.

Team, W. H. O., 2006. *Air quality guidelines - global update 2005*. [Online] Available at: [https://www.who.int/phe/health\\_topics/outdoorair/outdoorair\\_aqg/en/](https://www.who.int/phe/health_topics/outdoorair/outdoorair_aqg/en/) [Accessed 15 02 2020].

Thakur, P., 2019. Respirable Coal Dust, Combustible Gas and Mine Fire Control. In: *Advanced Mine Ventilation*. s.l.:Elsevier, pp. 189-210.

Tondy, H. R. & Tigga, A. M., 2019. An empirical evaluation and optimization of performance parameters of wire electrical discharge machining in cutting of Inconel 718. *Measurement*, Volume 140, pp. 185-196.

Vallero, D., 2014. *Controlling Air Pollution from Sources*. [Online] Available at: <https://sciencedirect.com/science/article/pii/B9780124017337000311> [Accessed 29 5 2020].

Vaughan, J., 2002. *Light Scattering Spectroscopy-Basic Theory and Instrumentation*. [Online] Available at: <https://sciencedirect.com/science/article/pii/B9780126137606500425> [Accessed 16 7 2020].

Virtanen, A., Marjamäki, M., Ristimäki, J. & Keskinen, J., 2001. Fine particle losses in electrical low-pressure impactor. *Journal of Aerosol Science*, 32(3), pp. 389-401.

- WHO, R. O. f. E., 2017. *Evolution of WHO air quality guidelines: past, present and future*. [Online]  
Available at: [https://www.euro.who.int/\\_data/assets/pdf\\_file/0019/331660/Evolution-air-quality.pdf](https://www.euro.who.int/_data/assets/pdf_file/0019/331660/Evolution-air-quality.pdf)  
[Accessed 26 06 2020].
- Wilson, W. E. et al., 2002. Monitoring of particulate matter outdoors. *Chemosphere*, 49(9), pp. 1009-1043.
- Win-Shwe, T.-T. & Fujimaki, H., 2011. Nanoparticles and neurotoxicity.. *International Journal of Molecular Sciences*, 12(9), pp. 6267-6280.
- Wong, D. et al., 2004. Break-up dynamics and drop size distributions created from spiralling liquid jets. *International Journal of Multiphase Flow*, 30(5), pp. 499-520.
- Wozniak, M., Jakubczyk, D., Derkachov, G. & Archer, J., 2018. Sizing of single evaporating droplet with Near-Forward Elastic Scattering Spectroscopy (vol 202, pg 335, 2017). *Journal of Quantitative Spectroscopy & Radiative Transfer*, Volume 205, p. 147.
- Wu, C. & Chu, B., 2000. *Chapter 1 – Light Scattering*. [Online]  
Available at: <http://sciencedirect.com/science/article/pii/B9780080506128500076>  
[Accessed 16 7 2020].
- Xu, Y., 2018. Evaluation of mineral dust aerosol optical depth and related components from the CHIMERE-DUST model using satellite remote sensing and ground-based observations. *Atmospheric Environment*, Volume 191, pp. 395-413.
- Yin, Z. et al., 2015. Size-resolved effective density of urban aerosols in Shanghai. *Atmospheric Environment*, Volume 100, pp. 133-140.
- YR, 2019. *www.yr.no*. [Online]  
Available at: <https://www.yr.no/>  
[Accessed 13 05 2019].
- Yuan, W., Chuanping, B. & Yuxin, Z., 2007. An Innovated Tower-fluidized Bed Prilling Process. *Chin. J. Chem. Eng.*, Volume 15, pp. 424-428.

## 10. APPENDIX

### 10.1. Unique ELPI Data Sheet for Impactor 10270

# **DEKATI ELPI+™ DATA SHEET**

DEKATI Impactor # **10270**

Cut points, downstream pressures and residence times:

Stage	D50% (µm)	Pressure (kPa)	Residence Times
1	0.0060	4.00	0.0010
2	0.0160	4.34	0.0024
3	0.0311	9.95	0.0056
4	0.0547	22.74	0.0127
5	0.0950	38.81	0.0222
6	0.156	69.52	0.0391
7	0.255	89.10	0.0505
8	0.380	97.06	0.0552
9	0.600	99.59	0.0585
10	0.944	100.48	0.0622
11	1.62	101.01	0.0571
12	2.46	101.18	0.0578
13	3.64	101.25	0.0736
14	5.35	101.30	0.1029
15	9.84	101.32	0.00
<b>inlet</b>		<b>101.33</b>	

Inlet Pressure: 1013.3 mbar  
 Outlet pressure: 40 mbar  
 Flow rate: 10.03 lpm

Calibration information

Date: 29.11.2018  
 Temperature: 20.5 °C

Diffusion loss parameters



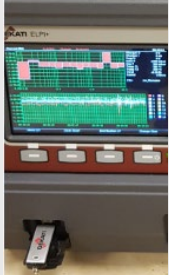
a	b	c
9.80E-08	-2.7300	0.05085
9.80E-08	-2.7300	0.05085
9.80E-08	-2.7300	0.05085
3.63E-08	-3.0600	0.03083
1.58E-06	-2.2600	0.02342
4.83E-06	-2.0600	0.02183
1.02E-05	-1.9000	0.02097
6.22E-05	-1.4900	0.01158
4.03E-05	-1.5600	0.00804
7.31E-05	-1.4000	0.00671
1.01E-04	-1.3100	0.00475
8.22E-05	-1.3500	0.00288
1.09E-04	-1.3100	0.00129
9.07E-05	-1.3600	0.00186

$$\text{Loss} = a \cdot D_i^b + c$$


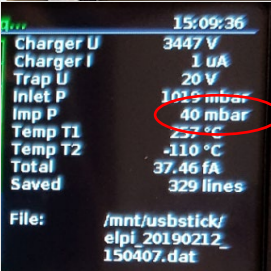
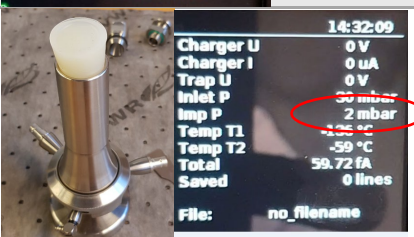

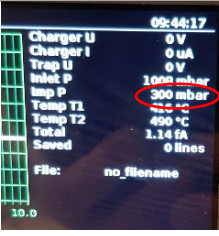
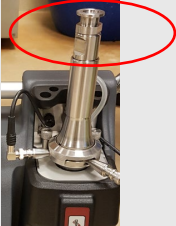
Charger Efficiency P<sub>neQ</sub>

Limit1	Limit2	
1.035	4.2820	
Mult1	Mult2	Mult3
1.83	1.8114	3.3868
Exp1	Exp2	Exp3
1.225	1.515	1.085

## 10.2. Operating Procedures for ELPI

	<p>Weight stage 15 collection plate before assembling impactor</p> <p>Check oil level and aspect in the vacuum pump</p>	<p>Use Sartorius balance Record results</p> <p>Level must be kept from mid-point up Oil must be transparent with no bubbles on it</p>	
	<p>Assemble ELPI setup with pump and dryer according to Manual</p>	<p>Step by step procedure is available on operations manual from supplier Dekati Ltd Set-up depends on technical analysis of sample location and dust/ air characteristics</p>	<div style="display: flex; justify-content: space-around;"> <div style="text-align: center;">  <p>setup ambient air</p> </div> <div style="text-align: center;">  <p>setup stack</p> </div> </div>
	<p>Perform leakage test on ELPI</p>	<p>See SPL 10.3</p>	
	<p>Perform zeroing test on ELPI</p>	<p>See SPL 10.4</p>	
	<p>Insert memory stick, got to menu 3/3, click control then click MOUNTED and start SAVING to FILE</p>	<p>Every time you remove memory stick and put it back you have to click SAVING to FILE</p>	
	<p>Switch on charger</p>	<p>After zeroing is important to remember switch OFF air pump and switch ON charger</p>	
	<p>Check parameters are ok:</p> <p>Inlet P~ 1000 mbar</p> <p>Imp P: 40 mbar</p> <p>Charger U ~3500 V</p>	<p>Inlet P is atmospheric pressure about 1000mbar Imp P from 35 to 45mbar is acceptable Charger U from 3000V to 4000V is acceptable Temperature shall be ignored once no sensor is installed</p>	
	<p>Run the test during planned time or until equipment is full</p>	<p>Equipment is full when Imp P starts to decrease quickly to below 35 mbar, even when adjusting the valve of ELPI to correct it for 40 mbar.</p>	

### 10.3. Perform Leakage Test on ELPI

<p>Adjust the pressure adjustment valve to get a reading of 40 mbar</p>	<p>Pressure from 38 to 42 mbar is acceptable</p>	<p>To see if assembling works fine in normal sampling conditions</p>	 
<p>Close tightly the inlet of the charger using e.g. the leakage check tool</p>	<p>Leakage tool is kept inside of the transparent box After a while, the pressure should reach less than 5 mbar</p>	<p>No external source of air besides leakages</p>	
<p>Close the pressure adjustment valve in the ELPI®+ unit front panel</p>	<p>Close it completely</p>	<p>Over pressurize the system to see if it is sealed</p>	
<p>Now check that the pressure reading does not increase more than 20 mbar per minute.</p>	<p>If the pressure increase is less than this the equipment is approved.  If pressures increases to end of scale (300 mbar) over the time go to step 5.</p>	<p>Leakage can affect reading and damage components due to erosion</p>	
<p>If you fail to get the values above, check that that the impactor is properly positioned in its support.</p>	<p>Generally, leakage is at the inlet of impactor, on the charging part or connection to sample dryer.  Remove upper connection piece to perform new leakage test</p>		



#### 10.4. Perform Zeroing Test on ELPI

z	Start ELPI®+ and leave it running for at least 20 min	Check charger is OFF	To ensure stable operation and successful zeroing
	Press the Menu button in the ELPI®+ display and select Zero air ON.	Start the zero air pump	Feed clean air through the stages
	Wait until the current values are stable.	There is always some noise in the electrometer readings but there should be no drift in the signal before the zeroing in started	
	Press the Menu button in the ELPI®+ display twice to go to the Main menu window. Choose Control, Choose Start Electrometer calibration.	<b>NOT touch the ELPI®+ during the zeroing</b>  Zeroing can take few minutes.	<b>Vibration in the unit can affect the zero level measurement.</b>
	Check that the zero levels are within acceptable limits (+-10 fA) with Zero air ON.	The zero levels should always be checked from the raw current values (view 7/7).	
	If zeroing is successful no response is given	Switch zero ai OFF Switch charger ON Check saving is ON	
	If not the alarm in red will say: zeroing sequence failed, wait 5min and try again		